

Bruce Hoppener

# MRI-Compatible Pneumatic Actuation Unit for a Self-Propelling Needle

# MRI-Compatible Pneumatic Actuation Unit for a Self-Propelling Needle

By

Bruce Hoppener

in partial fulfilment of the requirements for the degree of

**Master of Science**  
in Mechanical Engineering

at the Delft University of Technology,  
to be defended publicly on Thursday January 19, 2023 at 13:45

Student number:	4425626	
Supervisors:	ir. J. Bloembergen	TU Delft
	Prof. dr. ir. P. Breedveld	TU Delft
Thesis committee:	ir. J. Bloembergen	TU Delft
	Prof. dr. ir. P. Breedveld	TU Delft
	Dr.ir. G. Smit	TU Delft

An electronic version of this thesis is available at <http://repository.tudelft.nl/>.



## *Preface*

After a long, but definitely educational and fun period, I can finally say that I have finished my master thesis. The thesis is about the design and testing of an MRI-compatible pneumatic actuation unit for a self-propelling needle. The self-propelling needle is developed by the BITE (Bio-Inspired Technology) research group at the TU Delft. Previous versions of the needle were actuated by an actuation unit consisting of electromagnetic motors. Due to these motors not being able to be used inside of MRI-scanners, my goal was to design an actuation unit for the current needle design, that is MRI-compatible.

I would like to thank my supervisor, Jette Bloemberg for the helpful weekly meetings. Also, I would like to thank Paul Breedveld for the meetings we had, which I often left with a large amount of new creativity. Besides this, I also learned new ways how to solve designing problems and how to come up with more ideas. I remember one method was to think about a device in the year 3000 and ask yourself "how will the device look like then?". This method let me think the other way around and really sparked my creativity. I will take this with me for the rest of my engineering/design career. I would also like to thank Gertjan Mulder from the fluid mechanics department for the information on valves and for the help with the control unit design. Finally, I would like to thank the group of other students and supervisors for the meetings and workshops.

Bruce Hoppener  
Alkmaar, December 2022

# CONTENTS

<b>1</b>	<b>Introduction</b>	<b>1</b>
1.1	Focal Laser Ablation . . . . .	1
1.2	Wasp-Inspired Needles . . . . .	2
1.3	Problem Statement and Goal . . . . .	3
1.4	Structure . . . . .	3
<b>2</b>	<b>Requirements</b>	<b>3</b>
2.1	Must Haves . . . . .	3
2.1.1	Performance . . . . .	3
2.1.2	Dimensions . . . . .	4
2.1.3	Materials . . . . .	4
2.2	Nice to Haves . . . . .	4
<b>3</b>	<b>Design</b>	<b>5</b>
3.1	Actuation Unit . . . . .	5
3.1.1	Actuator Design . . . . .	5
3.1.2	Adjustable Stroke Mechanism . . . . .	5
3.1.3	Needle Attachment . . . . .	6
3.2	Final Layout . . . . .	6
<b>4</b>	<b>Prototype</b>	<b>7</b>
4.1	Materials . . . . .	7
4.2	Manufacturing . . . . .	7
4.2.1	Actuation Unit . . . . .	7
4.2.2	Needle . . . . .	10
4.2.3	Control Unit . . . . .	11
<b>5</b>	<b>Evaluation</b>	<b>11</b>
5.1	Goal . . . . .	11
5.2	Experimental Setup . . . . .	11
5.3	Experimental Procedure . . . . .	13
5.3.1	Functionality test . . . . .	13
5.3.2	Experiment 1: Variable Stroke . . . . .	13
5.3.3	Experiment 2: Variable Interval Time . . . . .	13
5.3.4	Data Analysis . . . . .	13
5.4	Experimental Results . . . . .	14
5.4.1	Experiment 1: Variable Stroke . . . . .	14
5.4.2	Experiment 2: Variable Interval Time . . . . .	15
<b>6</b>	<b>Discussion</b>	<b>16</b>
6.1	Main Findings . . . . .	16
6.2	Limitations and Recommendations . . . . .	16
6.2.1	Prototype . . . . .	16
6.2.2	Experiment . . . . .	17
6.3	Medical Application . . . . .	18
6.3.1	Focal Laser Ablation . . . . .	18
6.3.2	Medical Device Regulations . . . . .	18
6.4	Further Research . . . . .	18
6.4.1	Design Adjustments . . . . .	18
6.4.2	Control . . . . .	19
<b>7</b>	<b>Conclusion</b>	<b>19</b>
<b>8</b>	<b>Acknowledgements</b>	<b>19</b>
	<b>Appendix A. Morphological Chart</b>	<b>24</b>

<b>Appendix B. Old concepts and partial concepts</b>	<b>29</b>
<b>Appendix C. Technical Drawings Actuation Unit</b>	<b>33</b>
<b>Appendix D. Calculations and Variables as in the Matlab Script</b>	<b>42</b>
<b>Appendix E. Matlab Script for Dimensions, Force, and Frequency Calculations</b>	<b>46</b>
<b>Appendix F. Arduino Code</b>	<b>52</b>
<b>Appendix G. 3D-Print Iterations and Findings</b>	<b>53</b>
<b>Appendix H. Figures Data Analysis + Statistical Analysis</b>	<b>59</b>
<b>Appendix I. Matlab Script Data Analysis</b>	<b>64</b>
<b>Appendix J. Matlab Code Statistical Analysis</b>	<b>68</b>
<b>Appendix K. Components for the Control Unit</b>	<b>72</b>

# MRI-Compatible Pneumatic Actuation Unit for a Self-Propelling Needle

Bruce Hoppener

Mechanical Engineering, Delft University of Technology, Delft, The Netherlands



**Abstract**—Focal laser ablation is a new, promising method to treat tumors. The current focal laser ablation approach is to insert an optical fiber into the patient using rigid needles. A side effect of this approach is that during the needle insertion, tissue damage occurs. The larger the diameter of the needle, the more tissue damage. If the diameter of a rigid needle is reduced, the risk increases that buckling occurs during insertion. Buckling can result in tissue damage due to unwanted movements of the needle tip. By using wasp-inspired, self-propelling needles, the size of the needles can be reduced, thereby reducing tissue damage, while preventing needle buckling. The needle can advance through tissue with no net insertion force by moving parallel needle segments in a specific order. In this work, we present the design and evaluation of an MRI-compatible, pneumatic actuation unit for such a self-propelling needle. A prototype was created that was, except for the screws that were used, fully 3D printed with MRI-compatible materials. Guidelines were formed on how to approach such a 3D-printing process. The screws were also made of an MRI-compatible material. The prototype has the option to change the distance that the needle segments travel each cycle, called the stroke. By using a control unit for the air supply of the prototype, the needle segments were moved automatically. The needle consists of six needle segments with a diameter of 0.25 mm. We tested the performance of the prototype in 10 wt% gelatin tissue phantoms in terms of the slip ratio of the needle with respect to gelatin tissue phantoms. The results showed that the prototype was functional for small strokes (i.e., 2 mm and 4 mm), as the needle was able to advance through 10 wt% gelatin tissue phantoms using the self-propelling mechanism with a mean slip ratio of 0.912-0.955. The prototype is the next step in developing self-propelling needles suitable for focal laser ablation to treat tumors.

**Keywords**— additive manufacturing, pneumatic actuator, medical needle, magnetic resonance imaging, biologically inspired design.

## Abbreviations

PLA	Polylactic acid
SLA	Stereolithography
MRI	Magnetic resonance imaging

## Nomenclature

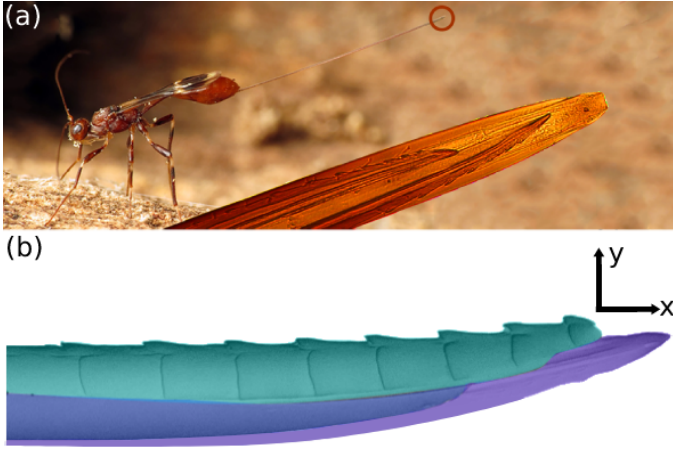
SR	Slip ratio
F	Force (N)
d	Distance (mm)
x	Position (mm)
P	Pressure (bar)

## 1 INTRODUCTION

### 1.1 Focal Laser Ablation

Ablative procedures are a popular, clinically accepted method to treat tumors. Although various ablative procedures exist, the instruments for these procedures all are needle-like instruments that are inserted into the tumor, whereafter the ablative procedure is started, eliminating the tumor by using some form of energy. An advantage of using ablative procedures is that the procedure is minimally invasive [1, 2]. A minimally invasive procedure is a procedure where the instruments are inserted through one or more small incisions called “ports” [3]. These types of procedures have shorter recovery times and less tissue damage compared to conventional surgical operations [4]. One form of such an ablative procedure is focal laser ablation. Focal laser ablation works by using an infrared laser, through an optical fiber, to locally eliminate the tumor with heat [5]. The laser creates precise and reproducible ablation zones while creating no or little changes in the tissue outside the ablation zones [6].

In current clinical usage, for the percutaneous approach, the flexible laser fiber is inserted by using rigid



**Fig. 1:** (a): Parasitic wasp with a close-up view of the tip of the ovipositor [12]. (b): Ovipositor of one of the parasitic wasp species, consisting of three valves, with each of the valves colored with a different color, adapted from [13].

needles or needle-like instruments [5–7]. These needles are inserted by pushing them through the tissue. Due to the complex cutting process during needle insertion, tissue damage and tissue deformation of tissue around the needle occurs [4, 8]. The tissue damage is partly due to the dragging of the needle surface along the tissue [4]. The larger the needle diameter, and thus the needle surface, the larger the tissue damage [9]. Although some methods to reduce tissue damage and tissue deformation during insertion were created, they frequently conflict with standard clinical needles and may be challenging to apply [4]. Van den Berg et al. [9] stated that the largest factor for tissue damage is the needle size, meaning that reducing the needle size will reduce the tissue damage. This holds for when the needle follows its desired trajectory. Needle-like instruments can lose their desired trajectory due to buckling. Buckling is a mechanical failure mode where a compressive load causes the needle to deflect laterally, making the configuration unstable. This can result in tissue damage due to unwanted movements of the needle tip [10]. Therefore, to minimize tissue damage for needle-like instruments that require a pushing force to advance through the issue, an optimum needle size should be found, as larger needles increase tissue damage, and smaller needles increase the risk of buckling [9, 11].

## 1.2 Wasp-Inspired Needles

In an attempt to minimize tissue damage and reduce the risk of buckling, self-propelling needles inspired by the egg-laying channel, the ovipositor, of parasitic wasps have been developed [14, 15]. These kinds of wasps lay their eggs by making holes in a variety of materials including wood [16]. In general, all species of parasitic wasps with an ovipositor have a similar ovipositor shape [11]. Figure 1a depicts one of the parasitic wasp species with a close-up of the tip of the ovipositor. The ovipositor

consists of three functional segments, also called valves [11]. Figure 1b depicts the ovipositor with each of the valves differently colored. These valves are connected by a joint and groove mechanism and can move relatively from each other in the axial direction (x-direction in Figure 1b) [13]. Some species have backward-facing teeth on the tip of the ovipositor, to anchor the ovipositor in the material [16, 17]. By pushing one valve at a time, while pulling at the other (anchored) valves, the valve that is being pushed advances in the tissue. By repeating this process for each valve, one valve at a time for a small distance, the ovipositor advances through the tissue [15, 16]. The ovipositor is a slender, hollow device, which makes it prone to buckling [11]. Although little about the buckling prevention mechanism is known, it is thought that buckling is prevented due to the small distance it travels each step of the repeated process [11]. By using the ovipositor as inspiration, needles can be developed that are small enough to reduce tissue damage, while having a buckling prevention mechanism [14].

Figure 2 shows the wasp-inspired needle, as developed by Scali [14]. The needle consists of six parallel needle segments held together by rings and a shrinking tube at the tip. Because the needle segments are of round shape, with a diameter of 0.25 mm, and do not have the joint and groove mechanism like the ovipositor, the total needle diameter is as low as 0.84 mm [14]. Although it does not use the same interlocking mechanism as the ovipositor, it does use the same method to advance through tissue. To advance the needle through tissue, the needle repeats cycles of motion. For a cycle to complete, first the segments advance through the tissue one by one, or in some cases, two by two, followed by a pulling motion on all segments simultaneously. Figure 3 schematically depicts the forces on the needle consisting of  $i$  needle segments, when advancing  $j$  number of segments through tissue. The insertion force,  $F_{in,i}$ , is the total insertion force acting on the needle. The friction force  $F_{fric,j}$  and the cutting force  $F_{cut,j}$  work on  $j$  number of advancing segments. The friction force acting on the stationary segments is  $F_{fric,k}$ . For the needle to be self-propelling, the net insertion force has to be zero:

$$\sum_{i=1}^N F_{in,i} = 0 \quad (1)$$

where  $N$  is the total number of segments. For Equation 1 to hold, the sum of the friction and cutting force of the advancing segments have to be equal to the friction force of the non-advancing segments:

$$\sum_{j=1}^a (F_{fric,j} + F_{cut,j}) = - \sum_{k=1}^{na} F_{fric,k} \quad (2)$$

where  $a$  is the number of advancing segments and  $na$  is the number of non-advancing segments [14, 15].

A number of studies researched the forces acting on a needle when inserted with a pushing force into

tissue. The force on the needle is positively correlated with insertion speed and insertion depth [18, 19]. For increasing speed, frictional forces increase considerably more quickly than cutting forces [20]. Another factor for increasing axial forces is the needle diameter. For larger diameters, the axial forces also increase [20]. Besides the needle speed, the insertion depth, and the needle diameter, the forces are also dependent on the material it is inserted in, and the shape of the needle tip [18–23]. In biological material, peaks in force can be measured when rupture events occur. Rupture events occur due to variability in the structure of biological tissue [21]. Due to the large number of variables that influence the forces on the needle during insertion, the needle-tissue interaction forces are hard to predict [19].

### 1.3 Problem Statement and Goal

Focal laser ablation happens under constant monitoring of an imaging technique. Magnetic resonance imaging (MRI) offers excellent soft-tissue contrast and allows for constant monitoring of the ablation zone, making it an excellent imaging technique for ablative procedures. MRI also allows for monitoring of temperature, in comparison with other imaging techniques, where temperature sensors are used to monitor the temperature of the ablation zone [25, 26].

To our knowledge, up to this date self-propelling, ovipositor-inspired needles are actuated manually [27] or by electromagnetic motors [15]. Electromagnetic motors allow for the adjustment of the cycle interval times, however, they interfere with the magnetic field inside MRI scanners. Although the manual actuation unit can be used inside MRI scanners, our prototype should be able to allow for adjustment of the interval times of the needle cycles. Thus, the main goal of this study is:

**To design an MRI-compatible, pneumatic actuation unit for a self-propelling, ovipositor-inspired needle consisting of six needle segments.**

Sub-goals of this study are:

- To design a pneumatic actuation unit with an adjustable output stroke, where the stroke is the distance that each needle segment travels per cycle.
- To design the actuation unit in such a way that it is possible to lock and change the needle segments of different sizes.
- To design a control unit, capable of actuating the actuation unit so that the output of the system is a cycle with an adjustable interval time, as previously described in Section 1.2, while using a single air input.
- To manufacture a complete prototype for the actuation unit and the needle consisting of MRI-compatible materials.
- To design the actuation unit in such a way that in the future, an optical fiber for focal laser ablation could be inserted in the core of the needle.

## 1.4 Structure

First, the requirements of the system are discussed in Section 2. Then, each part of the designed system is discussed in Section 3. Next, the prototype which is used for the experiments is discussed in Section 4. The evaluation of the prototype using experiments is discussed in Section 5. The discussion can be found in Section 6. Finally, Section 7 contains the conclusion.

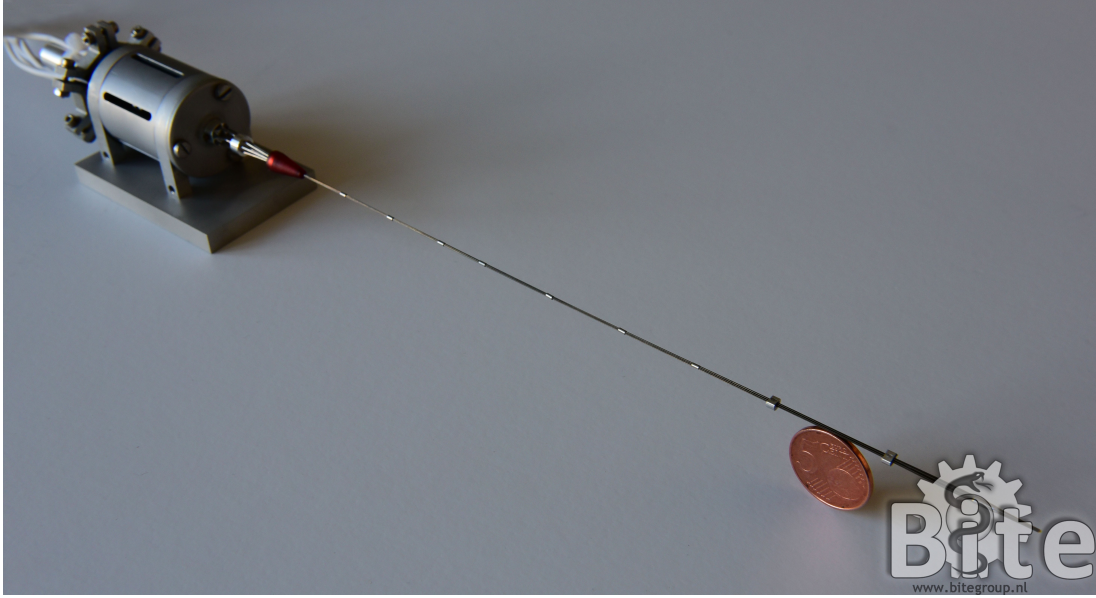
## 2 REQUIREMENTS

### 2.1 Must Haves

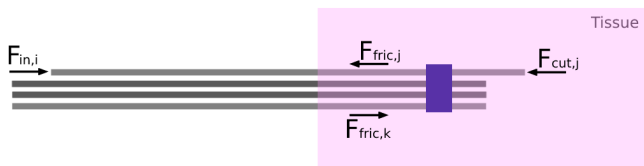
To start the design process, a list of requirements for the system (control unit, actuation unit, and needle) was created. The must-have requirements are the requirements that must be met in order for the system to be successful.

#### 2.1.1 Performance

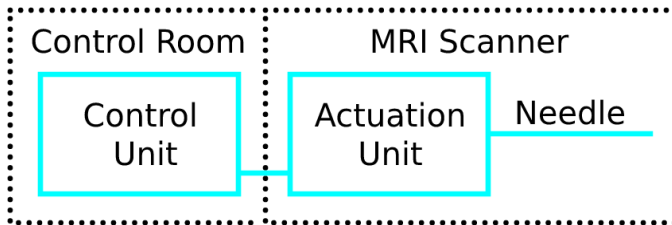
- 1) *Adjustable stroke.* The stroke of the needle segments should be adjustable between 1-10 mm in the actuation unit, with a precision of at least 1 mm. This is so it can be compared with the measurements done by Scali [14] and Pusch [15], who both used strokes of 2 mm, 4 mm, and 6 mm.
- 2) *Actuation cycle.* The actuation unit has to be able to move the segments in different orders, meaning each segment should be separately controllable for the forward motion. For the backward motion, the segments are moved back simultaneously.
- 3) *Input air pressure.* The minimum required input air pressure for the actuation unit to work should not be higher than 3.79 bar (55psig), as the range we found for medical air pressure is 3.79-7.2 bar [28–30]. For lower required air inputs a pressure regulator can lower the pressure.
- 4) *Force.* The output force of the actuation unit should be within the range of 0.3-0.75 N. Because, based on literature [18–23], it is hypothesized that this is sufficient, with a margin for uncertainty, for inserting needle segments with a diameter up to 0.25 mm into 10 wt% gelatin. Our needle size is comparable to the size of Aaboubout et al. [23], who use needles up to a diameter of 0.31 mm in biological tissue and measure maximum (peak) insertion forces of 0.6 N. A minimum of 0.3 N is chosen as this is thought to be sufficient to move the needle through the tissue. With 0.6 N as a maximum and a safety factor of 1.25, this results in a maximum force of 0.75 N.
- 5) *Segment attachment.* The needle segments can be attached and detached from the actuation unit.
- 6) *Speed* The output speed of the actuation unit should at least be 2 mm/s, to compare it with the state-of-the-art [14, 15].
- 7) *Safety.* The actuation unit is safe to use while the input air pressure is applied. Precautions for potential parts flying away should be taken.



**Fig. 2:** Wasp-inspired needle developed by Scali [14]. The needle consists of six parallel needle segments with a diameter of 0.25 mm per segment. The segments are actuated by an actuation unit with six linear stepper motors [24].



**Fig. 3:** Wasp-inspired needle insertion in tissue (pink), with shrinking tube (blue) at the tip of the needle. The needle segments are separately advanced through the tissue by insertion force  $F_{in,i}$ . The cutting force  $F_{cut,j}$  acting on the advancing segment is compensated by the static friction force on the stationary segments,  $F_{fric,k}$ .  $F_{fric,j}$  is the friction force on the advancing segments.



**Fig. 4:** Setup of the system, containing the control unit, the actuation unit, and the needle, inside the operating room. The control unit is placed in the control room, outside of the MRI scanner. The actuation unit and the needle are placed inside of the MRI scanner.

### 2.1.2 Dimensions

- 8) *Actuation unit.* For the instrument to be a handheld instrument, the length of the actuation unit is within the range of 50-150 mm. The largest diameter of the actuation unit is within the range of 10-60 mm.
- 9) *Option to implement laser fiber.* The actuation unit has the option to implement a laser fiber with a diameter of up to 0.5 mm, to comply with the dimensions of state-of-the-art laser fibers [31–33].
- 10) *Segment Compatibility.* The actuation unit is compat-

ible with needle segments with a diameter of 0.1-0.25 mm, to compare it with the state-of-the-art, where segments with a diameter of 0.125-0.25 mm were tested [14]. The minimum length of the needle segments is 100 mm.

- 11) *Maximum unsupported needle length.* The maximum unsupported needle length inside the actuation unit is 10 mm, to avoid buckling, as described by Pusch [15].

### 2.1.3 Materials

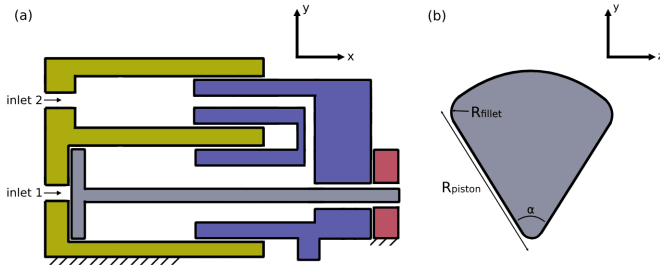
- 12) *MRI compatible.* The actuation unit and the needle will be used inside the MRI scanner (Figure 4). Thus, the materials used for the actuation unit and the needle should be MRI compatible, meaning they should be nonferrous [34].

## 2.2 Nice to Haves

Besides the functional requirements, a list of nice-to-have requirements was created. At this point, the concept does not have to fulfill the nice-to-have requirements, however, if these requirements can be met it would already be beneficial. The nice-to-have requirements that are not met can be an addition to future work.

- 13) *Costs.* The upper boundary for the total costs of the system, including the costs for the off-the-shelf components, is \$1000.
- 14) *Lightweight.* It is wished that weight of the actuation unit is within the range of 10-2000 g. As 2000 g is the highest weight that surgeons would tolerate for handheld tools according to Nakajima & Schwarz [35].





**Fig. 5:** (a): Design of the actuator with the piston housing (yellow), the piston stop (blue), the piston (grey), and the piston guidance (red). For forward motion (piston translates over the positive x-axis), air is inserted in inlet 1. For backward motion (piston translates over the negative x-axis), air is inserted in inlet 2. (b): Design of the piston base area.  $R_{piston}$  is the radius that is used to design the piston.  $R_{fillet}$  is the radius of the fillets.

- 15) *Bio-compatibility.* The materials of the needle that are in contact with the patient during focal laser ablation should be biocompatible.

### 3 DESIGN

#### 3.1 Actuation Unit

##### 3.1.1 Actuator Design

For the design, first, a morphological chart was created. The morphological chart contains geometrical functions, including shape, placement, and orientation. It also contains functions for some of the requirements. An example of this is the function to adjust the output stroke of the needle segments. Appendix A contains this morphological chart. Each solution comes with advantages and disadvantages over the others, only the main functions with the most promising solutions are discussed.

The actuator, depicted in Figure 5a, consists of the piston housing (yellow in Figure 5a), the piston stop (blue in Figure 5a), the piston (grey in Figure 5a), and the piston guidance (red in Figure 5a). The actuator is designed in such a way that the piston has one degree of freedom that is translation along the x-axis in Figure 5a. The piston housing is the housing in which the piston translates. The piston housing for one actuator contains two inlets that can be connected to an air supply to pressurize the chambers of the piston housing and the piston stop. By letting air through inlet 1 (see Figure 5a), the pressure builds up behind the base of the piston, causing the piston to move forward (positive x-direction). By letting air through inlet 2, the air will flow via the chamber in the piston stop until it reaches the piston base. Then, pressure builds up causing the piston to move backward (negative x-direction). By using this mechanism, the pressure pushes the piston back, rather than pulling it back with a negative gauge pressure. A theoretical minimum gauge pressure of -1 bar is achievable. In practice, this would not be reachable because the valves have a working range of up to -0.9 bar [36] and the actuator might not be fully airtight. To have the option to increase the pressure to more than 1 bar gauge pressure,

it is chosen to use a positive gauge pressure with two inlets.

Figure 5b depicts the shape of the base of the piston. As it is wished that the design of the actuation unit is as small as possible, the shape of the pistons can be an important factor in the total diameter of the actuation unit. To use the space as efficiently as possible, all pistons form a circle together. Since there are six pistons, each piston has the shape of 1/6th of a circle ( $\alpha = 60^\circ$ ), with  $R_{piston}$  as radius.  $R_{fillet}$  is the radius of the fillets. It was chosen to use a cylindrical design because the needle segments form a circle together. This way it allows for a simple design to actuate the needle segments and let them come together in a cylindrical shape. Besides this, a cylindrical design of the actuation unit also makes it easy for the instrument to be handheld in future design iterations of the pneumatic actuation unit for self-propelling needles.

As discussed in Section 2, Requirement 4 states that the output force of the actuation unit should be within the range of 0.3-0.75 N. Assuming that the actuator design is airtight enough, the output force of the actuation unit is related to the input pressure of the actuation unit with the following formula:

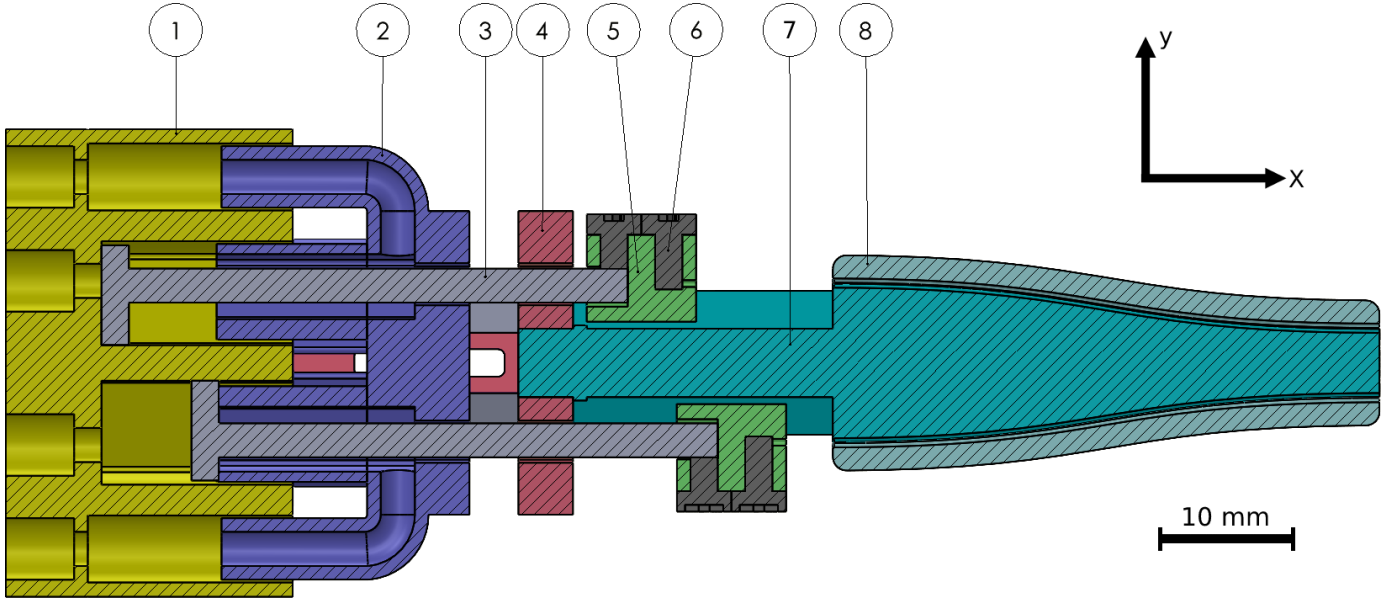
$$F = P * A \quad (3)$$

Where  $P$  is the gauge pressure,  $F$  is the force and  $A$  is the area of the piston base. The gauge pressure is the pressure in the actuator, relative to the ambient atmospheric pressure. Since the input air pressure can be adjusted within a range of 1-3.79 bar (Requirement 3), the output force can be adjusted by adjusting the input air pressure. This would mean that, in theory, the minimum area could be reduced as long as the pressure can be increased. However, due to limitations of the mechanical properties of the 3D-printed material, an optimum has to be found. To keep pressures inside the actuator as low as possible, the piston base area was calculated (Appendix E) by using a gauge pressure of 0.1 bar, which corresponds with an input pressure of 1.1 bar. At this pressure, an output force of 0.3 N was chosen to comply with the minimum force as stated in Requirement 4. In case this is not high enough, the force can be increased by increasing the input air pressure. This results in an area of the piston base of 30 mm<sup>2</sup>. For the final dimensions for the piston base,  $R_{piston}$  is 7.6 mm and  $R_{fillet}$  is 0.3 mm.

##### 3.1.2 Adjustable Stroke Mechanism

To adjust the piston stroke, an internal stop, the piston stop, was designed. The piston stop fits into the piston housing and is limited from sliding out of the housing by the piston guidance (red in Figure 5). The piston stop limits the axial movement of the piston base, therefore also limiting the axial movement of the piston itself. For the smallest stroke, the piston stop is moved and attached at a position closest to the piston housing (negative x-direction), whereas for the largest stroke the piston stop is moved and attached at a position furthest from the





**Fig. 6:** Cross-section of the actuation unit. With the piston housing (1), the piston stop (2), the piston (3), the piston guidance (4), the piston tip (5), screws to attach the piston tip to the piston, and the needle segment (6), the inner part of the nose (7), and the outer part of the nose (8). In the upper right corner is the coordinate system used to describe motions.

piston housing (positive x-direction). The piston guidance, which can be seen in the exploded view of the actuation unit (Figure 8), contains three bars to attach the piston guidance to the piston housing. To lock the piston stop at the desired stroke, plastic screws are used. These screws go through an opening in the bars of the piston guidance part, into a screw thread in the piston stop. When untightened, the screws can slide through this opening. Then, when tightened, the screws lock the piston stop in place. The opening in the piston guidance part contains stripe markings next to it. These markings are spaced linearly with 1 mm in between so the stroke can be read carefully with a precision of 1 millimeter.

### 3.1.3 Needle Attachment

To easily attach and detach the needle segments to the actuation unit, an add-on tip for the piston was created (5 in Figures 6 and 8). The tip has one opening on each side, one for the piston bar, and one for the needle segment. It also contains two openings that contain screw thread. Screws are chosen as this allows easy assembly and makes it easy to attach and detach the piston tip from both the piston itself and the needle segments.

The total actuation unit consists of six of the previously described actuators. These actuators are radially spaced with inlet 2 (Figure 5) positioned laterally pointing in the negative x-direction, creating a circular overall shape of the actuation unit. Inlet 2 is positioned laterally so there is a possibility to add a lumen through the center of the actuation unit for a possible laser fiber implementation, as per Requirement 9. Figure 6 and Figure 8 show the cross-section, and the exploded view of the total actuation unit, respectively. The needle segments enter the actuation unit at the tip of the nose of the

actuation unit. The nose guides the needle segments from the larger diameter inside the actuation unit to a smaller diameter at the tip of the actuation unit. By means of an S-curve, this happens gradually and without buckling. The largest diameter of the actuation unit is that of the piston housing, with 34.2 mm. The total length of the actuation unit is 100.5 mm.

## 3.2 Final Layout

The final layout of the design consists of the actuation unit and the needle. To compare the designed actuation unit with the state-of-the-art wasp-inspired, self-propelling needles, a needle like the one from Scali [14] is used. The needle consists of six nickel-titanium (Nitinol) segments. The segments have a diameter of 0.25 mm to be in line with Requirement 10. The length of the segments is 250 mm, to have enough length to attach it to the actuation unit, support the needle, insert the needle in the tissue, and advance in the tissue. At the tip, the needle segments are held together by a shrinking tube. By attaching the shrinking tube to one needle segment, the needle segments are free to move independently, while the shrinking tube stays at the tip of the needle.

To connect the air tubes to the actuation unit, a set of pins was designed. Figure 7 shows one of these pins. These pins allow the air tubes to be placed over them on one side, while the other side fits in the piston housing. Both sides fit with a tight fit, allowing for easy reassembly, without the need to use glue in the prototype. For each of the holes in the actuation unit, one pin was used, resulting in a total of 12 pins. Figure 8 shows the exploded view of the final actuation unit design, excluding the pins.



Fig. 7: One of the 12 3D-printed pins that connect the actuation unit with the input air tubes coming from the control unit. A tube fits over one side (left in the Figure) and the other side (right in the Figure) fits in the actuation unit.

## 4 PROTOTYPE

### 4.1 Materials

Table 1 lists the parts and the material of the actuation unit and the needle. Given that the actuation unit and the needle should be MRI-compatible, the materials used must be nonferrous [34]. Figure 9 shows the created prototype of the actuation unit, which, excluding the screws and the support structure, is made out of one material, Formlabs Model V2 resin. The screws in the piston tips and the screws to lock the piston stop are from Toolcraft and are made from Polyamide [37]. To support the prototype during the measurements, a support structure for the prototype was designed. Figure 9 shows this transparent support structure, which is made from polylactic acid (PLA). To ensure safety during the measurements, a case for the prototype, also from PLA, was designed. This is to prevent parts from shooting away in the case of the prototype blowing apart. The lubricant used for the actuation unit, as previously discussed in Section 4.2.1, is a multi-purpose synthetic grease, with syncolon (PTFE) [38].

The needle consists of six needle segments made from Nitinol. The magnetic properties of Nitinol are comparable to those of pure titanium, meaning it is paramagnetic and thus MRI-compatible [39]. An advantage of using Nitinol under MRI guidance is that it is clearly visible on the images [39, 40]. The shrinking tube that holds the needle segments together was made from polyester, has an inner diameter of  $0.81 \pm 0.05$  mm, and has a wall thickness of  $0.013 \pm 0.002$  mm [41]. The glue used to glue one of the segments to the shrinking tube was made from ethyl cyanoacrylate, which is popular due to the low curing and because it can be used on a wide range of substrates [42]. To support the needle segments, two support tubes made out of PLA were used. Finally, another support structure to support the needle was designed. This support structure was also made out of PLA.

TABLE 1: List of parts and the material they are made of for the prototype of the actuation unit and the needle.

Part(s)	Material
<b>Actuation unit</b>	
Actuation unit, excluding screws	Formlabs dental model V2 resin
Screws for the actuation unit (Toolcraft)	Polyamide plastic
Support structure & prototype case	PLA
Lubricant (Superlube)	Synthetic, with syncolon (PTFE)
<b>Needle</b>	
Needle segments	Nitinol
Shrinking tube (Nordson Medical)	Polyester
Gold gel glue (Pattex)	ethyl cyanoacrylate
Rigid needle guide tube	PLA
Support structure	PLA

PLA, polylactic acid.

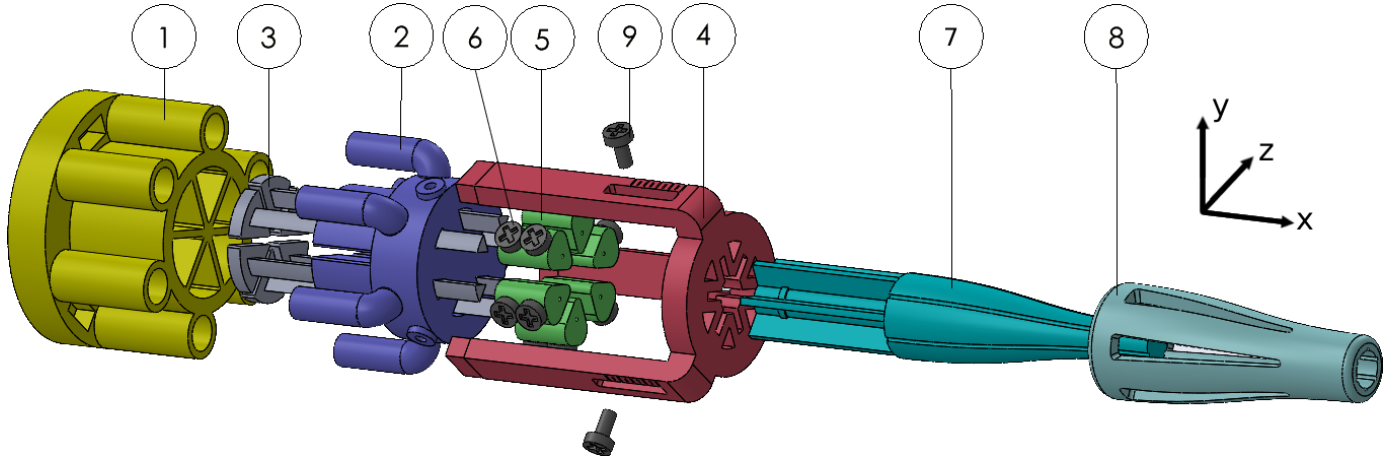
## 4.2 Manufacturing

### 4.2.1 Actuation Unit

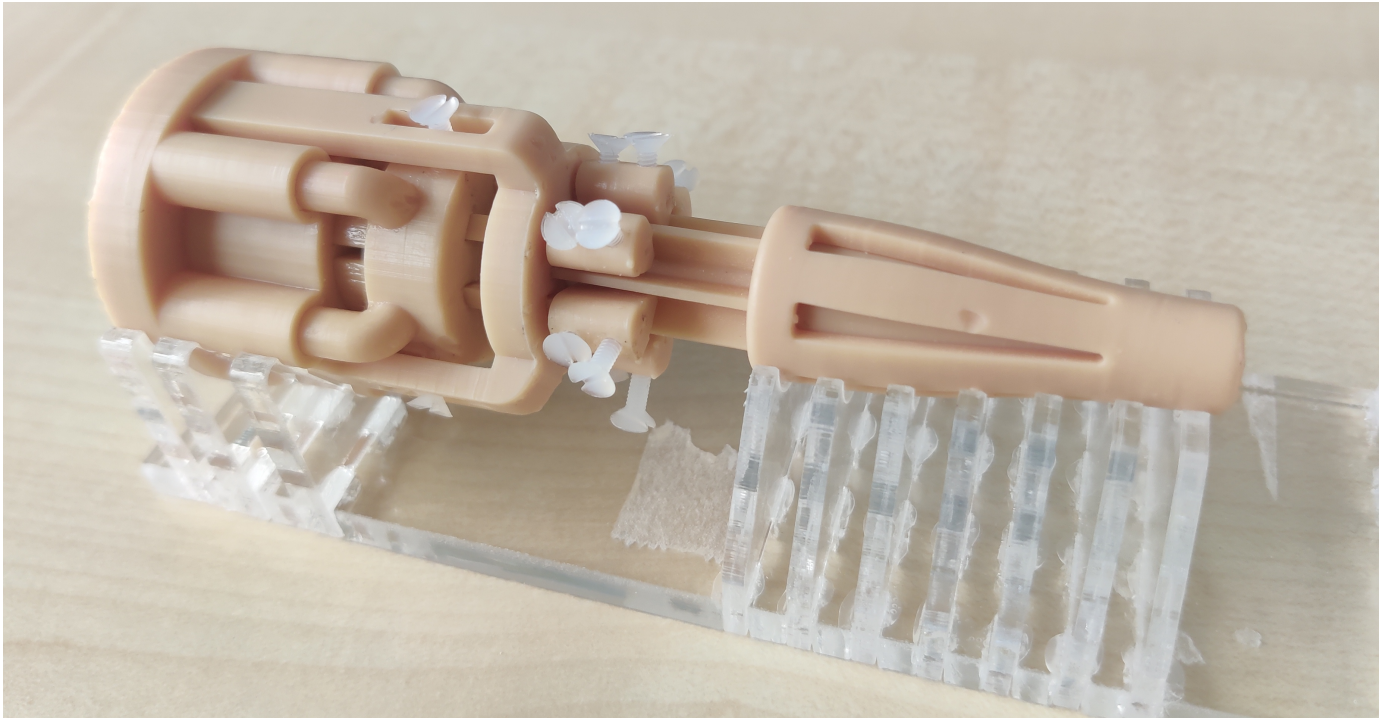
As discussed in Section 4.1, the prototype of the actuation unit, excluding the screws and the support structure, was made out of one material, Formlabs Model V2 resin. All these parts for the actuation unit were 3D printed with a stereolithography (SLA) printer (Form 3, Formlabs [43]). These types of printers use light-sensitive resins which are polymerized layer-by-layer during the printing. Although the materials available are limited, these printers are very accurate [44]. Figure 10 schematically shows the print process for printing with these types of printers. First, in Figure 10a the 3D model was created in Solidworks and prepared by loading it into the 3D printer software. During the preparation, the position of the model on the print bed is determined and support is added. Then, after uploading the model to the printer, the 3D printing of the model starts (Figure 10b). For SLA printers, the print bed moves upward while printing, while the resin stays stationary. Due to this print method, the model including support is printed upside down, hanging below the print bed. After the model is printed, the print bed can be detached and taken out of the printer. Now the print bed can be flipped vertically, placed on a work area, and the model can be removed. After removing the model from the print bed, the model contains excess fluid resin on it, which can be seen in Figure 11. To remove this excess resin, the model is washed in alcohol in the Formlabs washing station (Figure 10c) [45]. Finally, to maximize the material properties, the model is cured under 405 nm light in the Form Cure station (Figure 10d) [46]. At a number of stages of this process, the model can be adjusted if a certain function is required. By an iterative process of adjusting certain specifications at different steps in the process, guidelines were formed on how to approach such a 3D-printing process. In our case, the Form 3 by Formlabs [43] with model v2 resin [47] was used for all the prints. The next paragraphs discuss these guidelines.

### Model Design

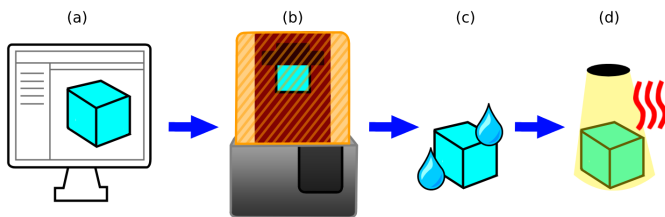
For moving parts, first, it is important to examine the



**Fig. 8:** Exploded view of the actuation unit. With the piston housing (1), the piston (3), the piston stop (2), screws to attach the piston tip to the piston and the needle segment (6), the piston tip (5), screws to lock the piston stop (9), the piston guidance (4), the inner part of the nose (7) and the outer part of the nose (8).



**Fig. 9:** Prototype of the actuation unit in its designed holder. The prototype, excluding screws and holder, was fully 3D printed.



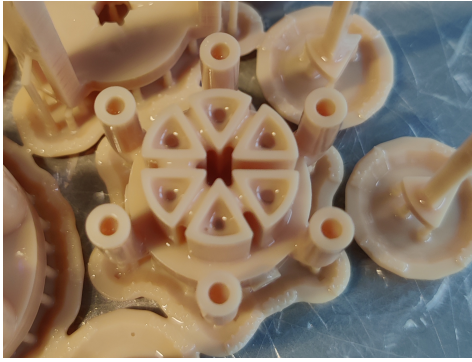
**Fig. 10:** Print process. (a): Creation and preparation of the 3D model, (b): printing of the model, (c): washing of the model, and (d): curing of the model

layering process of a 3D printer. A 3D printer builds the model layer by layer. Figure 12 shows this layering

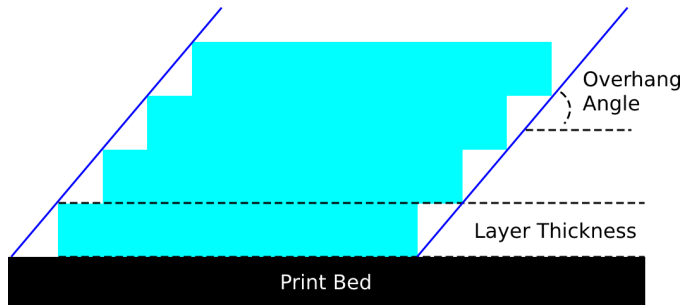
process. The part in light blue is the actual part, and the dark blue lines represent the desired profile of the part. Due to the layer thickness, the desired profile is not met. This is called the staircase effect. The lower the layer thickness, which is also called the print resolution, the more accurate the model [48, 49]. For our prints, the resolution was 25 microns, which was the lowest possible resolution for this printer.

This inaccuracy in printing means that when parts are required to move in or around other parts, the tolerance between the parts is of high importance. In addition to that, if the parts are also required to be airtight, an optimum tolerance that results in movable, airtight parts





**Fig. 11:** Piston stop with support after printing. The parts are still attached to the print bed. Excess resin can be seen in the openings of the piston stop.



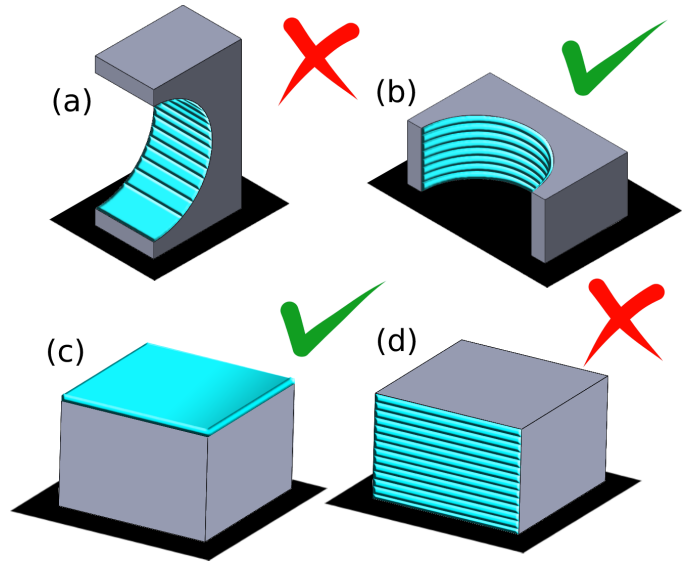
**Fig. 12:** Staircase effect when 3D printing a part (light blue) on the print bed (black). The dark blue lines represent the desired profile of the part. Due to the staircase effect, the desired profile is not printed correctly. Adjusted from [49].

should be found. In our case, as previously discussed, the moving parts all have one degree of freedom. This degree of freedom is a translation along one axis, the x-axis in Figures 6 and 8. It was found that for larger contact areas between moving parts, the tolerance needed was also larger. In our case, the tolerances are tested for a print area up to 34 mm<sup>2</sup>. In most places, the tolerance is 0.2 mm. Only for the piston base, which has the smallest contact area, the tolerance is 0.1 mm.

The nose of the actuation unit (parts 7 & 8 in Figures 6 and 8) was printed as two parts. The nose was split at the grooves where the needle segments slide through. When 3D printing with an SLA printer, sometimes clogging can occur. Clogging occurs when entrapped resin can not flow out of the channel where it is trapped before the next layer is printed. When the polymerization of the next layer happens, it is thought that this trapped resin also polymerizes, causing the channel to clog and thus not being printed correctly [50]. Although previous studies used a hive structure to prevent clogging while printing cable grooves [51], the current structure, with uninterrupted grooves, also proved to work, as all cable grooves were printed successfully.

### Print Layout

The print layout is the preparation of the model before



**Fig. 13:** Guidelines for the orientation with respect to the print bed (black) for 3D-printed parts with different sliding surfaces (light blue). (a & b): Parts with curved sliding surfaces. To prevent overhang, print the sliding surface perpendicular to the print bed. (c & d): Parts with straight sliding surfaces. For the best results print the sliding surface parallel to the print bed.

the model is printed (Figure 10a). At this step, the orientation of the model with respect to the printing bed is determined. The orientation of the part when printing is of a large influence on the tribology of the part [52]. In general, for straight sliding surfaces, printing parallel to the print bed results in the smoothest surfaces [52]. Hanon et al. [53] studied the friction when sliding two 3D-printed parts over each other. They found that sliding on the surface printed parallel to the print bed has a lower coefficient of friction than sliding on the surface printed perpendicular to the print bed.

However, one effect that should be considered for the orientation of the part is the previously mentioned staircase effect. Due to this effect, the roughness of the surfaces where this effect applies increases. When the overhang angle, the angle between the print bed and the desired profile (Figure 12), becomes less than 45 degrees, the roughness of this surface will be very high [49]. As it is wished to keep the roughness of the surface as low as possible, the print should be positioned in such a way as to prevent overhanging angles on the sliding surfaces as much as possible. A possible solution to minimize the roughness when the overhang angle becomes small is to add support to the model. However, when adding support to the model, the support has to be removed after the print, which also leaves roughness. Thus, it is recommended to not add support to sliding surfaces. Figure 13 depicts our guidelines for the part orientation with respect to the print bed (black) for 3D-printed parts with different sliding surfaces (light blue). When printing curved sliding surfaces (Figures 13a & 13b), the sliding surface should be printed perpendicular to the print bed. This way the overhang angle is always



**Fig. 14:** Two 3D-printed parts. On the left: the part after 3D printing, washing, and curing. The red arrow indicates where the 0.5 mm diameter hole was supposed to be. Due to clogging, only a small part of the hole was successfully printed. On the right: the same part after drilling the hole with a 0.5 mm drill.

90 degrees, resulting in the highest print accuracy. For straight sliding surfaces (Figures 13c & 13d), the sliding surface should be printed parallel to the print bed. This way the surface roughness is decreased as much as possible.

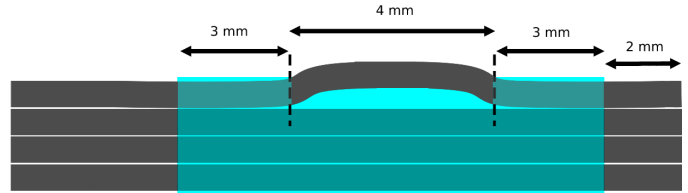
To summarize the main guidelines:

- Do not add support to sliding surfaces..
- Print sliding surfaces parallel to the print bed, unless it is a curved sliding surface. In that case print it perpendicular to the print bed, as in Figure 13.

### Post-Processing

After finishing the printing process, the post-printing process starts. First, the model was washed with the Form washing unit in Isopropanol 99% on the recommended settings. For our resin, this was ten minutes. Sometimes, after the washing cycle, in small openings, not all resin was removed. This was removed manually by squirting Isopropanol 99% through these openings with a syringe. After washing the model, the model was cured. Curing the model maximizes the material properties [46], but it also makes the model more brittle. We found that when screw thread is required at potentially breakable places, it is better to tap it before the curing process. Another interesting finding was that sometimes when printing the same part, some prints fitted better in the same housing than others. This is because there are a lot of factors that influence the reproducibility of a 3D print [54]. Some examples of these factors are print layout [55], machine accuracy, and post-processing accuracy [54]. Another observation was that small holes (tested up to a 0.5-millimeter diameter) were not printed correctly. This is due to the previously described clogging effect. These holes were drilled with a 0.5 mm drill after the print was cured. Figure 14 shows the part before (left) and after drilling (right).

To fill the spaces between moving parts and to make the actuation unit as airtight as possible, a synthetic grease lubricant (Super Lube) was used. First, the



**Fig. 15:** Needle tip with the shrinking tube (light blue) and needle segments (grey). In this configuration, where no needle segments are moved relatively from each other, all segments have a 2 mm distance between the tip and the shrinking tube. One segment is zig-zagged between the cuts in the shrinking tube which are shown with a dashed line.

lubricant was lightly attached to the model. To move the piston with the model lightly lubricated, a large amount of air was needed. The piston moved relatively easily. After attaching a thick layer of the lubricant to the model, it was observed that the model was more airtight and a lower amount of air could move the piston. Another thing noted was that the air could be added more slowly, with the pressure building up inside the actuator. Thus, the conclusion was that a thick layer of lubricant is beneficial to maximize air tightness.

To summarize the main guidelines:

- Check for excess resin after washing the model. Remove this manually with a syringe with washing Isopropanol before curing.
- When tapping thread at potentially breakable places, tap before curing the model.
- When needed, use sanding to fit the printed parts properly. Due to inaccuracies in the printing, not every print is the same. It was found that some of the same parts fitted better than others in the same openings.
- Small holes (tested for 0.5 mm diameter) require additional drilling after the print is finished.
- For moving parts that require airtightness, use a thick layer of lubricant to fill up the tolerances between these moving parts to make it as airtight as possible.

### 4.2.2 Needle

To compare the experimental results of the actuation unit with the state-of-the-art, a similar needle design as Scali [14] was created. Six needle segments of 0.25 mm were used. For the manufacturing of the needle tip, first, six needle segments of equal length were cut from one longer Nitinol wire. After this, four needle segments were put through the 10-mm-long shrinking tube. Then, by using a sharp knife the shrinking tube was cut open in two places, as schematically shown in Figure 15. The cuts were made 3 mm from the edges of the shrinking tube, leaving 4 mm in between the cuts. A fifth segment was then put through the cuts and the opening of the shrinking tube in a zig-zag pattern. The tip of this fifth needle segment was positioned so that there was a 2 mm

space between the tip and the shrinking tube. Next, the sixth segment was put through the shrinking tube. By using the previously mentioned gold gel glue, the zig-zag positioned segment was glued to the shrinking tube with a drop of glue. While the glue dried out, the five other, non-glued, segments were moved to make sure they did not also get glued to the shrinking tube.

### 4.2.3 Control Unit

The control unit is the unit that controls the air pressure of the system and the airflow for the inlets of the actuation unit. Appendix K contains the full list of components used for the control unit. To regulate the pressure of the system, a pressure regulator was attached after the air supply, which is a single air inlet. To digitally measure this pressure, right after the pressure regulator, a T-connector connects a digital pressure sensor with the airflow that goes through the system. By using a valve system, the single air inlet was divided over the six actuators. Each actuator was connected to one electrically controlled, magnetically switched, mono-stable 5/2-way valve from Festo [36]. A 5/2-way valve has two outputs. When no signal is sent to the valve, air flows through the first output. Then, while applying an electrical signal, the air flows through the second output. After the signal is stopped the air flows through the first output [56]. The first output was connected to the inlet of the actuator that moves the piston back (inlet 2 in Figure 5). So, when no electrical signal was sent to the valves, the piston was pushed backward (negative x-direction in Figures 6 and 8). The valve system consisted of six valves together with a valve manifold. The automated control of the valves was done via an Arduino One microcontroller. The Arduino code is given in Appendix F. To power the valves, the valves were connected to a 24V power supply. The power supply and the microcontroller were both connected to transistors to regulate the power when switching the valves on and off. Since the control unit contains ferrous materials and the tubes can be of sufficient length, the actuation unit was located outside of the MRI scanner. For safety precautions, the control unit should also be placed in a fixed structure to prevent it from being accelerated toward the magnet [34].

## 5 EVALUATION

### 5.1 Goal

The experiments' primary goal was to investigate the performance behavior of the needle actuated by the actuation unit for different stroke lengths and different piston interval times. To evaluate the performance behavior, the slip of the needle with respect to phantom tissue was used as the performance measure. The slip ratio gives insight into the amount of slip of the needle segments while the needle advances through the tissue and is given by the following formula:

$$SR = 1 - d_{\text{measured}}/d_{\text{theoretical}} \quad (4)$$

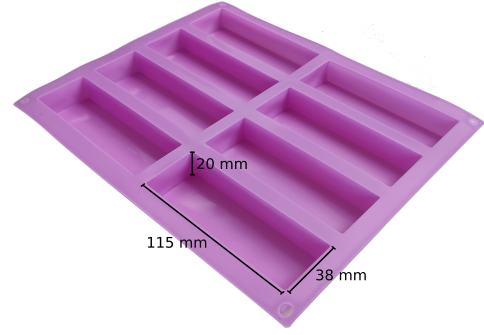


Fig. 16: Mold that was used to make the gelatin samples. The mold contains a total of eight sections, for which the dimensions are given. Per mold, eight gelatin samples were created.

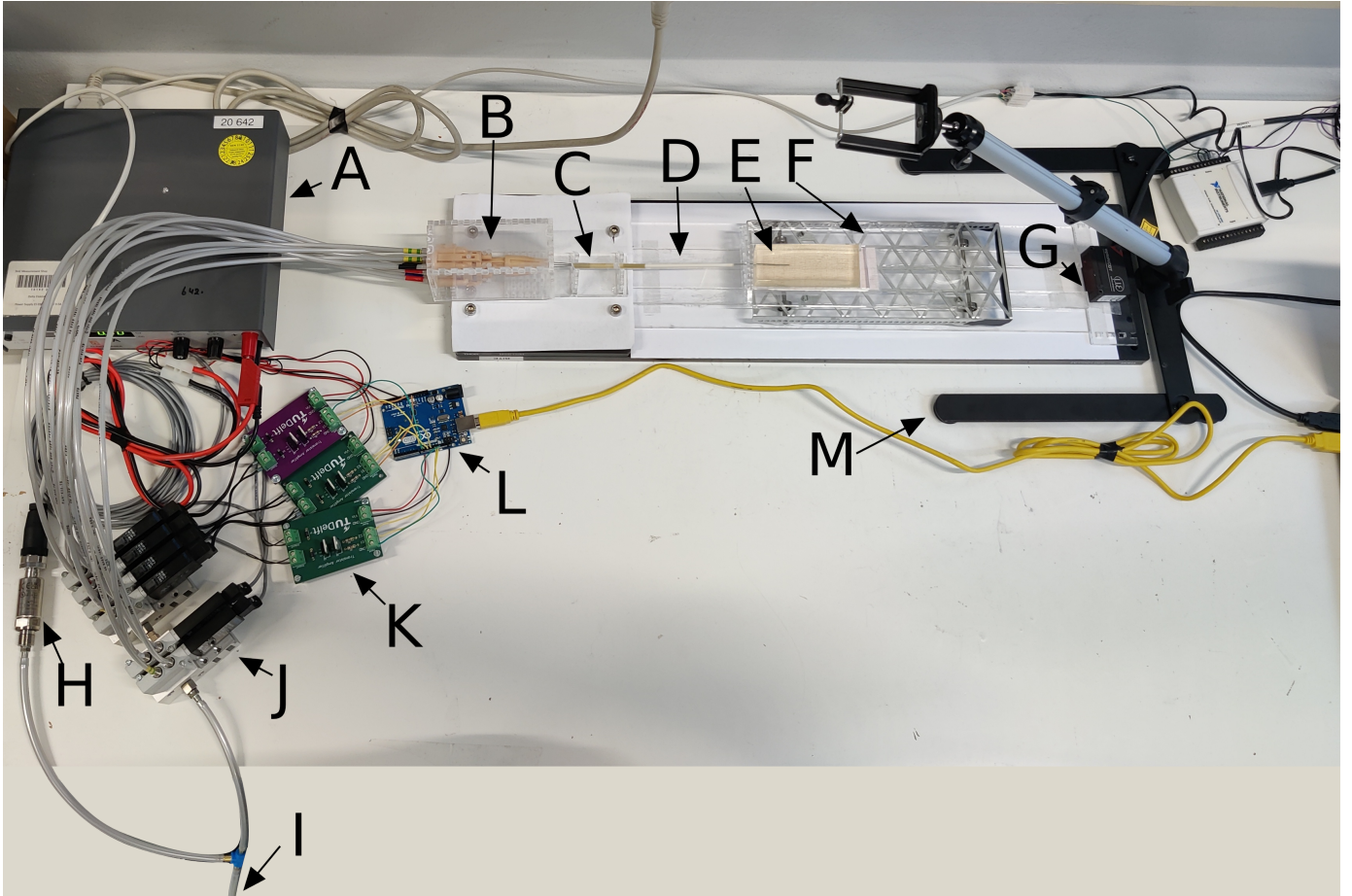
where  $SR$  is the slip ratio,  $d_{\text{measured}}$  is the measured distance that the needle travels, and  $d_{\text{theoretical}}$  is the theoretical distance that the needle travels. Meaning that for one actuation cycle,  $d_{\text{theoretical}}$  is equal to the stroke.

### 5.2 Experimental Setup

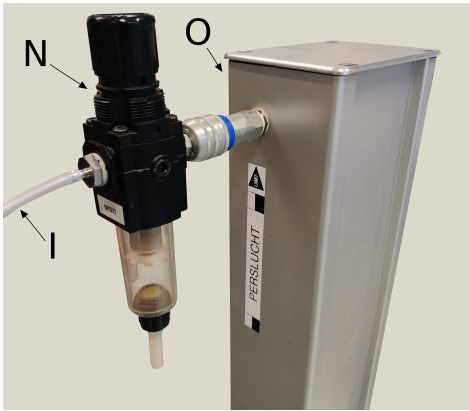
To mimic tissue, and to compare results with previous studies [14, 15], gelatin was used for needle insertion for both measurements. For each measurement, a new gelatin phantom was created. Gelatin powder (Dr. Oetker) was used to create phantoms of 10 wt% gelatin. The powder was added to boiling water, whereafter it was carefully stirred. After the gelatin powder was dissolved, the mixture was added to a flexible silicone mold. The mold contains eight sections, all of the same size. Figure 16 depicts this mold, including the dimensions of one of the eight sections. After filling each mold with the gelatin mixture, the molds were put in a refrigerator overnight at 5 degrees Celsius. After the cooling process, the gelatin was carefully taken out of the mold by folding the mold. Then, one side of the gelatin was cut to get a final dimension of 100x38x20 mm. The weight was kept constant at 62.53 g, with a standard deviation of 4.22 g.

Figure 17 shows the full experimental setup, excluding the pressure regulator. The pressure regulator can be seen in Figure 18. The input air came from the air supply (O). The pressure regulator (N) was connected to the experimental setup via a tube (I). A T-connector was used to split the air coming from the pressure regulator into two ways: one going to the pressure sensor (H), and one going to the valves (J). The valves were powered by a power supply (A), via transistors (K). To control the valves, an Arduino microcontroller (L) was used. The actuation unit (B) was surrounded by a protective housing and attached to the needle. Instead of moving the needle toward the gelatin, the gelatin was placed on a low-friction cart (F) and moved toward the actuation unit over rails from PLA (D). The actuation unit was fixed to the base of the test setup, at the end of the rails. The self-propelling mechanism works if the needle advances through the gelatin, resulting in the gelatin moving to-





**Fig. 17:** Experimental setup. With power supply (A), actuation unit in its designed protective case (B), guidance tubes that support the needle (C), rails (D), gelatin (E), gelatin cart (F), laser sensor (G), pressure sensor (H), air tube that comes from the pressure regulator (I), valves (J), transistor plates (K), Arduino microcontroller (L), and camera stand (M).



**Fig. 18:** Pressure regulator (N), which is connected to the experimental setup via a tube (I). The pressure regulator regulates the pressure coming from the air supply (O).

ward the actuation unit. This is the same approach as Scali [14] and Pusch [15].

The needle goes through two guidance tubes of different diameters (C). One guidance tube is slightly larger than the other tube, making it possible for the tubes to slide over each other. This makes it possible to support

the full length of the needle during the measurements. When the cart moves toward the actuation unit, it pushes the tubes over each other like a telescopic tube. The cart contains four ball bearings used to move the cart with low friction. The base of the cart is an aluminum plate (220x90 mm). On that base, a printed plate (PLA) with a 40x100 mm opening was fixed. At the base of the cart, at the location of the opening, a laminated millimeter sheath was attached. The gelatin (E) was placed into the opening of the printed plate, on the laminated millimeter sheath. At one side of the cart, a part created for needle support and guidance, also from PLA, was attached. This part contains a hole which the needle can be inserted through. To record the measurements with a cellphone, a camera stand (M) was used. The linear laser displacement sensor (optoNCDT) (G) to record the position of the gelatin cart was attached to the rails by using double-sided tape.

Because the needle works based on a friction difference between the non-advancing and the advancing wires, this friction difference should be high enough for the self-propelling mechanism to work. To make sure that the friction forces become high enough, the needle was inserted into the tissue at a certain distance. At this

distance, the friction forces become high enough for the self-propelling mechanism to work. Scali [14] describes that an insertion depth of 25 mm is sufficient for the system to work. However, after trying the insertion depth of 50 mm it was found that for this insertion depth the slip is constant from the beginning of the measurements. As it is wished to use as less gelatin as possible, for our measurements, an initial insertion depth of 35 mm was chosen.

### 5.3 Experimental Procedure

The experimental procedure for each of the individual measurements per condition was as follows:

- 1) Take the gelatin out of the mold and cut it to the correct size.
- 2) Measure the weight of the gelatin.
- 3) Add the prototype to the experimental setup and the needle through the tubes.
- 4) Insert the needle 35 mm in the gelatin.
- 5) Extend the guidance tubes so that they cover the full length of the needle outside the gelatin.
- 6) Cover the prototype with the protective case.
- 7) Record with the cellphone camera.
- 8) Record the data with Labview.
- 9) Make sure safety glasses are on.
- 10) Start the measurements of a random condition from the experiment by starting the Arduino script.
- 11) The actuation unit runs for 30 cycles.
- 12) Stop the cellphone camera and the Labview recordings.
- 13) Remove the needle from the gelatin.
- 14) Take the prototype out of the experimental setup and clean the needle with water and alcohol.

#### 5.3.1 Functionality test

The goal of the functionality test was to test for what working pressure the actuation unit was able to execute all desired piston movements, and if the self-propelling mechanism of the needle works. For each measurement, the actuation unit was programmed to perform 30 cycles. For these measurements, the independent variables are the pressure and the stroke. The control variables are the interval time and the number of cycles. The initial working pressure was slightly increased before each measurement until an optimal pressure was found for strokes of 2, 4, 6, 8, and 10 mm. We defined the optimal working pressure as the pressure at which all six pistons could move over all specified strokes (i.e., 2, 4, 6, 8, 10 mm) for three consecutive measurements. It was found that for strokes up to 4 mm, the actuation unit was functional (i.e., all pistons could move over the stroke) for a working pressure of 0.5 bar. For strokes of 6, 8, and 10 mm, the system was not functional up to a pressure of 1.5 bar. For 1.5 bar, with a 6 mm stroke, the system showed some functionality, but not all pistons were able to execute the full backward motion. After the

TABLE 2: Conditions for Experiment 1.

Condition	Stroke (mm)	Pressure (bar)	Interval time (s)	Number of cycles	Number of repetitions
s2-p05-i05	2	0.5	0.5	30	10
s4-p05-i05	4	0.5	0.5	30	10
s6-p05-i05	6	0.5	0.5	30	4*
s8-p05-i05	8	0.5	0.5	30	4*
s10-p05-i05	10	0.5	0.5	30	4*

\*: fewer repetitions due to the actuation unit not being functional for these strokes at this pressure.

TABLE 3: Conditions for Experiment 2.

Condition	Stroke (mm)	Pressure (bar)	Interval time (s)	Number of cycles	Number of repetitions
s4-p05-i05	4	0.5	0.5	30	10
s4-p05-i03	4	0.5	0.3	30	10
s4-p05-i01	4	0.5	0.1	30	10

third measurement at a pressure of 1.5 bar, one piston broke, meaning the maximum working pressure was exceeded and an optimal working pressure that works for all specified strokes of the current prototype does not exist. Therefore, we decided to set the working pressure at 0.5 bar for Experiments 1 and 2.

#### 5.3.2 Experiment 1: Variable Stroke

The goal of the first experiment was to investigate the performance behavior of the actuation unit for different strokes in terms of the slip of the needle with respect to the gelatin. The independent variable is the stroke. The dependent variable is the position of the cart, which was used to calculate the slip ratio. The control variables are the pressure, which was 0.5 bar at the start of each measurement, the interval time between the pistons, which was 0.5 seconds, and the number of cycles, which was set to 30. Table 2 contains the conditions that were tested for Experiment 1. The first two conditions were tested ten times. The conditions with a stroke equal to or larger than 6 mm were tested four times. Since, as described in Section 5.3.1, with a pressure of 0.5 bar, the actuation unit proved not to be functional for strokes 6, 8, and 10 mm.

#### 5.3.3 Experiment 2: Variable Interval Time

The goal of the second experiment was to investigate the performance behavior of the actuation unit for different time intervals between the piston movements in terms of the slip of the needle with respect to the gelatin. The independent variable is the time interval between the piston movements. The dependent variable is the position of the cart, which was used to calculate the slip ratio. The control variables are the stroke, the pressure, and the number of cycles. Table 3 contains the conditions for Experiment 2. Condition s4-p05-i05 was already tested ten times in Experiment 1, and thus, it was not repeated for the measurements of Experiment 2.

#### 5.3.4 Data Analysis

For both experiments, the data from the laser sensor and the pressure sensor was collected via Labview 2014 and exported to Excel. The data was then loaded into



Matlab R2019b and processed (Appendix I). By plotting the pressure and position data against the time, the first plots were created. Then, the slip ratio per cycle was calculated by first smoothing the position data by using a Savitzky-Golay filter. Whereafter each cycle was determined by first detecting the peaks of the signal with the findpeaks function of Matlab. The peaks in the position data indicate the start of a cycle. To find the  $d_{measured}$  for each cycle, the difference in position between peaks was calculated by using the following formula:

$$d_{measured,j} = x_{j+1} - x_j \quad (5)$$

where  $d_{measured,j}$  is the measured distance traveled for  $j$ th cycle,  $x_{j+1}$  is the position at the end of that cycle, and  $x_j$  is the position at the start of that cycle. Finally, to calculate the slip, Equation 4 was used.

To test if the data meets the parametric assumptions, first, a histogram was plotted (Appendix H), since this is the easiest way to visually observe if the data is normally distributed [57]. It was observed that the data is skewed, and thus a number of normality tests were conducted. The tests were conducted by using the Matlab function from Öner & Deveci Kocakoc [58]. The function contains ten different normality tests. The four conditions used to calculate the slip ratio per cycle were tested first. The data for all four conditions proved to be not normally distributed for all ten normality tests. This means that the parametric assumptions are not met, and thus nonparametric statistic tests were used (Appendix J). To examine if there were significant differences between the data from the conditions for Experiment 1, a Wilcoxon signed-rank test was conducted. Note that this is conducted for conditions s2-p05-i05 and s4-p05-i05, because the other conditions of Experiment 1 did not lead to position data. To statistically compare the data from Experiment 2, a Friedman test was conducted. To further examine the differences between the data, three Wilcoxon signed-rank tests were conducted.

For the pressure data of Experiment 1, it was observed that there is a difference in pressure between the start of the cycle and the moment when all valves were activated. To calculate the maximum differences in pressure per cycle, first, the data was smoothed with a Savitzky-Golay filter. Then by using the findpeaks function of Matlab, the peaks and the valleys were located. Then the following formula was used:

$$dP_j = P_{peak,j} - P_{valley,j} \quad (6)$$

Where  $dP_j$  is the pressure difference for  $j$ th cycle,  $P_{peak,j}$  is the pressure at the peak of that cycle, and  $P_{valley,j}$  is the pressure at the valley of that cycle. To test if these pressure differences were significantly different for the different strokes, statistical analyses were conducted. In the same way as the slip ratio data, the data was first tested if it meets the parametric assumptions. Although the pressure data for some of the conditions is fully normally distributed according to the ten tests,

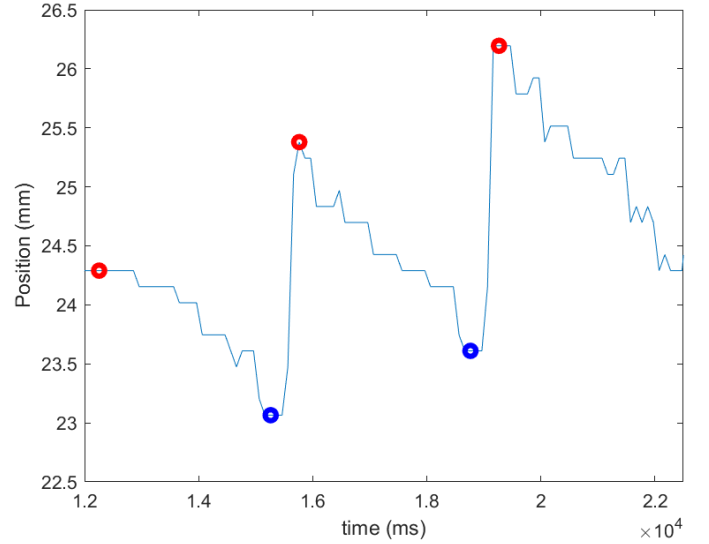


Fig. 19: Plot of the raw data of the position of the cart [mm] vs. time of the experiment [ms] for an s4-p05-i05 measurement. The position is the position of the gelatin cart with respect to the laser sensor. The red markings indicate the start of the cycles, and the blue markings indicate the moment when all six valves were activated, meaning all six pistons were moved forward. The plotted data between two red markings corresponds to a single cycle. The plotted data between a blue and a red marking is the moment when all six pistons were pulled backward.

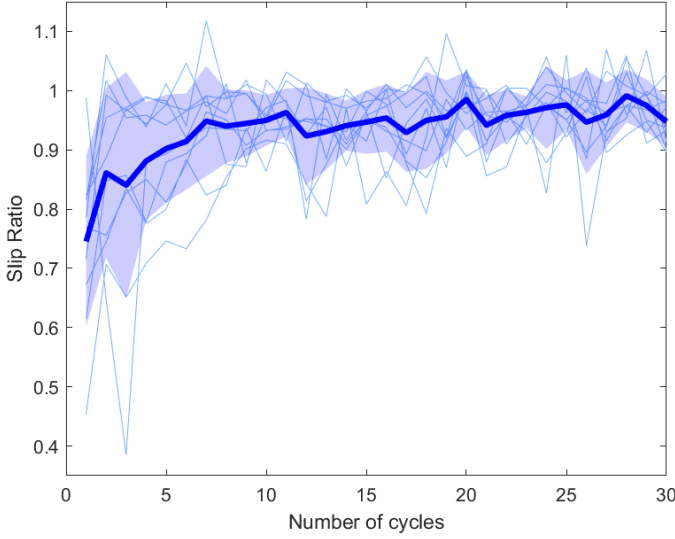
the pressure data for other conditions proved to be not normally distributed. It was chosen to use the same approach as for the slip ratio. After conducting a Friedman test, Wilcoxon signed-rank tests were conducted to show differences between condition pairs. To examine the differences between the groups with a different sample size due to fewer measurements, a Wilcoxon rank-sum test was conducted. For all statistical analyses, the value for statistical significance,  $\alpha$ , was chosen to be less than 0.05.

## 5.4 Experimental Results

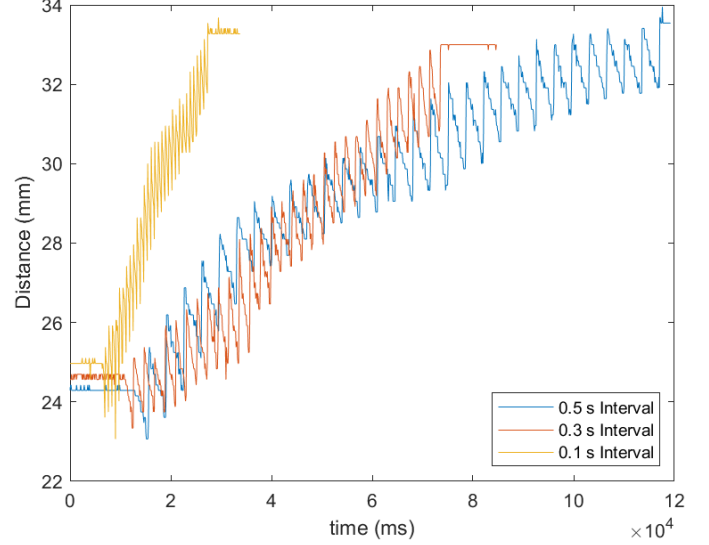
### 5.4.1 Experiment 1: Variable Stroke

The raw data of the position of the cart [mm] vs. time of the experiment [ms] for two cycles of one measurement from the s4-p05-i05 condition is shown in Figure 19. The raw data shows that for each piston moving forward, the cart moves backward (away from the actuation unit). Theoretically, if no slip occurs, the position change of the cart, and thus of the needle with respect to the gelatin for one cycle will be equivalent to the stroke. However, due to slip of the needle with respect to the gelatin, in practice, this is less. Figure 20 shows the slip ratio per cycle for each cycle for the s4-p05-i05 measurements. One thing to note is that sometimes, a slip ratio larger than 1 was measured. In that case, the cart moved away from the actuation unit during the cycle. An observation for the slip ratio data is that the slip ratio was generally lower in the first few cycles.

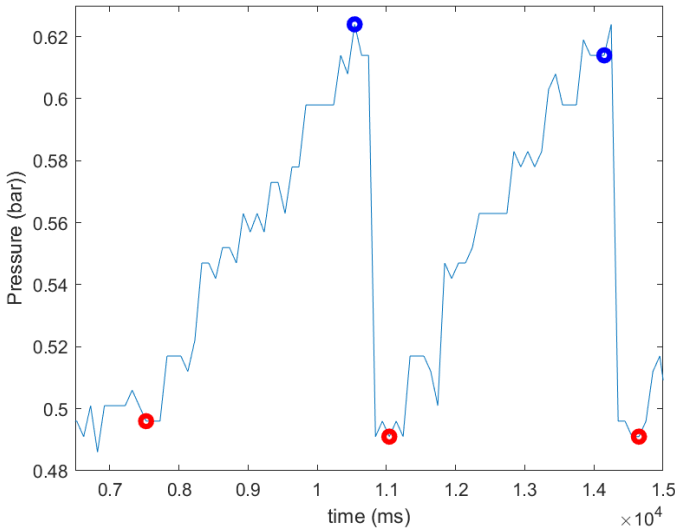
Table 4 shows the means and standard deviation for the slip ratio and pressure difference per cycle, for all conditions. For conditions s2-p05-i05 and s4-p05-i05,



**Fig. 20:** Plot of the slip ratio per cycle vs. the number of cycles for the s4-p05-i05 measurements. The light blue lines represent the data from each of the ten measurements, the thick blue line represents the mean of the ten measurements, and the blue shaded area represents the standard deviation.



**Fig. 22:** Plot of the raw data of the position of the cart [mm] vs. time [ms] for one measurement of each of the conditions for Experiment 2. The blue line represents one measurement for the s4-p05-i05 condition, the orange line represents one measurement for the s4-p05-i03 condition, and the yellow line represents one measurement for the s4-p05-i01 condition.



**Fig. 21:** Plot of the raw data of the pressure in the system [bar] vs. time of the experiment [ms] for an s4-p05-i05 measurement for two cycles. The red markings indicate the start of the cycles, and the blue markings indicate the moment when all six valves were activated, meaning all six pistons were moved forward. The period between two red markings is a cycle.

**TABLE 4:** Results of Experiment 1 and 2. List of the means and standard deviation for the stroke and pressure difference per cycle, for all conditions.

Condition	Mean slip ratio (mm)	Mean pressure difference per cycle (bar)
s2-p05-i05	0.926±0.123	0.111±4.3e-3
s4-p05-i05	0.935±0.089	0.108±3.6e-3
s6-p05-i05	*	0.116±5.6e-3
s8-p05-i05	*	0.092±7.6e-3
s10-p05-i05	*	0.070±3.1e-3
s4-p05-i03	0.912±0.081	*
s4-p05-i01	0.955±0.049	*

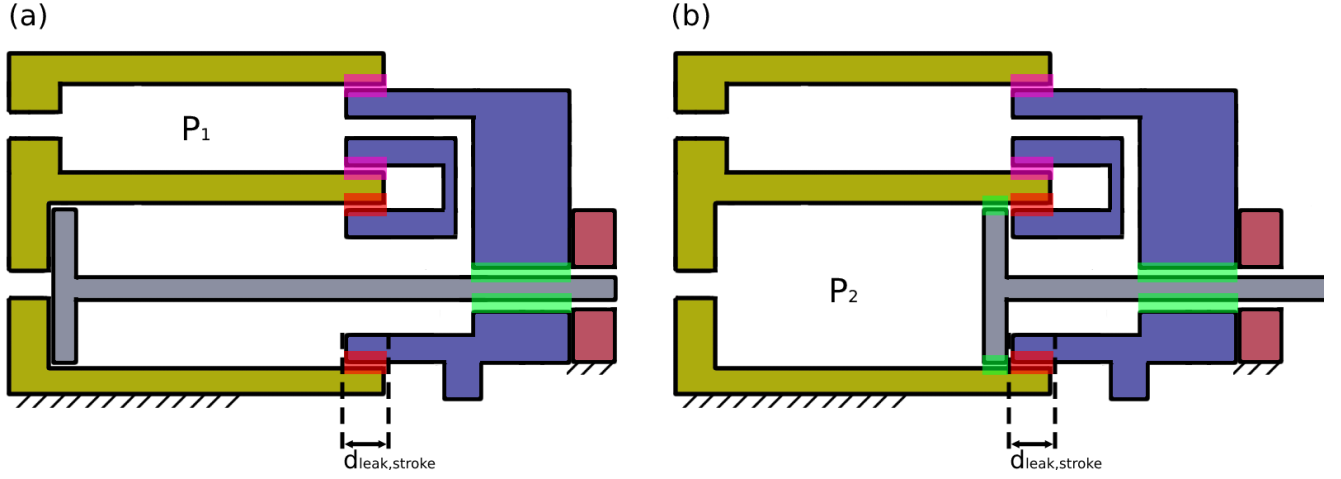
\*: no data available

the means and standard deviations are  $0.926 \pm 0.123$  and  $0.935 \pm 0.089$ , respectively. A Wilcoxon signed rank test showed that there is no significant difference between both conditions ( $z = -0.662$ ,  $p = 0.508$ ). An interesting result that came from the data of the pressure sensor was that during the measurements, the pressure was not constant. Figure 21 depicts the raw time vs. pressure data for two cycles from one of the s4-p05-i05 measurements. Initially, the pressure was set to approximately 0.5 bar. After starting the Arduino script, each time a valve switched on, the pressure built up. In the case of this specific s4-p05-i05 measurement, it led to a maximum pressure of approximately 0.62 bar.

After conducting a statistical analysis on the data of pressure differences per cycle, it was found that all means are significantly different. An interesting result was that for the condition with the largest stroke (s10-p05-i05), the mean pressure difference per cycle is significantly lower than the means of the other conditions. Besides this, the mean pressure difference per cycle for the condition with the second largest stroke is also significantly lower than those of the conditions with a smaller stroke (s2-p05-i05, s4-p05-i05, and s6-p05-i05).

#### 5.4.2 Experiment 2: Variable Interval Time

Figure 22 contains the unfiltered data for one measurement of each of the conditions for Experiment 2. The mean and standard deviation for the slip ratio for conditions s4-p05-i05, s4-p05-i03, and s4-p05-i01 are  $0.935 \pm 0.089$ ,  $0.912 \pm 0.081$ , and  $0.955 \pm 0.049$ , respectively. A Friedman test ( $p = 1.588e-10$ ) showed that there are at least two conditions with significant differences from each other. Further examination with a Wilcoxon signed



**Fig. 23:** Actuator design with the places of air leakage marked. With (a): Moment after the backward motion, when the chamber is pressurized with pressure  $P_1$ , and (b): Moment after the forward motion, when the chamber is pressurized with pressure  $P_2$ . The places marked with a green square are thought to have constant air leakage. Note that when the chamber is pressurized by  $P_2$ , the piston forms an extra barrier before the air can leak. The places marked with red and purple are the places of variable air leakage, depending on the position of the piston stop (blue). distance  $d_{\text{leak,stroke}}$  is the distance that the piston stop overlaps the piston housing (yellow).

rank test showed that condition s4-p05-i01 has significant differences from both condition s4-p05-i05 ( $z = -2.905$ ,  $p = 0.37\text{e-}3$ ) and s4-p05-i03 ( $z = -8.230$ ,  $p = 1.881\text{e-}16$ ). Conditions s4-p05-i05 and s4-p05-i03 also proved to be statistically different ( $z = 3.59$ ,  $p = 3.294\text{e-}4$ ).

## 6 DISCUSSION

### 6.1 Main Findings

In this work, we created a prototype for an MRI-compatible actuation unit for a self-propelling needle. The results of this study show that the locking mechanism for the piston stop worked, because it stayed in position during the experiments, even during the ones with increased air pressure up to 1.5 bar. The production cost of the prototype of the actuation unit is relatively low because almost every part of the prototype was 3D printed. However, the current control unit is expensive due to the valves being expensive (£124,78 per valve). Appendix K contains a full list of the costs for the parts of the control unit. The total costs were within the range to fulfill Requirement 13. The largest diameter of our actuation unit is 34.2 mm, and the length of our actuation unit is 100 mm, making it a handheld device. The weight of our prototype of the actuation unit, including the pins for tube attachment, is 31 g. The dimensions and the weight fulfill Requirements 8 and 14. All desired requirements regarding the design of the system were fulfilled.

After testing the prototype, it was found that the prototype was not functional at larger strokes (i.e., 6, 8, and 10 mm). Although at 6 mm it showed some functionality, it did not perform all desired movements. This means that for this test setup, Requirement 1, regarding the adjustable stroke, is not fully met. For smaller strokes (i.e., 2 mm and 4 mm), it was found that the actuation unit was functional for a working (gauge) pressure of

0.5 bar. For lower working pressures (i.e., 0.2 bar), it was found that the forward motion of the pistons was possible, however, the backward motion was only achieved for a working pressure of 0.5 bar. For the larger strokes (i.e., 6, 8, and 10 mm), the results of this study show that for lower working pressures (i.e., 0.5 bar) the forward motion was possible, but the backward motion was not. This indicates that the forces during the forward motion were high enough to overcome the cutting and friction forces on the needle segments. Compared to previous work done by Scali [14], the measured mean slip ratio from our measurements is high. Scali [14] researched the slip ratio for the needle advancing through gelatin of 5 wt%, whereafter it entered another layer of 10 wt% gelatin. The tissue was placed on the same cart as our experiments, but only the box to hold the tissue was different. For six segments of 0.25 mm diameter, with a stroke of 4 mm, and an insertion speed of 2 mm/s, she found that the mean slip ratio when the needle entered the 10 wt% gelatin layer was 0.3. The mean slip ratio of our experiments with a 4 mm stroke and a 0.5 s piston interval (condition s4-p05-i05) is 0.935. Although during the testing Requirement 1 was not fully met, and the slip ratio was high, the prototype still proved to be functional (i.e., the needle could self-propel through the gelatin) and thus is considered a successful prototype.

### 6.2 Limitations and Recommendations

#### 6.2.1 Prototype

The main difference between the prototype and ideal design is the air-tightness. Due to the limitations of 3D printing, as discussed in Section 4.2, a completely airtight design is not possible. Figure 23 depicts the places in a single actuator, for two piston positions, where air leakage occurs. It was observed that the pressure during the measurements increased with each piston moving

forward. Initially, when the pressure was set at 0.5 bar, all pistons were in a backward position (Figure 23a). Then, when the pistons were moved forward (Figure 23b) the pressure measured by the pressure sensor increased. A reason for this could be that when the piston was in a backward position, it is hypothesized that air leakage occurred in a greater number of places than when the piston was in the forward position because the volume under pressure existed within multiple (moving) parts. This is why we believe that the places marked with pink leaked more air when pressure  $P_1$  was applied, compared to when pressure  $P_2$  was applied. Besides this, when pressure  $P_2$  was applied, the piston itself was placed in such a way that it formed another barrier for the air to escape.

Furthermore, for larger strokes, the pressure differences per cycle were found to be statistically lower. This could mean that for larger strokes, more air leakage occurred. Distance  $d_{\text{leak,stroke}}$  is the distance that the piston stop overlaps the piston housing. It is hypothesized that for small  $d_{\text{leak,stroke}}$ , and thus for large strokes, the air leakage is high because if the overlap is small, the chance of a good seal between the surfaces reduces. For smaller strokes,  $d_{\text{leak,stroke}}$  increases, resulting in a better chance of a good seal between the surfaces. Thus, for the least air leakage with the current prototype, it is recommended to keep the stroke sufficiently small (i.e., under 4 mm).

No needle buckling happened inside the prototype due to the sufficiently small unsupported needle length, fulfilling Requirement 11. Buckling only happened where the needle came out of the prototype before entering the first guidance tube since here the unsupported needle length was larger than 10 mm. Figure 24 depicts the moment that the segment indicated with the red arrow was pushed forward and buckled. This was observed during the measurements of Experiment 2, it only happened to the segment that was attached to the shrinking tube, and was only observed a few times in all the measurements. To reduce buckling as much as possible, it is recommended to use tubes to cover the full length of the needle that is not in the tissue.

The actuation unit failed after a few measurements with high working pressure because one of the pistons broke. One could argue that this is a failure, and thus, to make the pistons more resistant to high working pressures. On the other hand, if the piston is the first part to fail, the actuation unit fails in a relatively safe way. This failure method will do no harm to the patient and surgeon because there will be no parts shooting away. Besides this, it is easily visible to the surgeon that the part has failed, since the part is visible from the outside. Thus, for the current actuation unit to be functional with less chance of failure, it is recommended to operate at lower pressures (i.e., 0.5 bar).

### 6.2.2 Experiment

A reason for the high slip ratio could be the influence of friction in the test setup. In our experiments, the friction

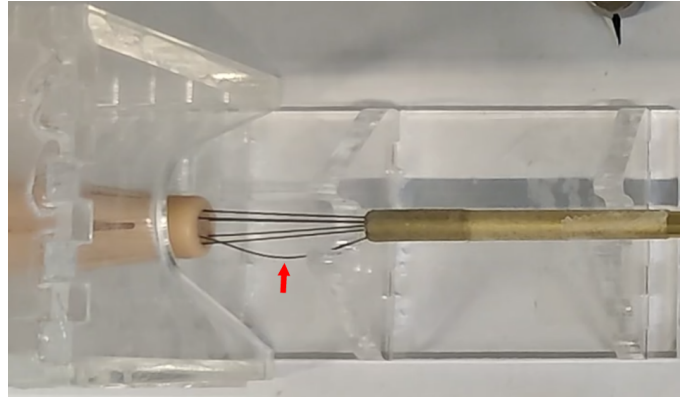


Fig. 24: Nose of the actuation unit, the needle, and the first guidance tube, at the moment that the segment indicated with the red arrow was pushed forward and buckled. This figure was taken from video footage of a measurement of the s4-p05-i03 condition.

between the cart and the rails was high. For the cart to be pulled toward the actuation unit, the pulling force on the cart, exerted by the needle, had to overcome the friction force between the cart and the rails. If the needle advanced through the tissue with no slip, the pulling force on the needle had to be equal to the friction force between the needle and the tissue. Slip occurred when the pulling force was greater than the friction force between the needle and the tissue. This means that for constant friction between the needle and the tissue, an increase in the friction between the cart and the rails could have contributed to a higher slip ratio. The larger the weight of the gelatin cart, the higher the friction between the cart and the rails. The cart is relatively large for the amount of gelatin that is on it. Also, it was found that the needle never got to the end of the gelatin during the experiments, meaning that a smaller piece of gelatin could have been used. Additionally, the bearings used for the cart were old, which could have added to the friction. These factors could have contributed to the high slip ratio observed in our work compared to previous work by Scali [14].

Another possible reason for the high mean slip ratio may be that the cart moved backward with each movement of the piston, as shown in the raw time vs. position plot (Figure 19). This also is the reason for the slip ratio being larger than 1 sometimes. This could be explained by the high insertion speed of the independent needle segments. Gerwen et al. [59] suggested that for needle insertion in artificial materials the friction force increases with increasing velocity. This increase in friction force could be due to the increase in viscous friction, which is proportional to the relative speed between the two materials [60, 61]. The high friction between the needle and the tissue may have caused the cart to move backward rather than advancing the needle segment through the tissue. This increase in friction force may also be a reason for the high amount of buckling observed in the advancing needle segments when no tubes were used. Additionally,



the mean slip ratio per cycle was found to be lower at the start of the measurements and at a lower number of cycles. This could be because, at deeper insertion distances, the friction force between the needle and tissue acted on a longer needle distance, leading to a higher chance of moving the cart backward. Therefore, it is suggested that the high insertion speed of the individual segments has a negative impact on the performance of the prototype.

For the piston interval of 0.1 s, with a stroke of 4 mm, it was observed that the last piston of the actuation cycle was not able to execute the full forward and backward movement within the specified interval. Although the actuation unit proved to work for this piston interval, the mean slip ratio was significantly higher than the slip ratio of the other conditions. An idea for further research would be to investigate whether for this piston interval (i.e., 0.1 s) the slip ratio is lower for a stroke of 2 mm than for a stroke of 4 mm. No significant differences were found between 2 mm and 4 mm strokes for a 0.5 s piston interval. This could mean that if the piston is able to execute the full desired motion for a 2 mm stroke at a 0.1 s piston interval, the slip ratio could be less than the slip ratio measured during the current 0.1 s interval measurements. This is interesting to investigate since the speed of the needle insertion then increases while having a similar slip ratio. Additionally, according to Mahvash & Dupont [8], a higher insertion speed can also reduce tissue damage.

## 6.3 Medical Application

### 6.3.1 Focal Laser Ablation

As previously tested by Pusch [15], the needle can implement a seventh segment in the center of the six segments described in this article. This seventh segment could be replaced by a functional element such as a laser fiber. Our actuation unit, as stated in Requirement 9, has the option to incorporate a hollow core to implement such a laser fiber as the seventh segment. For medical applications, this could mean that the instrument can be used as a focal laser ablation instrument, where the laser fiber can be placed in the desired location in the patient.

Previous research has also explored the possibility of steering wasp-inspired needles [14, 15]. If implemented in our needle, one potential application could be for the treatment of kidney tumors. Currently, rigid needle-like instruments are manually inserted while the patient holds their breath, as the kidneys can move up to 30 mm while breathing [62]. A flexible, steerable needle could be a solution for this because potential errors can be compensated for with the steering.

### 6.3.2 Medical Device Regulations

To use a medical device inside patients, it has to meet certain norms. One group of these norms is the norms regarding sterilization [63, 64]. The needle described in this article potentially will be used inside of the patient

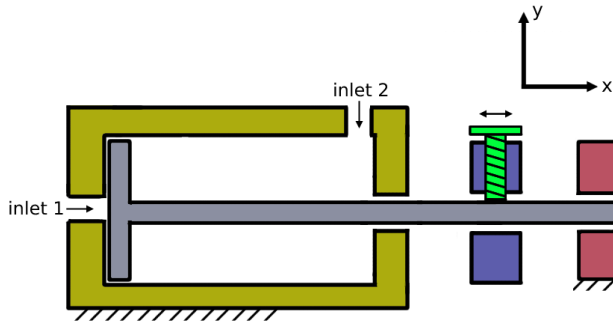
in a normally sterile area. This means it is classified as a critical device, which means that the needle should be properly sterilized [65]. For the current needle design, the Nitinol segments can be sterilized [66], just like the shrinking tube [67]. However, it is uncertain if the shrinking tube and the glue that is used to glue the shrinking tube to the needle segment can be sterilized without losing their function. If this can not be sterilized, to use the needle in a patient, a different connection mechanism to bundle the needle segments at the tip has to be used.

It is important to consider the reusability of an instrument when thinking about the medical application. On the one hand, single-use instruments are cost-effective [68] because the instruments are cheaper and they have no additional costs for sterilization and maintenance [69]. On the other hand, single-use surgical equipment from the operating room is a major source of waste [69]. With environmental issues becoming a more popular topic, we think it is important to reuse the instrument as much as possible. This means that the instrument should follow procedures like sterilization in between the operations and the use of reusable packaging [70]. If the materials are determined to be unsuitable for reuse, the instrument could be reprocessed by a reprocessing company. These types of companies collect medical single-use instruments from hospitals, then reprocess them, whereafter they sell them back to the hospitals at a lower cost than the original cost. This results in lower costs for the hospitals and less environmental damage [71]. To our knowledge, these companies do not yet exist in every country so a solution like this is not available to every hospital. In summary, before the medical application of the instrument, it is important to think about whether or not the instrument is reusable, and if not, how environmental damage can be reduced.

## 6.4 Further Research

### 6.4.1 Design Adjustments

One thing that followed from the testing of the prototype is that the fixation of the piston stop at the correct stroke was hard to do accurately. This is because the movement is a continuous movement, where the piston stop has to be manually fixed at the desired stroke. The markings on the bars of the actuation unit help with this, however, the distance between the bar and the piston stop is of such a large size that when not looking perfectly perpendicular to the surface, it can give a wrong view of the stroke. An idea for further research would be to make the movement discrete, so it is easier to know the exact stroke. An example could be to use a teeth-like system with a step size of 1 millimeter, so there are ten different strokes possible. This would also enhance the reproducibility of the measurements. However, for future models, it could be argued that the adjustment of the stroke is not needed, as an optimum stroke could have been found. In this



**Fig. 25:** Actuator design for the alternative design with an external piston stop (blue). By attaching the piston stop at a certain position in the x-direction at the piston, the stroke is adjusted. The piston stop is attached to the piston with a screw (green).

case, the model would be designed around a fixed stroke requirement.

Another way to improve the design of the actuation unit is to change the actuators so that less air leakage occurs. Figure 25 depicts an alternative design for the actuator. Unlike the actuator used in our experiments, which has an internal piston stop, this actuator has an external piston stop that is attached to the piston with a screw. As the piston moves, the attached piston stop moves with it, thereby limiting the forward motion of the piston, because the forward motion of the piston stop is limited by the piston guidance (red in Figure 25). While this design requires each piston to be separately attached to the piston stop, which may make it less convenient to change the stroke during experiments, it may offer a more airtight design.

#### 6.4.2 Control

The current system requires a control unit, as described in Section 4.2.3, to regulate the cycles of the system. This requires multiple valves and a microcontroller. These valves are the most expensive part of the whole system, and thus it is wished to either have fewer or no valves in future prototypes. For further research, an interesting direction to look at would be making the actuation unit compatible with a single, continuous air input, where the cycle is mechanically implemented. An idea could be to take inspiration from Walschaerts valve gear [72] and implement such a system with the pistons. The input air can then create a rotating motion, which is the input motion of the system. This rotation then can be converted into a translational motion that actuates the pistons in a specific order. Such a mechanism could also reduce the insertion speed of the individual segments, potentially decreasing friction during insertion.

If during needle insertion the slip ratio would be constant, the slip ratio can be pre-programmed so that the needle can follow a programmed trajectory. However, in biological tissue, the slip most likely is not constant. When inserting a needle in biological tissue, sudden tissue ruptures occur due to tissue heterogeneity [8]. In

that case, it may be beneficial to implement a feedback loop that adjusts the input pressure or valve opening time until the piston reaches its desired position. Adding a feedback loop increases the level of automation. This is because in that case, the human operator does not have to check whether the piston movement is successful. The human operator now is taken out of the loop. To further increase the level of automation, an idea for further research could be to let the instrument work together in an automated way with imaging techniques such as MRI. This could be done by letting the needle follow a pre-planned path toward a pre-planned target location specified on the MR images. In the future, MRI-ready, pneumatic, self-propelling needles that can follow a pre-planned path toward a pre-planned target location could be used for MRI-guided needle insertion procedures, while reducing tissue damage.

## 7 CONCLUSION

In this work, we created and evaluated a prototype of an MRI-compatible, pneumatic actuation unit for a self-propelling, ovipositor-inspired needle. The actuation unit has the option to implement an optical fiber, which can be used with the needle for focal laser ablation to treat tumors. The prototype's components were 3D printed using MRI-compatible materials, or, in the case of the screws, made of an MRI-compatible material. The input air for the actuation unit was controlled and divided over the inputs of the actuation unit, using a control unit. By moving the pistons in a specific order, the so-called cycles for the six needle segments were performed, resulting in the desired needle segment motion for the self-propelling mechanism to work. The actuation unit allows the user to change the distance that the needle segments travel each cycle, called the stroke. It was found that for smaller strokes (i.e., 2 and 4 mm) at a gauge pressure of 0.5 bar, the actuation unit was able to actuate the self-propelling needle, resulting in the needle advancing through 10 wt% gelatin tissue phantoms. However, for larger strokes (i.e., 6, 8, and 10 mm), it was found that the actuation unit was not able to actuate the self-propelling needle. The prototype is the next step in developing self-propelling needles suitable for focal laser ablation to treat tumors.

## 8 ACKNOWLEDGEMENTS

I would like to thank Jette Bloemberg and Paul Breedveld for the helpful meetings during the whole period of the project. Also Gertjan Mulder from the fluid mechanics department for the info on valves and for the help with the control unit design. Finally, I would like to thank the group of other students and supervisors for the graduating student meetings and workshops.

## REFERENCES

- [1] M. Ahmed, C. L. Brace, F. T. Lee Jr, and S. N. Goldberg. Principles of and advances in percutaneous

- ablation. radiology. *Med. Phys.*, page 351–369, 2011. doi: <https://doi.org/10.1148/radiol.10081634>.
- [2] C. J. Cooper, M. Teleb, A. Dwivedi, G. Rangel, L. A. Sanchez, S. Laks, N. Akle, and Z. Nahleh. Comparative outcome of computed tomography-guided percutaneous radiofrequency ablation, partial nephrectomy or radical nephrectomy in the treatment of stage T1 renal cell carcinoma. *Rare Tumors*, 7(1):20–25, 2015. doi: [10.4081/rt.2015.5583](https://doi.org/10.4081/rt.2015.5583).
  - [3] Yale. Minimally invasive surgery. retrieved from <https://www.yalemedicine.org/conditions/minimally-invasive-surgery>, date accessed: 24-01-2022.
  - [4] A. Leibinger, M. Oldfield, and F. Rodriguez y Baena. Minimally disruptive needle insertion: a biologically inspired solution. *Interface Focus*, page 20150107, 2016. doi: <http://dx.doi.org/10.1098/rsfs.2015.0107>.
  - [5] S. Natarajan, S. Raman, A. M. Priester, J. Garritano, D. J. A. Margolis, P. Lieu, M. L. Macairan, J. Huang, W. Grundfest, and L. S. Marks. Focal laser ablation of prostate cancer: Phase i clinical trial. *The Journal of Urology*, pages 68–74, 2016. doi: [10.1016/j.juro.2015.12.083](https://doi.org/10.1016/j.juro.2015.12.083).
  - [6] H. Wenger, A. Yousuf, A. Oto, and S. Eggner. Laser ablation as focal therapy for prostate cancer. *Current opinion in urology*, page 236–240, 2014. doi: <https://doi.org/10.1097/MOU.0000000000000044>.
  - [7] E. Walser, A. Nance, L. Ynalvez, S. Yong, J. Aoughsten, E. J. Eyzaguirre, and S. B. Williams. Focal laser ablation of prostate cancer: Results in 120 patients with low- to intermediate-risk disease. *Journal of Vascular and Interventional Radiology*, pages 401–409, 2019. doi: <https://doi.org/10.1016/j.jvir.2018.09.016>.
  - [8] M. Mahvash and P. E. Dupont. Fast needle insertion to minimize tissue deformation and damage. *IEEE International Conference on Robotics and Automation*, pages 3097–3102, 2009. doi: [10.1109/ROBOT.2009.5152617](https://doi.org/10.1109/ROBOT.2009.5152617).
  - [9] N. J. van den Berg, F. C. Meeuwssen, M. Doukas, G. Kronreif, A. Moelker, and J. J. van den Dobbels. Steerable needles for radio-frequency ablation in cirrhotic livers. *Scientific Reports*, 2021. doi: <https://doi.org/10.1038/s41598-020-77869-3>.
  - [10] A. Sakes, D. Dodou, and P. Breedveld. Buckling prevention strategies in nature as inspiration for improving percutaneous instruments: a review. *Bioinspir. Biomim.*, page 021001, 2016. doi: <https://doi.org/10.1088/1748-3190/11/2/021001>.
  - [11] U. Cerkvénik, B. van de Straat, S. W. S. Gussekloo, and J. L. Leeuwen. Mechanisms of ovipositor insertion and steering of a parasitic wasp. *Proceedings of the National Academy of Sciences*, pages 7822–7831, 2017. doi: <https://doi.org/10.1073/pnas.1706162114>.
  - [12] M. Scali (BITE-Group). 3d printed wasp-ovipositor replica: Reverse engineering approach (closed). retrieved from <https://www.bitegroup.nl/assignments/3d-printed-wasp-ovipositor-replica-reverse-engineering-approach/>, date accessed: 19-12-2022.
  - [13] M. Ghara, L. Kundanati, and R. M. Borges. Nature’s swiss army knives: Ovipositor structure mirrors ecology in a multitrophic fig wasp community. *PLoS One*, page e23642, 2011. doi: <https://doi.org/10.1371/journal.pone.0023642>.
  - [14] M. Scali. Self-propelling needles: From biological inspiration to percutaneous interventions. 2020. doi: <https://doi.org/10.4233/uuid:523e3e5f-08f0-4acb-ab45-abaa7ace3967>.
  - [15] T. P. Pusch. From the wasp ovipositor to a 3d steerable needle for solid-tissue interventions. 2016.
  - [16] F. V. V. Vincent and M. J. King. The mechanism of drilling by wood wasp ovipositors. *Biomimetics*, pages 187–201, 1995.
  - [17] D. L. J. Quicke and M. G. Fitton. Ovipositor steering mechanisms in parasitic wasps of the families gasteruptiidae and aulacidae hymenoptera). *Proceedings: Biological Sciences*, pages 99–103, 1995.
  - [18] S. P. DiMaio and S. E. Salcudean. Needle insertion modeling and simulation. *IEEE TRANSACTIONS ON ROBOTICS AND AUTOMATION*, pages 864–875, 2003.
  - [19] A. M. Okamura, C. Simone, and M. D. O’Leary. Force modeling for needle insertion into soft tissue. *IEEE TRANSACTIONS ON BIOMEDICAL ENGINEERING*, pages 1707–1716, 2004.
  - [20] D. J. van Gerwen. Needle-tissue interaction by experiment. 2013.
  - [21] M. Mahvash and P. Dupont. Mechanics of dynamic needle insertion into a biological material. *IEEE TRANSACTIONS ON BIOMEDICAL ENGINEERING*, pages 934–943, 2010.
  - [22] Y. Fukushima and K. Naemura. Estimation of the friction force during the needle insertion using the disturbance observer and the recursive least square. *ROBOMECH Journal*, pages 1–8, 2014. doi: <https://doi.org/10.1186/s40648-014-0014-7>.
  - [23] Y. Aaboubout, N. Soares, E. M. Barroso, L. C. van der Sar, A. Bocharnikov, I. Usenov, V. Artyushenko, P. J. Caspers, S. Koljenović, T. C. Bakker Schut, J. J. van den Dobbels, and G. J. Puppels. Experimental study on needle insertion force to minimize tissue deformation in tongue tissue. *Medical Engineering Physics*, pages 40–46, 2021. doi: <https://doi.org/10.1016/j.medengphy.2021.10.003>.
  - [24] BITE-Group. Self propelled devices. retrieved from <https://www.bitegroup.nl/category/self-propelled-devices/>, date accessed: 19-09-2022.
  - [25] E. Knull, A. Oto, S. Eggner, D. Tessier, S. Guneyli, A. Chatterjee, and A. Fenster. Evaluation of tumor coverage after mr-guided prostate focal laser ablation therapy. *Med. Phys.*, pages 800–810, 2019. doi: [10.1002/mp.1405](https://doi.org/10.1002/mp.1405).
  - [26] R. J. Leveillee, S. M. Castle, V. Gorbatiy, N. Salas, G. Narayanan, G. Morillo-Burgos, M. Jorda, and

- M. M. Faraday. Oncologic outcomes using real-time peripheral thermometry-guided radiofrequency ablation of small renal masses. *Journal of Endourology*, 27(4):480–489, 2013. doi: 10.1089/end.2012.0305.
- [27] J. Bloembergen, F. Trauzettel, B. Coolen, D. Dodou, and P. Breedveld. Design and evaluation of an mri-ready, self-propelled needle for prostate interventions. *PLoS ONE*, page e0274063, 2022. doi: <https://doi.org/10.1371/journal.pone.0274063>.
- [28] Compressed Air Best Practices. Nfpa 99 medical air dewpoint requirements. retrieved from <https://www.airbestpractices.com/standards/nfpa-99-medical-air/nfpa-99-medical-air-dewpoint-requirements#:~:text=Medical%20air%20is%20produced%2C%20by,Level%201%20or%202%20applications.>, date accessed: 05-10-2022.
- [29] Compressed Air Systems. Medical application. retrieved from <https://www.compressedairsystems.com/application/medical/>, date accessed: 11-10-2022.
- [30] R. Jacob and D. A. Kumaresh. Medical grade compressed air. *Update in Anaesthesia*, pages 2–3.
- [31] Elesta. Elesta echolaser thermoablation. retrieved from <https://www.elesta-echolaser.com/termoterapia/?lang=en>, date accessed: 22-11-2022.
- [32] F. Morra, M. De Landro, S. Korganbayev, A. Wolf, A. Dostovalov, A. Cigada, and P. Saccomandi. Spatially resolved thermometry during laser ablation in tissues: Distributed and quasi-distributed fiber optic-based sensing. *Optical Fiber Technology*, page 102295, 2020.
- [33] F. Panthier, S. Doizi, C. Gorny, and O. Berthe, L. and Traxer. Impact of laser fiber diameter and irrigation fluids on induced bubble stream dynamics with thulium fiber laser: An in vitro study. *Journal of Endourology*, 2020. doi: 10.1089/end.2020.0766.
- [34] H. Elhawary, Z. T. H. Tse, A. Hamed, M. Rea, B. L. Davies, and M. U. Lamperth. The case for mr-compatible robotics: a review of the state of the art. *Int J Med Robotics Comput Assist Surg*, pages 105–113, 2008. doi: 10.1002/rcs.192.
- [35] K. Nakajima and O. Schwarz. How to use the ovipositor drilling mechanism of hymenoptera for developing a surgical instrument in biomimetic design. *Int. J. of Design Nature and Ecodynamics.*, page 177–189, 2014. doi: 10.2495/DNE-V9-N3-177-189.
- [36] Eriks. Festo magneetventiel. retrieved from <https://shop.eriks.nl/nl/pneumatische-componenten-ventielen-ventielen/magneetventiel-mhp2-ms1h-5-2-m5-525105-11644608/?searchTerm=MHP2-MS1H-5%2f2-M5&searchType=102>, date accessed: 28-09-2022.
- [37] Conrad. Toolcraft screws. retrieved from <https://www.conrad.nl/nl/p/toolcraft-839944-verzonken-schroeven-m2-10-mm-sleuf-din-963-kunststof-polyamide-10-stuk-s-839944.html>, date accessed: 03-10-2022.
- [38] Super Lube. Multi-purpose synthetic lubricant with syncolon® (ptfe). retrieved from <https://www.superlube.com/multi-purpose-lubricant-with-syncolon-ptfe>, date accessed: 10-10-2022.
- [39] D. Stoeckel. Nitinol-a material with unusual properties. *Endovascular Update*, pages 1–8, 1998.
- [40] A. Melzer, S. Michitsch, S. Konak, G. Schaefer, and T. Bertsch. Nitinol in magnetic resonance imaging. *Minimally Invasive Therapy Allied Technologies.*, pages 261–271, 2004. doi: 10.1080/13645700410020269.
- [41] Nordson Medical. Heat shrink tubing. retrieved from <https://www.nordsonmedical.com/Shop/Heat-Shrink-Tubing/Products/103-0139/mm>, date accessed: 22-11-2022.
- [42] P. Klemarczyk. Adhesion studies of mixtures of ethyl cyanoacrylate with a difunctional cyanoacrylate monomer and with other electron-deficient olefins. *The Journal of Adhesion*, pages 293–306, 1999. doi: 10.1080/00218469908017232.
- [43] Formlabs. Formlabs form 3. retrieved from <https://formlabs.com/eu/3d-printers/form-3/>, date accessed: 30-09-2022.
- [44] M. Park and S. Shin. Three-dimensional comparative study on the accuracy and reproducibility of dental casts fabricated by 3d printers. *THE JOURNAL OF PROSTHETIC DENTISTRY*, pages 861.e1–861.e7, 2018.
- [45] Formlabs. Form wash. retrieved from <https://formlabs.com/eu/store/post-processing/form-wash/>, date accessed: 06-10-2022.
- [46] Formlabs. Form cure. retrieved from <https://formlabs.com/eu/store/post-processing/form-cure/>, date accessed: 06-10-2022.
- [47] Formlabs. Formlabs model v2 resin. retrieved from <https://dental.formlabs.com/store/materials/model-resin-v2/>, date accessed: 30-09-2022.
- [48] J. S. Cuellar, G. Smit, A. A. Zadpoor, and P. Breedveld. Ten guidelines for the design of non-assembly mechanisms: The case of 3d-printed prosthetic hands. *J Engineering in Medicine*, pages 962–971, 2018. doi: 10.1177/0954411918794734.
- [49] A. Charles, A. Elkaseer, T. Müller, L. Thijs, M. Torge, V. Hagenmeyer, and S. Scholz. A study of the factors influencing generated surface roughness of down-facing surfaces in selective laser melting. 2018. doi: 10.3850/978-981-11-2728-1\_57.
- [50] M. J. Männel, L. Selzer, R. Bernhardt, and J. Thiele. Optimizing process parameters in commercial micro-stereolithography for forming emulsions and polymer microparticles in nonplanar microfluidic devices. *Advanced Materials Technologies*, page 1800408, 2018. doi: <https://doi.org/10.1002/admt.201800408>.
- [51] C. Culmone, P. W. J. Henselmans, B. van Starkenburg, and P. Breedveld. Exploring non-assembly 3d printing for novel compliant surgical devices. *PLoS ONE*, 2020. doi: <https://doi.org/10.1371/journal.pone.0232952>.
- [52] A. Pavone, G. Stano, and G. Percoco. On the fabrication of modular linear electromagnetic actuators

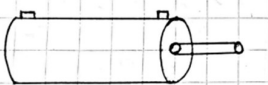
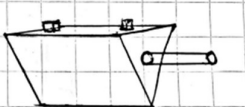
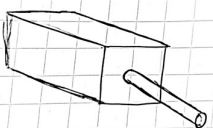
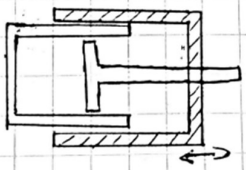
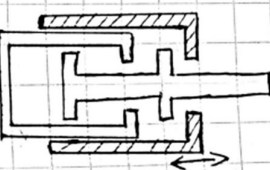
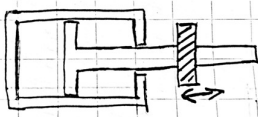
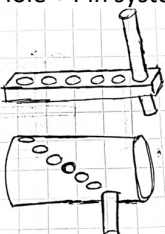

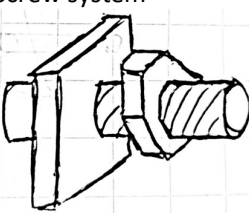
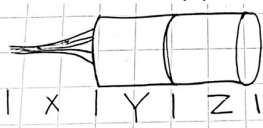
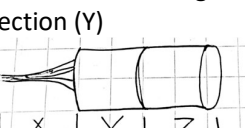
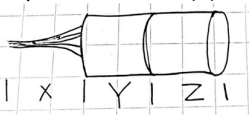
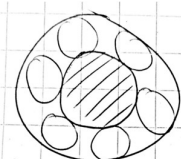
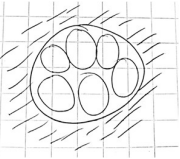
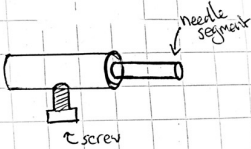
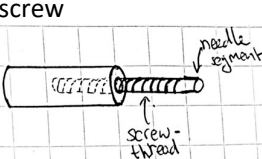
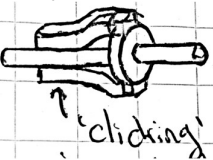
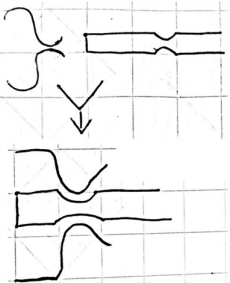


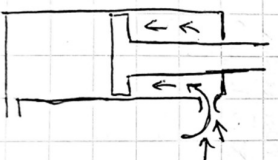
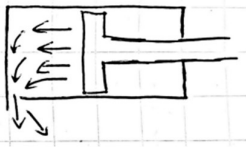
- with 3d printing technologies. *V CIRP Conference on Biomanufacturing*, page 139–144, 2022. doi: 10.1016/j.procir.2022.06.026.
- [53] M. M. Hanon, R. Marczis, and L. Zsidai. Impact of 3d-printing structure on the tribological properties of polymers. *Industrial Lubrication and Tribology*, pages 811–818, 2020. doi: <https://doi.org/10.1108/ILT-05-2019-0189>.
- [54] E. George, P. Liacouras, F. J. Rybicki, and D. Mitsouras. Measuring and establishing the accuracy and reproducibility of 3d printed medical models. *Radiographics*, pages 1424–1450, 2017. doi: 10.1148/rg.2017160165.
- [55] J. S. Shim, J. Kim, S. H. Jeong, Y. J. Choi, and J. J. Ryu. Printing accuracy, mechanical properties, surface characteristics, and microbial adhesion of 3d-printed resins with various printing orientations. *The Journal of Prosthetic Dentistry*, pages 468–475, 2020. doi: <https://doi.org/10.1016/j.prosdent.2019.05.034>.
- [56] Festo. Wegventielen. retrieved from [https://www.festo.com/net/nl-be\\_be/SupportPortal/Files/706426/Wegventielen.pdf](https://www.festo.com/net/nl-be_be/SupportPortal/Files/706426/Wegventielen.pdf), date accessed: 03-10-2022.
- [57] K. R. Das and A. H. M. R. Imon. A brief review of tests for normality. *American Journal of Theoretical and Applied Statistics*, pages 5–12, 2016. doi: 10.11648/j.ajtas.20160501.12.
- [58] M. Öner and Ý. Deveci Kocakoç. A compilation of some popular goodness of fit tests for normal distribution: Their algorithms and matlab codes (matlab). *Journal of Modern Applied Statistical Methods*, 2017. doi: 10.1080/00218469908017232.
- [59] D. J. van Gerwen, J. Dankelman, and J. J. van den Dobbelen. Needle–tissue interaction forces – a survey of experimental data. *Medical Engineering Physics*, pages 665–680, 2012. doi: <http://dx.doi.org/10.1016/j.medengphy.2012.04.007>.
- [60] H. Kataoka, T. Washio, K. Chinzei, K. Mizuhara, C. Simone, and A. M. Okamura. Measurement of the tip and friction force acting on a needle during penetration. *International conference on medical image computing and computer-assisted intervention*, pages 216–223, 2002.
- [61] R. Kelly, J. Llamas, and R. Campa. A measurement procedure for viscous and coulomb friction. *IEEE TRANSACTIONS ON INSTRUMENTATION AND MEASUREMENT*, pages 857–861, 2000.
- [62] P. Moreira, A. Momen, and S. Misra. Towards physiological motion compensation for flexible needle interventions. *2015 IEEE/RSJ International Conference on Intelligent Robots and Systems (IROS)*, pages 831–836, 2015.
- [63] G. C. C. Mendes, Brandão T. R. S., and C. L. M. Silva. Ethylene oxide sterilization of medical devices: A review. *American Journal of Infection Control*, pages 574–581, 2007. doi: <https://doi.org/10.1016/j.ajic.2006.10.014>.
- [64] T. J. A. G. Munker, S. E. C. M. van de Vijfeijken, C. S. Mulder, V. Vespasiano, A. G. Becking, C. J. Klevverlaan, L. Dubois, L. H. E. Karssemakers, D. M. J. Milstein, P. R. A. M. Depauw, F. W. A. Hoefnagels, W. P. Vandertop, T. J. J. Maal, E. Nout, M. Riool, and S. A. J. Zaat. Effects of sterilization on the mechanical properties of poly(methyl methacrylate) based personalized medical devices. *Journal of the Mechanical Behavior of Biomedical Materials*, pages 168–172, 2018. doi: <https://doi.org/10.1016/j.jmbbm.2018.01.033>.
- [65] S. Govindaraj and M. S. Muthuraman. Systematic review on sterilization methods of implants and medical devices. *International Journal of ChemTech Research*, pages 897–911, 2015.
- [66] B. T. M. Tabrizian and O. S. L. Yahia. Effects of sterilization processes on niti alloy: Surface characterization. *Journal of Biomedical Materials Research*, pages 88–98, 1999. doi: [https://doi.org/10.1002/\(SICI\)1097-4636\(200001\)49:1<88::AID-JBM11>3.0.CO;2-I](https://doi.org/10.1002/(SICI)1097-4636(200001)49:1<88::AID-JBM11>3.0.CO;2-I).
- [67] Nordson Medical. Heat shrink tubing specifications. retrieved from <https://www.nordsonmedical.com/Components-and-Technologies/Heat-Shrink-Tubing/PET-Heat-Shrink-Tubing/Technical-Information/>, date accessed: 23-11-2022.
- [68] D. K. Manatakis and N. Georgopoulos. Reducing the cost of laparoscopy: Reusable versus disposable laparoscopic instruments. *Minimally Invasive Surgery*, 2014. doi: 10.1155/2014/408171.
- [69] J. Siu, A. G. Hill, and A. D. McCormick. Systematic review of reusable versus disposable laparoscopic instruments: costs and safety. *ANZ Journal of Surgery*, 87:28–33, 2016. doi: 10.1111/ans.13856.
- [70] H. Schlautmann. Reprocessing of surgical instruments. *101 of Surgical Instruments*, pages 205–221, 2022. doi: <https://doi.org/10.1007/978-3-662-63632-9>.
- [71] K. Ubaldi. Reprocessing single-use devices in the ambulatory surgery environment. *AORN Journal*, 109(4):452–462, 2019. doi: <https://doi.org/10.1002/aorn.12639>.
- [72] B. Spencer. Walschaert valve gear design. *JOURNAL OF THE INST. OF LOCO. ENGINEERS.*, pages 555–576, 1924.

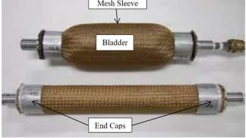
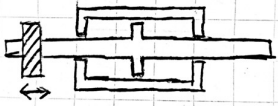
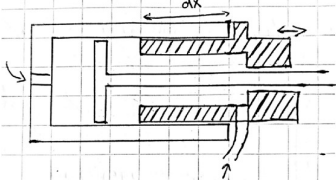
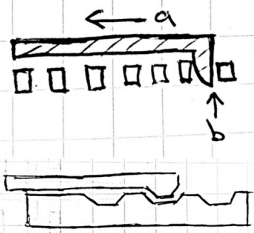
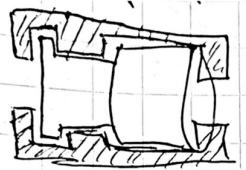
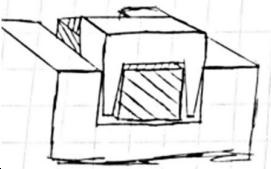

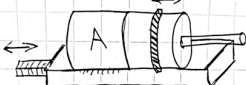



## Appendix A. Morphological Chart

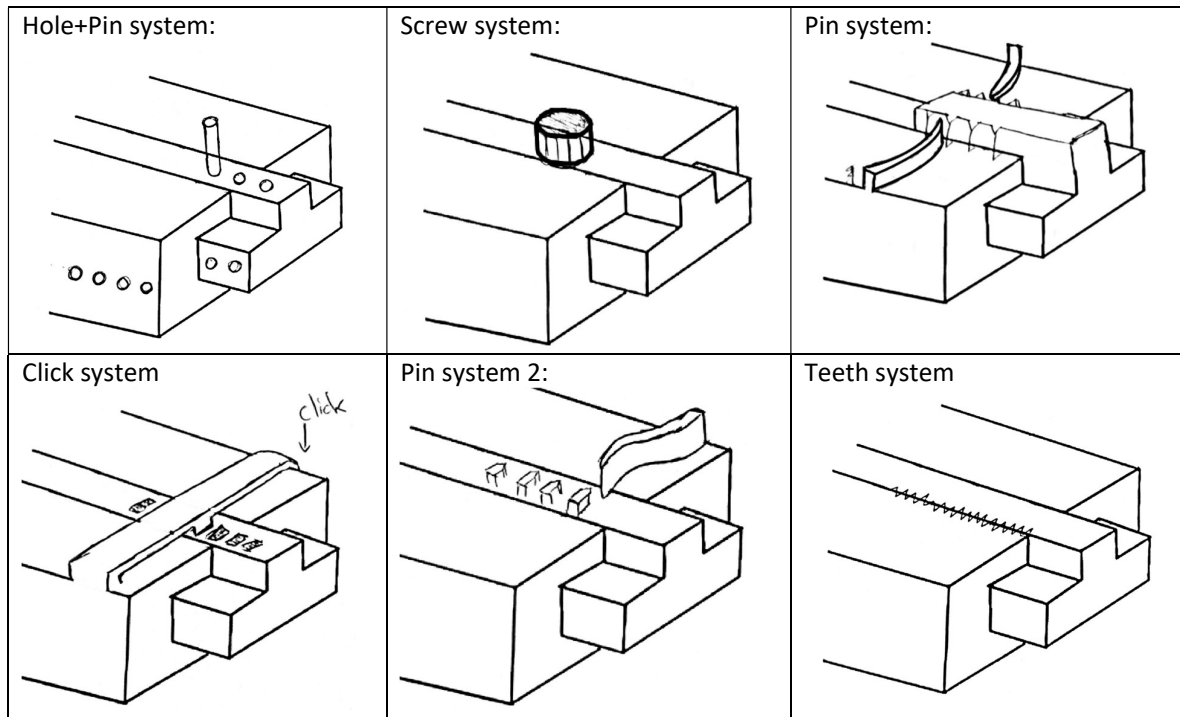
This appendix contains the morphological chart, including some morphological charts for solutions to problems that were present at a later phase in the design phase.

Function	Solution A	Solution B	Solution C
Actuator Type	Cylinder-shaped 	Triangle-shaped 	Cube-shaped 
Adjustable stroke mechanism	Change end of actuator 	Use external "wall" 	Change second piston "stop" 
Locking mechanism for axial adjustment	Hole + Pin system 	Teeth system 	Screw system 
Locking mechanism position	At cable section (X) 	At actuator housing section (Y) 	At piston section (Z) 
placement of air tubes for pushing pistons back	In center 	Out center 	
Piston orientation	Needle attached to piston	Needle attached to actuator housing	
Locking + changing the needle segments	Use a screw to fasten 	Use needle segment as screw 	Compliance  

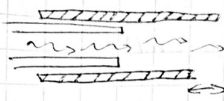
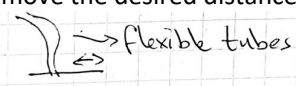
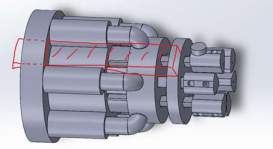
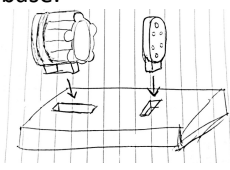
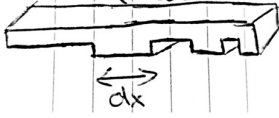
Mechanism to move the actuator back	By using positive pressure (2 inlets) 	By using negative pressure (1 inlet) 	
-------------------------------------	--	--	--

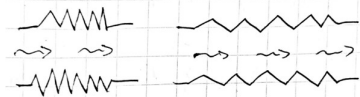
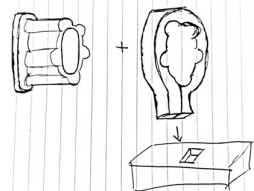
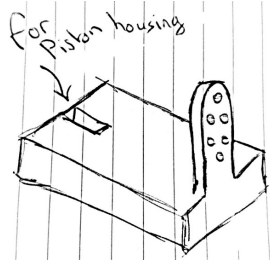
Function	Solution D	Solution E	Solution F
Actuator Type	Pneumatic stepper motor	Soft robotics/muscle actuator 	
Adjustable stroke mechanism	Change second "stop" at other side 	Use internal stop 	
Locking mechanism for axial adjustment	Compliant click system 	External click-on On whole structure:  On part after base: 	Tie-wrap-like system 
Locking mechanism position	After the base, with A fixed to the base 		
Locking + changing the needle segments	Move ring over two tube segments to lock 	Use (detachable) tip that connects segment with piston stick.	

Ideas for locking in case of a base where the model moves through: (for concept 1 in Appendix B)



Solutions to other problems that were encountered at a later moment in the design process:

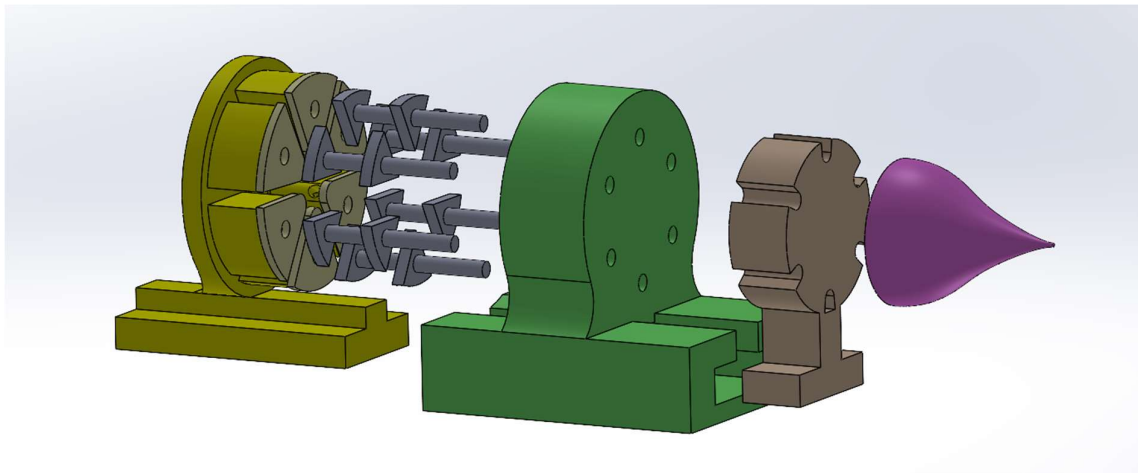
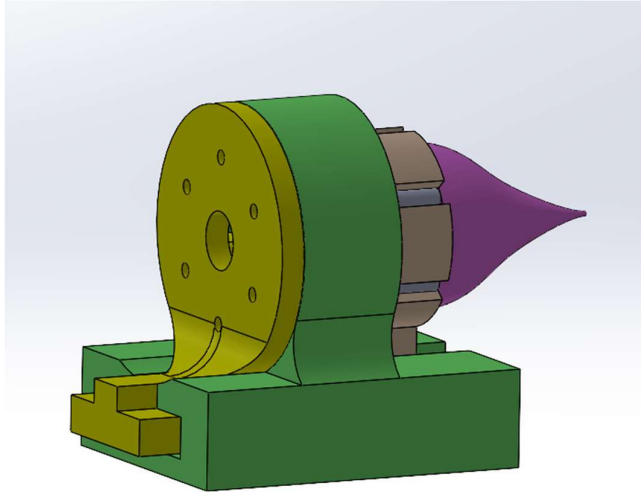
Function	Solution A	Solution B
<b>Option for the "return" air tube</b>	Two tubes moving over each other. 	Flexible tubes, with enough space to move the desired distance. 
<b>Locking the piston guidance + piston housing at the correct position</b>	bars on the side, attached to the piston guidance, attachable and detachable to the housing. 	Attach to a base by modifying the prints with a part that fits in the base.  Options: <ul style="list-style-type: none"><li>- Pins</li><li>- Compliant click system</li><li>- Screws</li></ul>
<b>Locking the piston stop at the correct position</b>	Slide through the base/bars and lock on the sliding parts.  Options: <ul style="list-style-type: none"><li>- Pins</li><li>- Compliant click system</li><li>- Screws</li></ul>	Use bars with shapes fitted for each stroke. 

Function	Solution C	Solution D
<b>Option for the "return" air tube</b>	Accordion expanding tubes. 	
<b>Locking the piston guidance + piston housing at the correct position</b>	Attach to a base by using an external part.  Options: <ul style="list-style-type: none"><li>- Pins</li><li>- Compliant click system</li><li>- Screws</li></ul>	Piston guidance is part of the base. The piston housing is attached to the base. * # 

## Appendix B. Old concepts and partial concepts

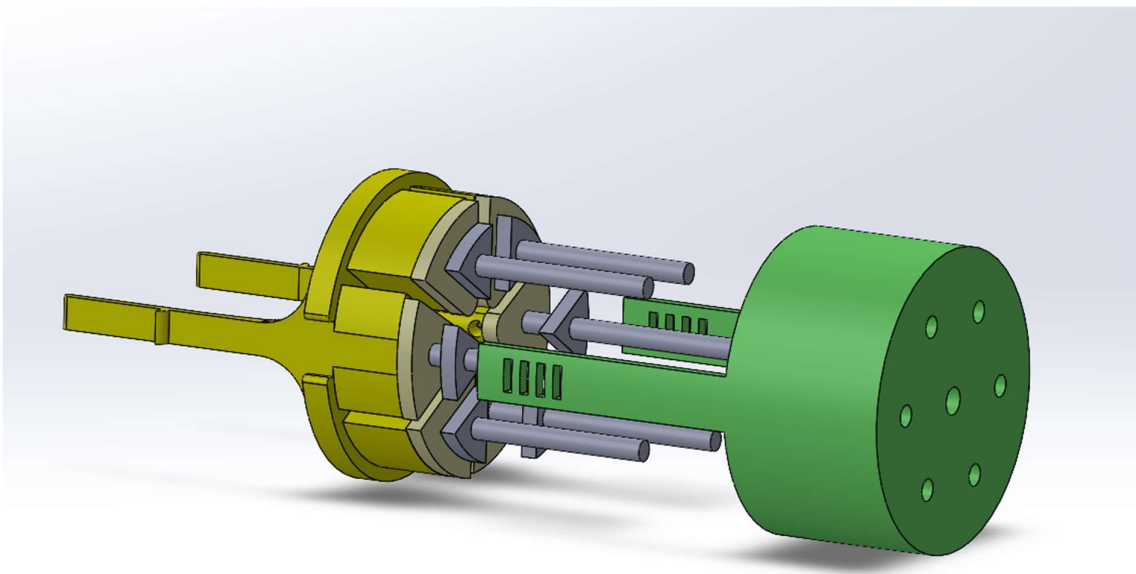
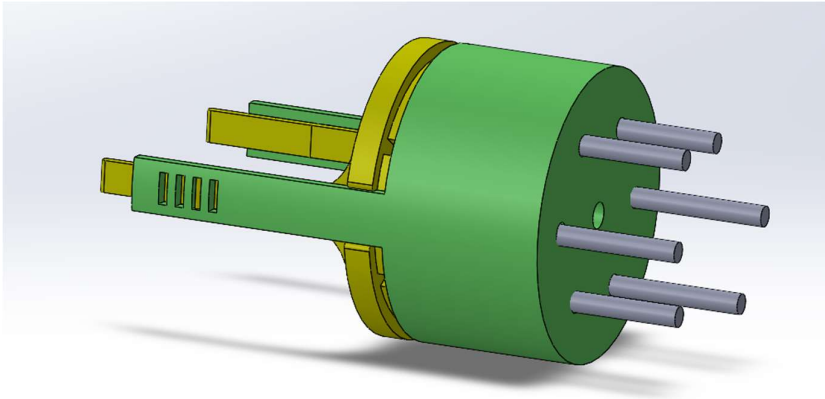
This appendix contains designs of old (partial) concepts.

1. External wall piston sliding through a solid base.

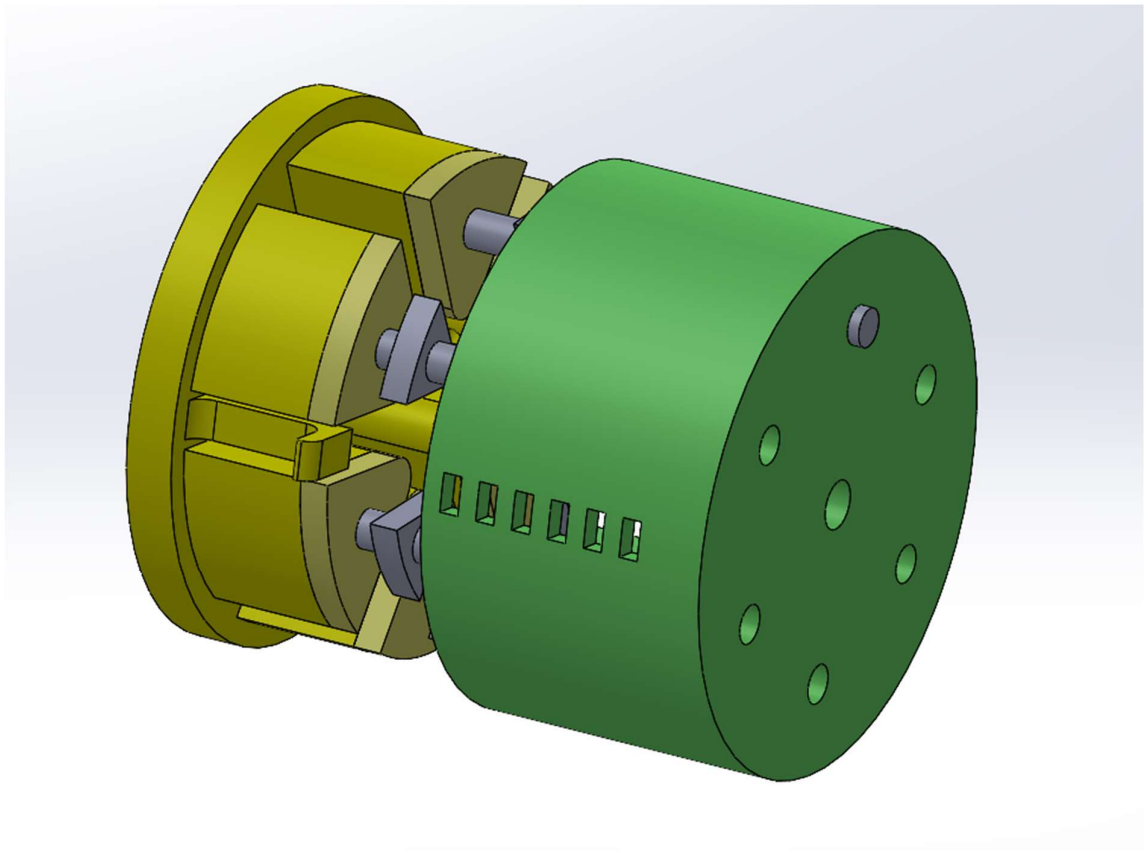
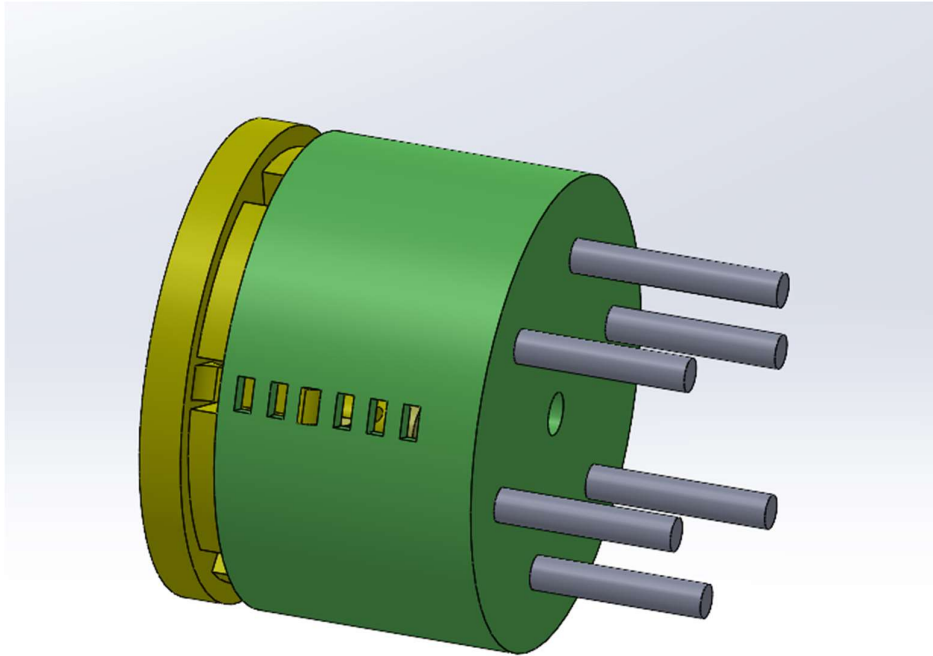




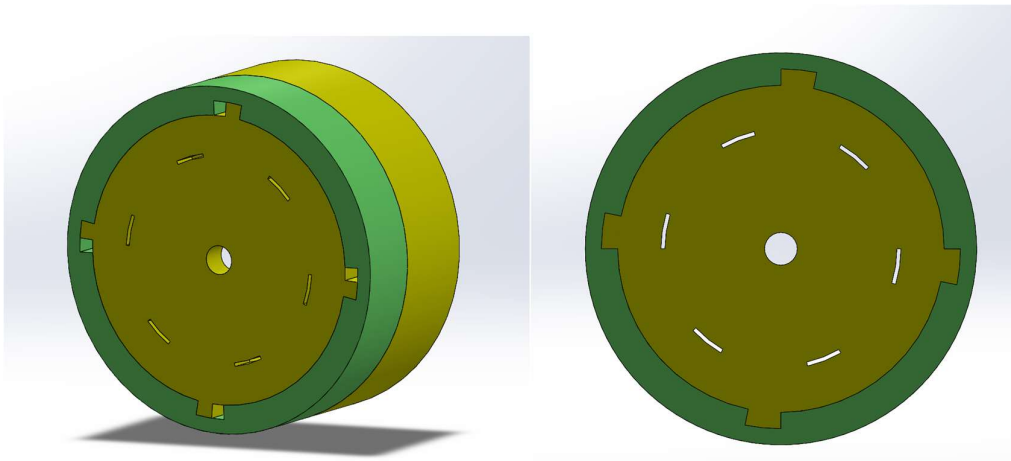
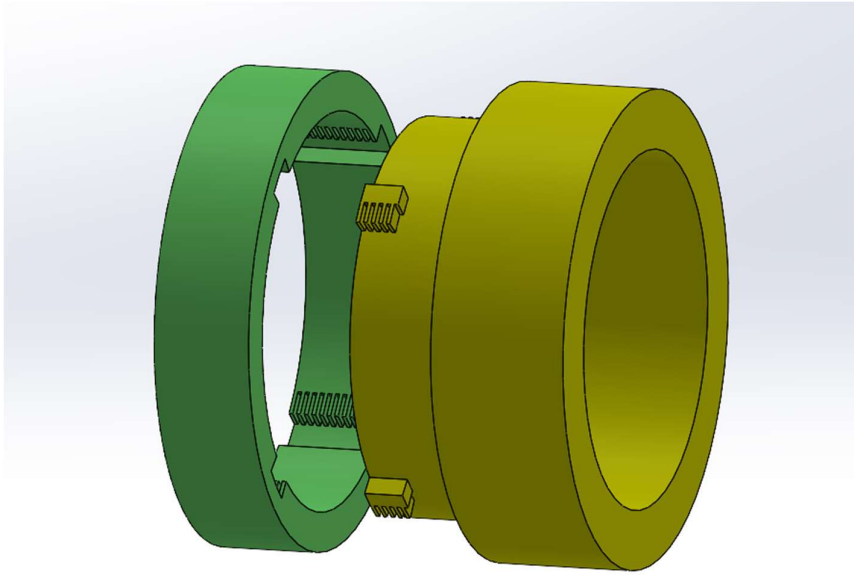
2. External wall piston with compliant stroke change mechanism on outside



3. External wall piston with compliant stroke change mechanism on inside



4. Rotate to change stroke idea



## Appendix C. Technical Drawings Actuation Unit

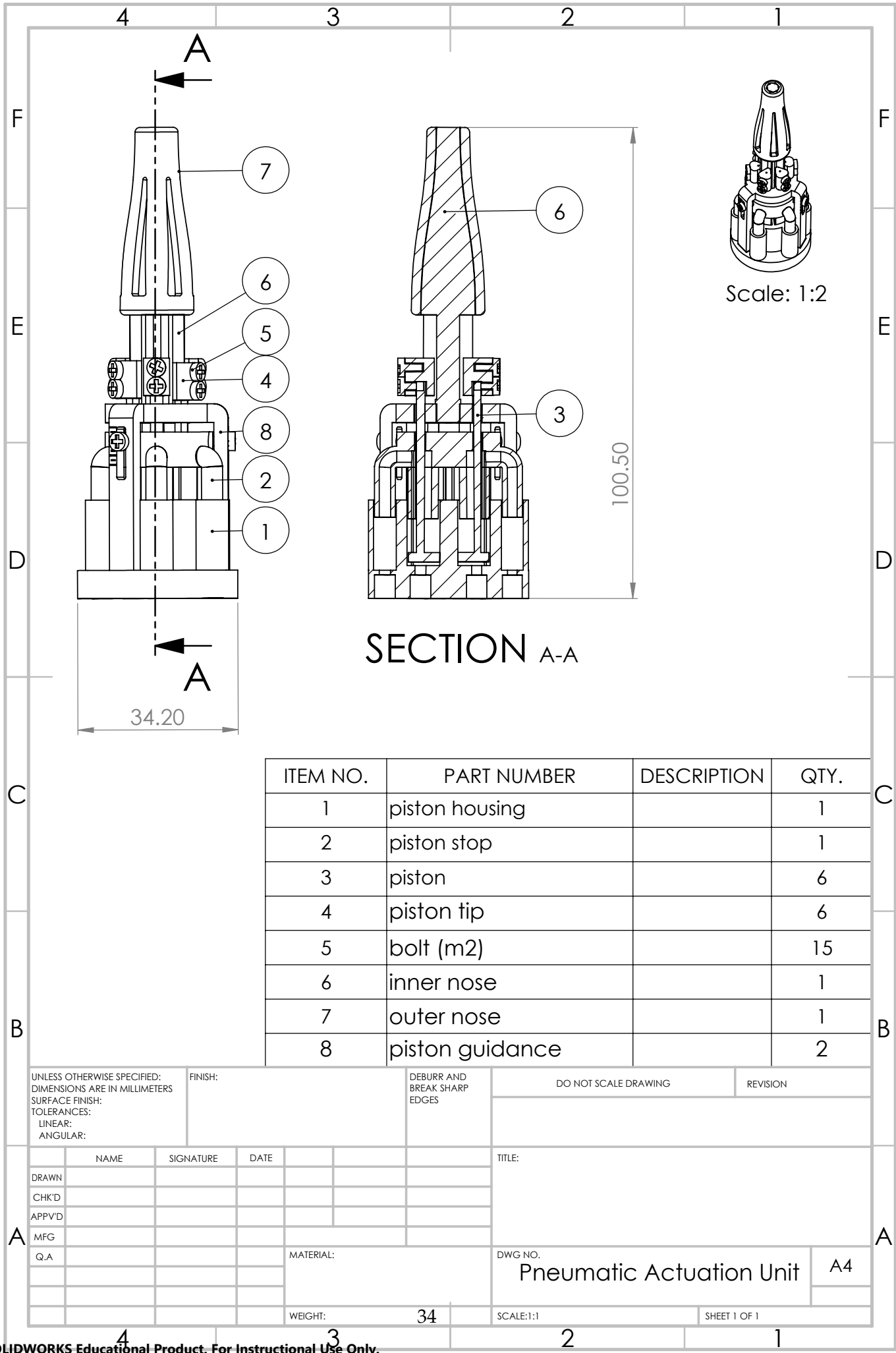
The following technical drawings of the designed pneumatic actuation unit can be found in this appendix:

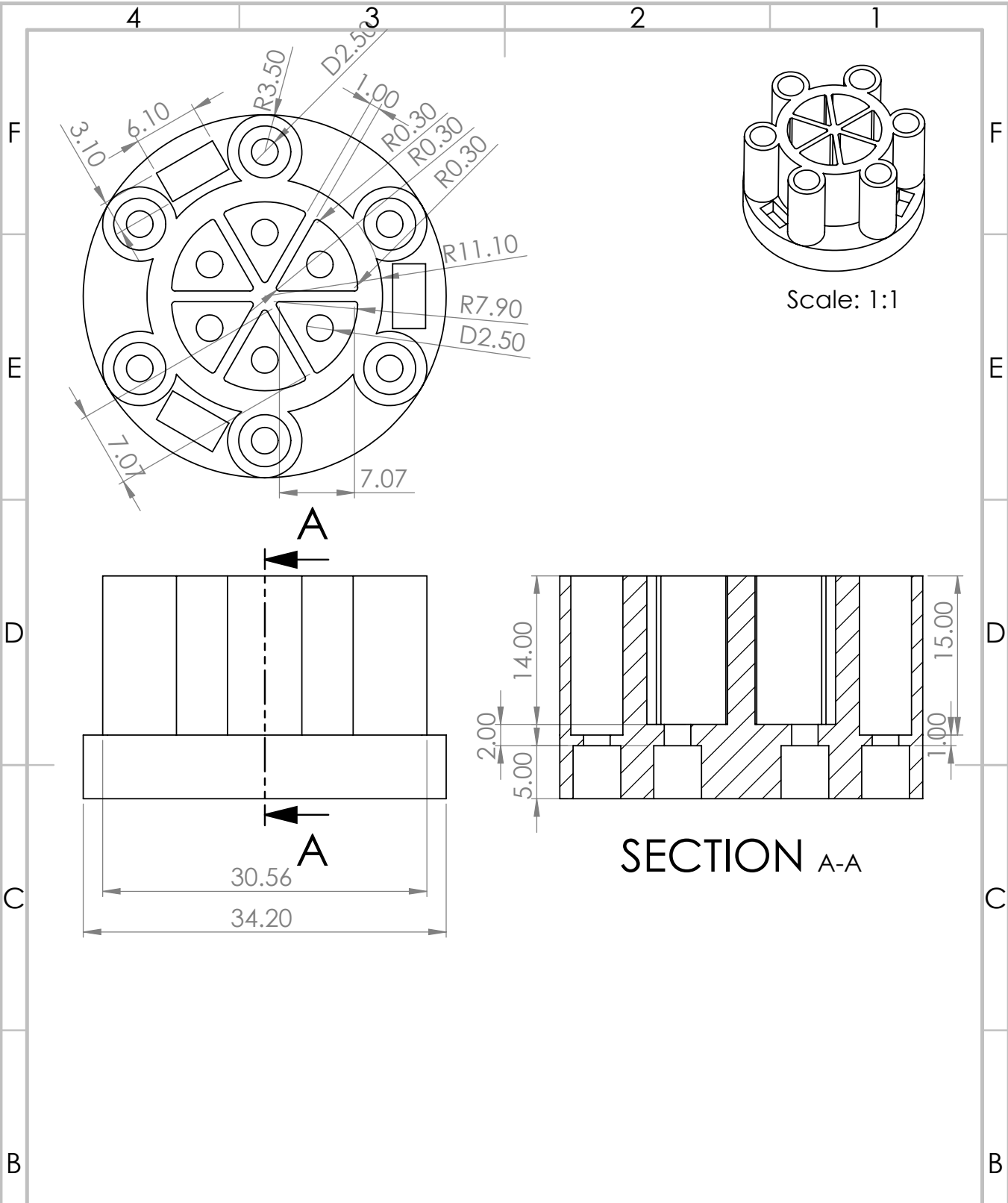
### Assembly drawings

- Pneumatic actuation unit

### Part drawings

- Piston housing
- Piston stop
- Piston
- Piston tip
- Inner nose
- Outer nose
- Piston guidance



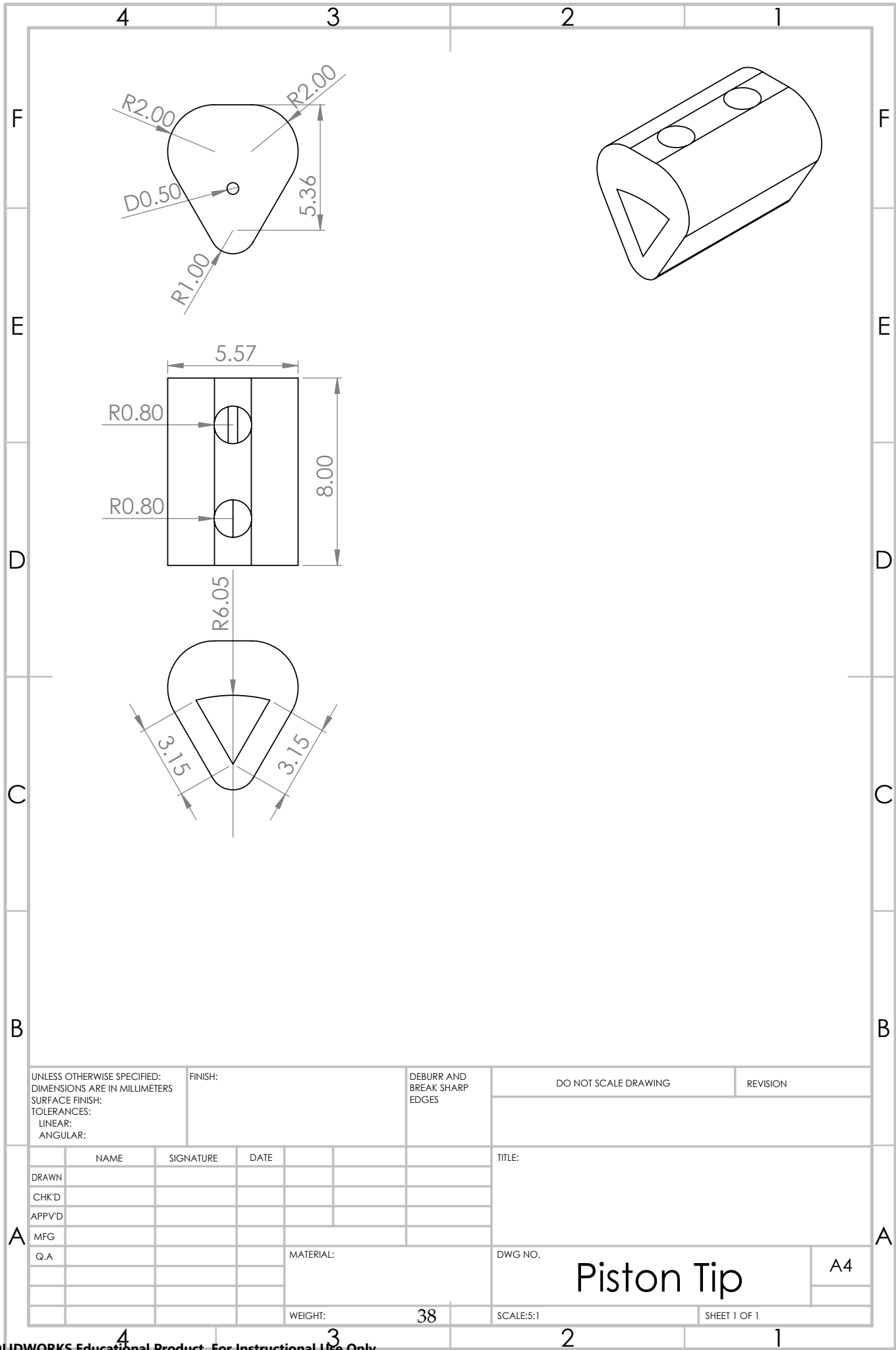


UNLESS OTHERWISE SPECIFIED: DIMENSIONS ARE IN MILLIMETERS SURFACE FINISH: TOLERANCES: LINEAR: ANGULAR:				FINISH:		DEBURR AND BREAK SHARP EDGES		DO NOT SCALE DRAWING		REVISION	
DRAWN				NAME		SIGNATURE		DATE		TITLE:	
CHK'D										Housing	
APPV'D										DWG NO.	
MFG										piston housing	
Q.A.										A4	
										SCALE:2:1	
										SHEET 1 OF 1	
										WEIGHT: 35	

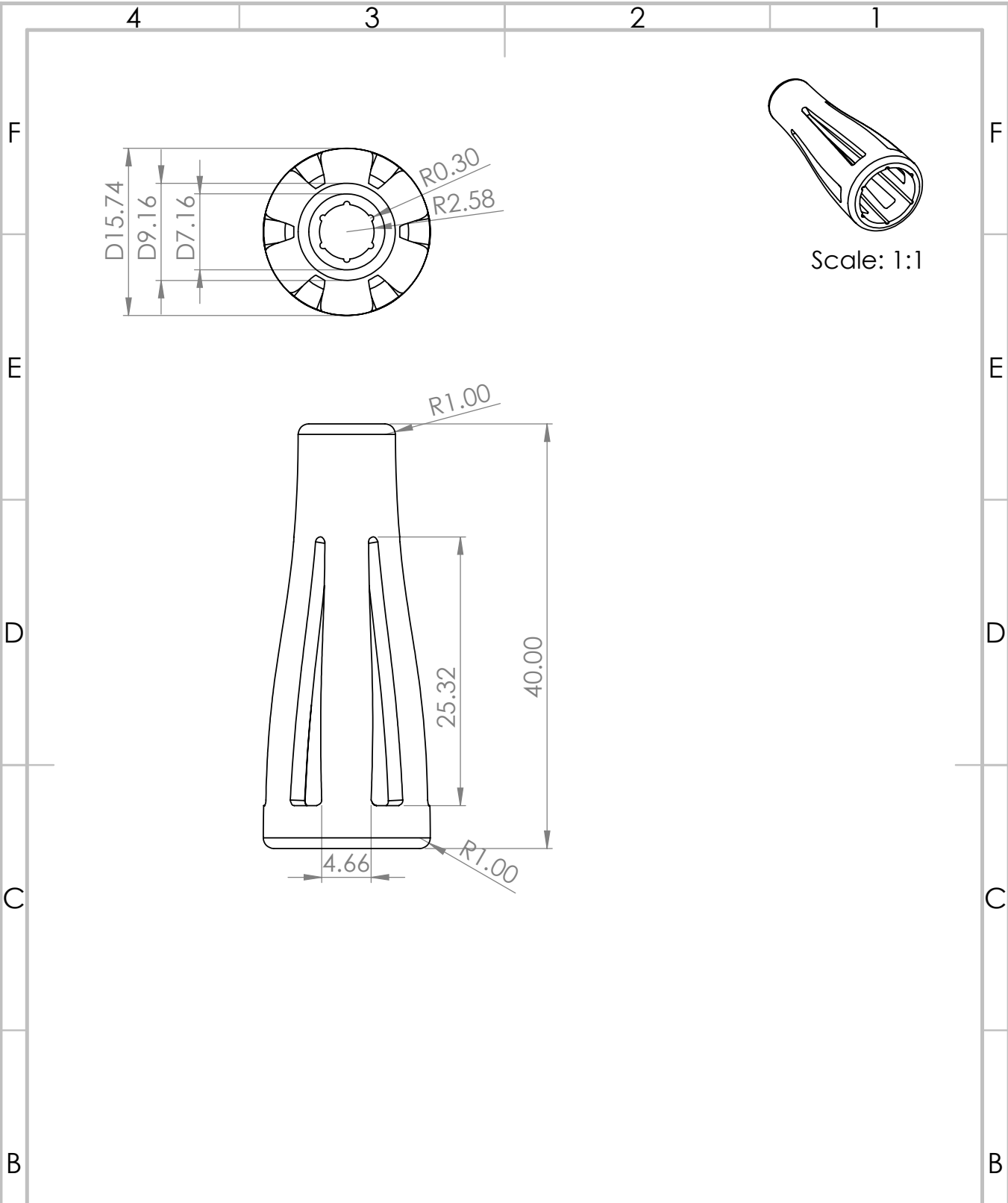










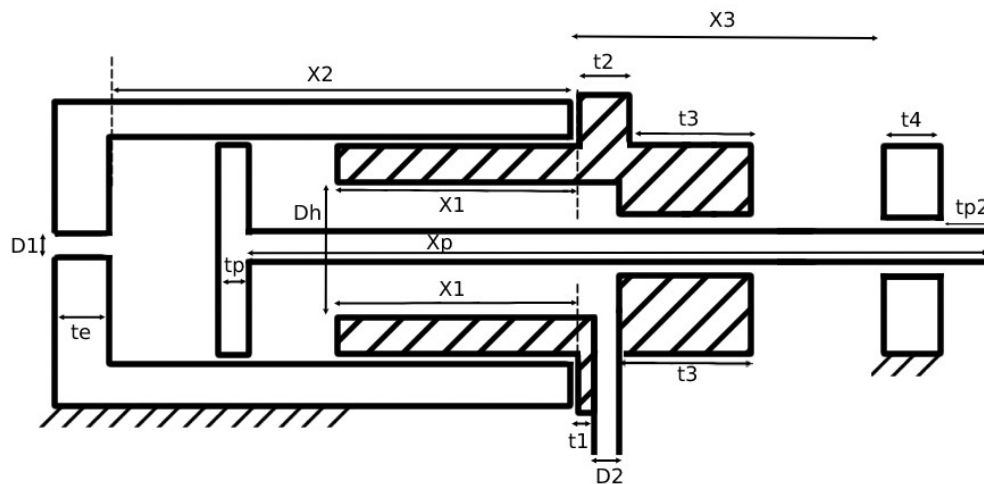


UNLESS OTHERWISE SPECIFIED: DIMENSIONS ARE IN MILLIMETERS SURFACE FINISH: TOLERANCES: LINEAR: ANGULAR:				FINISH:		DEBURR AND BREAK SHARP EDGES		DO NOT SCALE DRAWING		REVISION	
DRAWN	NAME	SIGNATURE	DATE			TITLE:					
	CHK'D										
	APP'VD										
	MFG										
	Q.A										
				MATERIAL:		DWG NO.					
				WEIGHT: 40		SCALE:2:1					
						SHEET 1 OF 1					

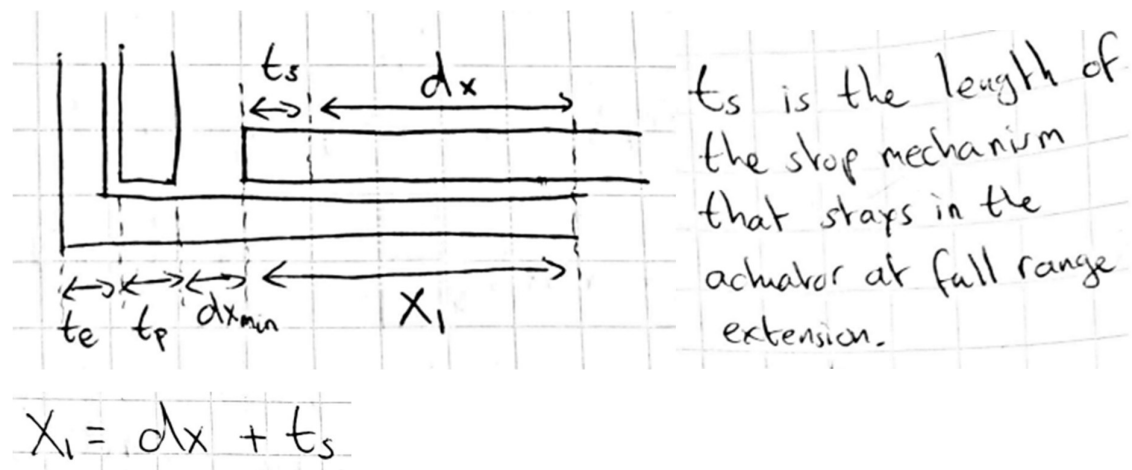


## Appendix D. Calculations and Variables as in the Matlab Script

Piston dimensions as referred to in the matlab script.

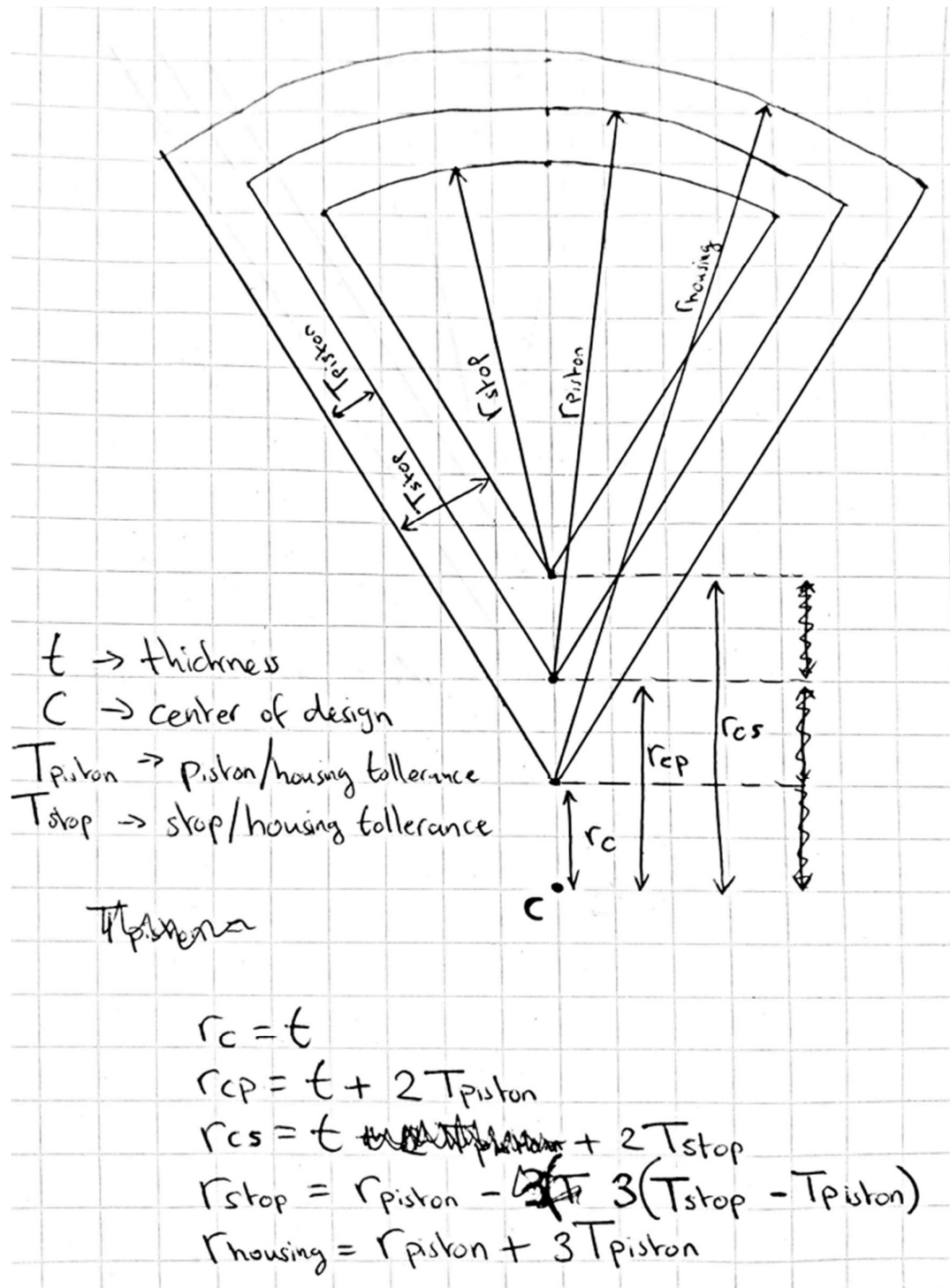


### Piston Length Calculations for Inner stop:





# Piston dimensions (for tolerance)



Calculate the losses in area due to the fillets:

### Surface loss from fillets



$$\tan \alpha = \frac{r}{x}$$
$$x = r / \tan \alpha$$

$$\left. \begin{aligned} A_{\text{total}} &= r \cdot x \\ A_{\text{total}} &= A_{\text{fillet}} + A_{\text{loss}} \end{aligned} \right\} A_{\text{loss}} = r x - A_{\text{fillet}}$$

$$A_{\text{fillet}} = \frac{2\gamma}{360^\circ} \times 2\pi r^2$$

$$\gamma = 180^\circ - 90^\circ - \alpha = 90^\circ - \alpha$$

$$A_{\text{fillet}} = \frac{2(90^\circ - \alpha)}{360^\circ} \times 2\pi r^2$$

$$\rightarrow A_{\text{loss}} = r x - \frac{2(90^\circ - \alpha) \pi r^2}{360}$$

$$A_{\text{loss}} = r x - \frac{(90^\circ - \alpha) \pi r^2}{180^\circ}$$

# Piston Frequency calculations (Theoretical)

~~215mm~~ orifice diameter of valve and tubes:  
 $D_{vt}$ ,  $r_{vt}$  is orifice radius

$$Q = v \cdot A$$

$\downarrow$  Volumetric flow rate     $\downarrow$  flow velocity     $\rightarrow$  area

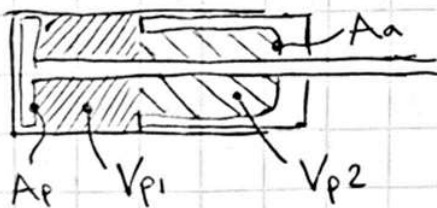
$$A = \pi r_{vt}^2$$

$$Q = v \cdot A \rightarrow Q = v \cdot \pi r_{vt}^2$$

time to pressurize the piston volume:  $t = V_p / Q$

$V_p$  depends on  $dx$  (stroke)

$$f = 1/t, \text{ so } f = Q / V_p$$



$$V_p = \overbrace{dx \cdot A_p}^{V_{p1}} + \overbrace{(x_1 + t_2) \cdot A_a}^{V_{p2}}$$

$$A_a = \frac{60}{360} \times \left( \frac{1}{2} \times \pi \times r_{stop}^2 \right)$$

$A_p \rightarrow$  (optimal) piston area from matlab code

## Appendix E. Matlab Script for Dimensions, Force, and Frequency Calculations

```
% Piston Length Dimensions Calculations, for internal stop
clear all
close all
clc

dx_max = 10; %mm
dx_min = 1; %mm

tp = 2; %mm
te = 2; %mm
D1 = 2; %mm
D2 = 3.5; %mm
t1 = 0; %mm
t3 = 4; %mm
t4 = 3; %mm
ts = 2; %mm
tp2 = 5; %mm (1mm safety factor + 4mm to attach to the tip)

t2 = t1 + D2;
X1 = (dx_max - dx_min) + ts;
X2 = tp + dx_min + X1;
X3 = t2 + t3 + (dx_max - dx_min);
Xp = (X2 - tp) + X3 + t4 + tp2;
```

```

%% A visualisation of the output forces per surface area and working pressure
clear all
close all
clc

%At minimum pressure p, what is the output force per piston area?

%working pressure range
pmin = 1.1E5;%Pa
pmax = 8E5; %maximum working range pressure

%gauge pressure
pgmin = pmin - 1E5;
pgmax = pmax - 1E5;

%Diameter of the piston
Dmin = 1;
Dmax = 30;

p = [pgmin:0.1E5:pgmax];
D = [Dmin:1:Dmax]; %mm
A = 0.25*pi*(D*1E-3).^2; %Calculate the area as if the piston is circular

F = zeros(length(p),length(A));

for i = 1:length(p)

    F(i,:) = p(i)*A;

end

Amin = 3E-5; %The determined area (After iterating with tollerances)
Fmin = pgmin*Amin;

%For a piston with area A
figure
plot(A,F)
ylabel('Force (N)')
xlabel('Piston Area (m^2)')
title('output force per piston diameter for pmin to pmax working range')
xline(Amin);
set(gca,'YTick',(0.5:0.5:15))
ylim([0 11])
xlim([0 1E-4])

```

```

%% Piston Diameter Dimensions Calculations
clear all
close all
clc

%constants
xpist = 6; %Number of pistons
A_optimal = 3E-5; %Optimal area, as calculated in piston_force_calculations (in m^2)
Dmin = 2E-3; %Minimum 'free' center diameter, (in m)
rfillet = 0.3E-3; %Radius of the fillets in the three corners (in m)
tmin = 1E-3;%minimum specified wall-thickness
tminmm = tmin*1E3; %tmin in mm
Tstop = 0.2E-3; %Tolerance between the piston stop and the piston housing (in m)
Tpiston = 0.1E-3;%Tolerance between the piston and the piston housing (in m)

%calculations

phi = 360/xpist; %angle of the piston to the center (in degrees)

%Fillet area losses
alpha_center = phi/2;
alpha_edges = 45; %assume the angles at the other two corners are 90 degrees
Aloss_center = rfillet*(rfillet/tand(alpha_center)) - ((90-alpha_center)*pi*(rfillet^2))/180; %Area losses in the center due to the fillet (in m^2)
Aloss_edges = rfillet*(rfillet/tand(alpha_edges)) - ((90-alpha_edges)*pi*(rfillet^2))/180; %Area losses in the center due to the fillet (in m^2)
Aloss = Aloss_center + 2*Aloss_edges; %Total area loss due to fillets

Ap = A_optimal + Aloss; %Calculate the new required area, including losses due to the fillets

%Calculate the optimum wall thickness, based on the given minimum "free"
%center diameter
topt = 0.5*Dmin - rfillet;
toptmm = topt*1E3;
fprintf('Based on the given minimum "free" center diameter, the optimal whall thickness t is %s mm\n',toptmm)

%check which wall-thickness (minimum or calculated optimal) must be used
if topt < tmin
    t = tmin;
    fprintf('As this is less than the minimum wall thickness, the wall thickness used is %s mm \n',tminmm)
else
    t = topt;
    disp('The optimal wall-thickness will be used since it is not less than the minimum specified wall-thickness')
end

%Calculate radius of the piston part
r = sqrt(6*Ap/pi); % m
rmm = r*1E3; %mm
fprintf('The minimum value for r is %s mm\n',rmm)

%Calculate the distance of the piston hole to the center of the design
rh = t + (2/3)*r; %assume the center is at 2/3 r.
rhmm = rh*1E3;

fprintf('The distance of the piston center to the center is %s mm\n',rhmm)

%Calculate the radius and center distance of the piston housing and piston
%stop
rstop = r - 3*(Tstop - Tpiston)
rcs = t + 2*Tstop

rhousing = r + 3*Tpiston
rcp = t + 2*Tpiston

```



```

%% Piston frequency calculations

%A script that checks if the theoretical (calculated) frequency or the
%specified valve frequency limits the design.

clear all
close all
clc

%variables
Dvt = 2E-3; %orifice diameter of the valve(in m)
v = 343;%maximum flow velocity of air in an air valve,
    %at 20 degrees celcius(in m/s)
Qvn = 90/1000/60;%nominal flow rate, specified for the valve (in m^3/s)
rstop = 0.0073; %From piston_dimensions_calculations (in m)
dxmin = 1E-3; %minimum stroke (in m)
dxmax = 10E-3; %maximum stroke (in m)
X1 = 11E-3; %distance X1 (in m)
t2 = 8E-3; %distance t2 (in m)
fspec = 300; %maximum valve switch frequency (in Hz)
Ap = 3E-5;%area of the piston, from the optimized area script (in m^2)

%Calculations
%flow
A = (1/4)*pi*Dvt^2; %The area where the air flows through (m^2)
Qvc = v*A; %The calculated flow rate of the air through the valve (m^3/s)

%dimensions
Aa = (60/360)*(0.5*pi*rstop^2); %Area of the moving piston part

%Check which flow rate (calculated vs nominal) limits the flow rate, use
%this flow rate.
if Qvc > Qvn
    Q = Qvn;
else
    Q = Qvc;
end

%Maximum and minimum piston volume calculations (in m^3)
Vplmin = dxmin*Ap;
Vplmax = dxmax*Ap;
Vp2 = (X1+t2)*Aa;
Vpmin = Vplmin + Vp2;
Vpmax = Vplmax + Vp2;

```

```

tvmin = Vpmin/Q; %minimum time to pressurize the piston, for the minimum range dxmin
fvmin = 1/tvmin; %frequency for the minimum range dxmin
tvmax = Vpmax/Q; %minimum time to pressurize the piston, for the maximum range dxmax
fvmax = 1/tvmax; %frequency for the maximum range dxmax

fprintf('The caculated maximum frequency for operating with minimum volume is %s Hz\n',fvmin)
fprintf('The caculated maximum frequency for operating with maximum volume is %s Hz\n',fvmax)

%Check which frequency (calculated or specified) limits the design (for the
%miniumum volume and for the maximum volume)

if fvmin < fspec
    fvmin = fvmin;
    disp('The frequency for operating with minimum volume is determined by the calculated frequency')
else
    fvmin = fspec;
    disp('The frequency for operating with minimum volume is determined by fspec')
end

if fvmax < fspec
    fvmax = fvmax;
    disp('The frequency for operating with maximum volume is determined by the calculated frequency')
else
    fvmax = fspec;
    disp('The frequency for operating with maximum volume is determined by fspec')
end

```

```

%% Volume calculations

%Lengths per stroke 2 and 10 mm
Ls2 = 2E-3;
Ls10 = 10E-3;

%Volume per stroke 2 and 10 mm
Vs2 = Ap*Ls2;
Vs10 = Ap*Ls10;

%Calculate Volume inside the piston stop
Lstop1 = (X1+t2)*1E-3;
Aa = (60/360)*(0.5*pi*rstop^2); %Area of the moving piston part
Vstop1 = Lstop1*Aa;

Lstop2 = 14E-3;
Dstop2 = 2.5E-3;
Astop2 = (0.25)*pi*Dstop2^2;
Vstop2 = Astop2*Lstop2;

Vstop = Vstop1+Vstop2;

%Calculate the volume in one of the air tubes
Dcable = 2.6E-3; %Inner diameter of the cable
Lcable = 0.4;
Vcable = Dcable*Lcable;

%Calculate the total volumes for both stroke legths, for the backward
%piston position
Vbackward_s2 = Vs2 + Vstop + Vcable;
Vbackward_sl0 = Vs10 + Vstop + Vcable;

%Calculate the total volumes for both stroke legths, for the forward
%piston position
Vforward_s2 = Vs2 + Vcable;
Vforward_sl0 = Vs10 + Vcable;

%Calculate the volume difference for forward and backward motion per stroke length
Vf_s2 = Vforward_s2/Vbackward_s2
Vf_sl0 = Vforward_sl0/Vbackward_sl0

%Calculate the volume increase for the difference in stroke
Vincrease_forward = Vforward_sl0/Vforward_s2
Vincrease_backward = Vbackward_sl0/Vbackward_s2

```

## Appendix F. Arduino Code

```
// Setup millis
unsigned long startMillis;
unsigned long currentMillis;

// period between the piston movements
int DELAY = 1000;

//Number of Cycles
unsigned long totalCycles = 2;

//set the current cycle to zero
unsigned long currentCycle = 0;

// Declaring pins
int PIST1 = 13;
int PIST2 = 12;
int PIST3 = 11;
int PIST4 = 10;
int PIST5 = 9;
int PIST6 = 8;

void setup() {
  // put your setup code here, to run once:
  pinMode(PIST1, OUTPUT);
  pinMode(PIST2, OUTPUT);
  pinMode(PIST3, OUTPUT);
  pinMode(PIST4, OUTPUT);
  pinMode(PIST5, OUTPUT);
  pinMode(PIST6, OUTPUT);
  startMillis = millis(); //initial start time
}

void loop() {
  currentMillis = millis(); //get the current "time" (actually the number of milliseconds since the program started)

  if (currentMillis - startMillis >= DELAY && totalCycles - currentCycle > 0) //test whether the period has elapsed
  {
    digitalWrite(PIST1, HIGH);
  }

  if (currentMillis - startMillis >= 2*DELAY && totalCycles - currentCycle > 0) //test whether the period has elapsed
  {
    digitalWrite(PIST2, HIGH);
  }

  if (currentMillis - startMillis >= 3*DELAY && totalCycles - currentCycle > 0) //test whether the period has elapsed
  {
    digitalWrite(PIST3, HIGH);
  }

  if (currentMillis - startMillis >= 4*DELAY && totalCycles - currentCycle > 0) //test whether the period has elapsed
  {
    digitalWrite(PIST4, HIGH);
  }

  if (currentMillis - startMillis >= 5*DELAY && totalCycles - currentCycle > 0) //test whether the period has elapsed
  {
    digitalWrite(PIST5, HIGH);
  }

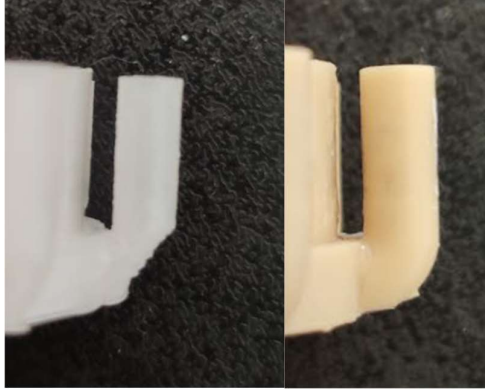
  if (currentMillis - startMillis >= 6*DELAY && totalCycles - currentCycle > 0) //test whether the period has elapsed
  {
    digitalWrite(PIST6, HIGH);
  }

  if (currentMillis - startMillis >= 7*DELAY && totalCycles - currentCycle > 0) //test whether the period has elapsed
  {
    digitalWrite(PIST1, LOW);
    digitalWrite(PIST2, LOW);
    digitalWrite(PIST3, LOW);
    digitalWrite(PIST4, LOW);
    digitalWrite(PIST5, LOW);
    digitalWrite(PIST6, LOW);
    startMillis = currentMillis; // update the time
    currentCycle = currentCycle + 1;
  }
}
```

## Appendix G. 3D-Print Iterations and Findings

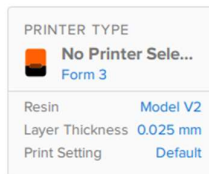
### First print: preform vs ultimaker

- Ultimaker quality is poorer, especially the curved tubes, which were printed at a 45 degrees angle instead of a smooth curve. Also the pistons were printed very poorly with no details.



### First print preform

Specs: 0.5mm tolerance in most places. 0.25mm tolerance for the outer tubes and varying (0.1, 0.2,



0.4mm) tolerance for the piston stick.

### Notes:

- Jamming can occur if it slides at a slight angle. Maybe due to the large tolerances. Lubrication helps.
- The design is not airtight enough. Forward motion works, but backward motion via the outer tubes is not possible. Even when most gaps are filled, it still doesn't work. It is assumed this is due to the gap between piston and housing.
- At this design the 0.1mm tolerance for the piston stick seems to work.

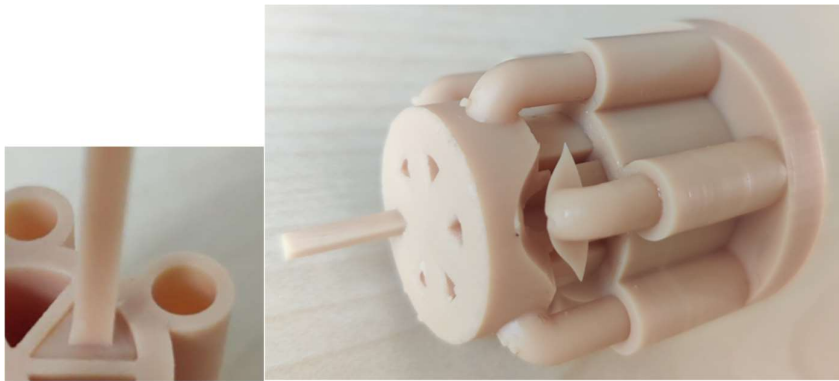


### Second print preform

Specs: 0.1mm tolerances everywhere. The part where the piston stick slides through is increased in length from 1 to 4mm. It is believed that this will guide the piston better and that it will make the design more airtight.

Notes:

- Between the piston and the housing, the 0.1mm tolerances were sufficient.
- At the other places, the 0.1mm tolerance was too tight. It could go in but getting it out was a lot harder.
- The tolerance at the piston pole and the piston guidance was also too tight, it is believed that this is due to the fact that this is a smaller hole and thus tolerances play a larger role(?)
- For the piston base it is found that some holes move better than the other, however it is believed that this can be fixed by sanding the jamming pistons.
- A positive point was that when the piston stick was sanded and the design was put together, the forward and backward motion of the piston worked very well.

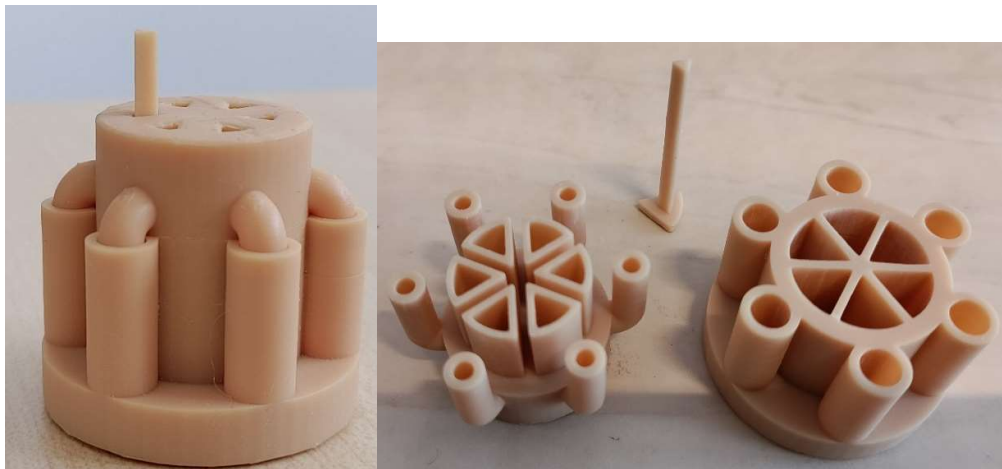


### Third print ultimaker

Specs: 0.2mm tolerances, except for the tolerance between piston and housing, where it is 0.1mm.

Notes:

- Only minor jamming, which is easily fixed by sanding some parts.
- Forward and backward motion is going smooth.





### Prototype 1.0

- Holes for needle segments in the piston tip needs to be drilled, because the hole is not printed that good.
- The bars on the side that were laser cutted do not fit in the housing, only after sanding.
- The nose does not fit 100%, this is believed to be due to the inner part that was printed using support. The part was sanded and after that both parts fit together better, but still not with a 100% fit.
- The play between piston tip and piston is still pretty large, the piston tip could be printed with a lower tolerance.



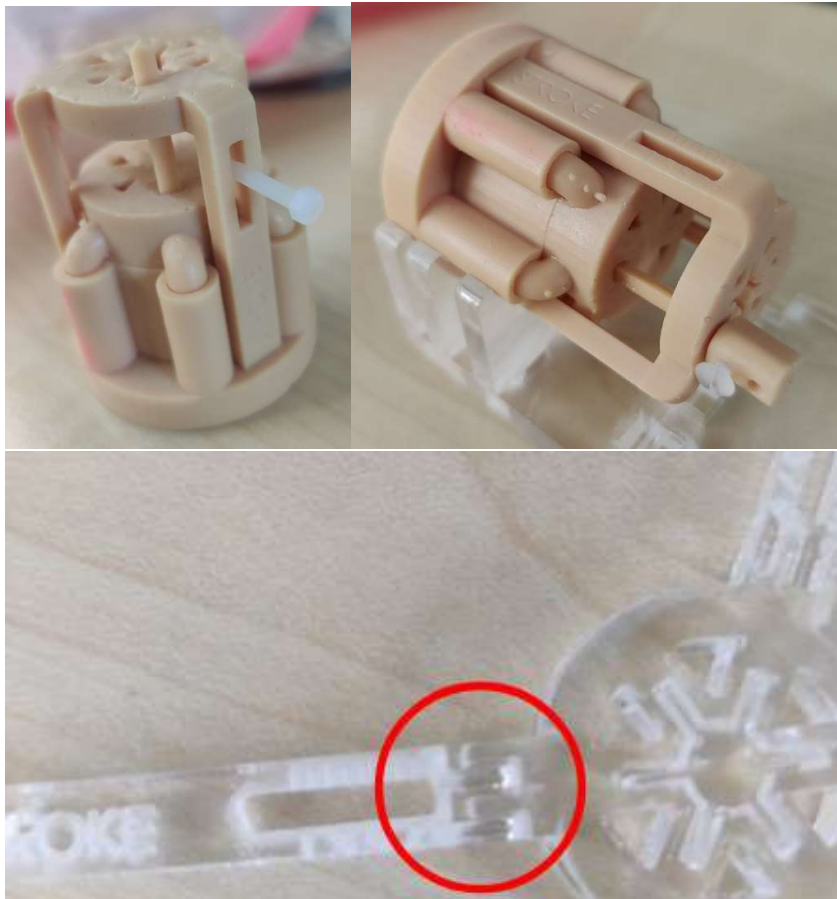
## Prototype 2.0

### Adjusted:

- 0->0.05 tolerance for the bar/housing attachment
- Piston tip 0.1->0.05 tolerance.
- No print support attached to the inner part of the nose
- Nose tolerance 0.05->0.075
- Made holes for the screws in the piston stop deeper.
- Tolerance between screw holes and bars 0.6->0.2
- Tried 3d printing of bars + piston guidance, together with laser cutting to compare the differences.

### Results:

- piston tip tolerance fits perfectly, less play than before.
- The nose fits almost the same, could be 0.1 in the future.
- Bars + guidance printed fits better and more precise, only forgot tolerance between support and nose attachment.
- More tolerance between screw and bar (see picture) is needed, as this jams.
- Less jamming of the piston stop when the 3d printed Bar/guidance part is used, so this part will be used for the final concept.
- The Screw system to fix the piston stop works well.



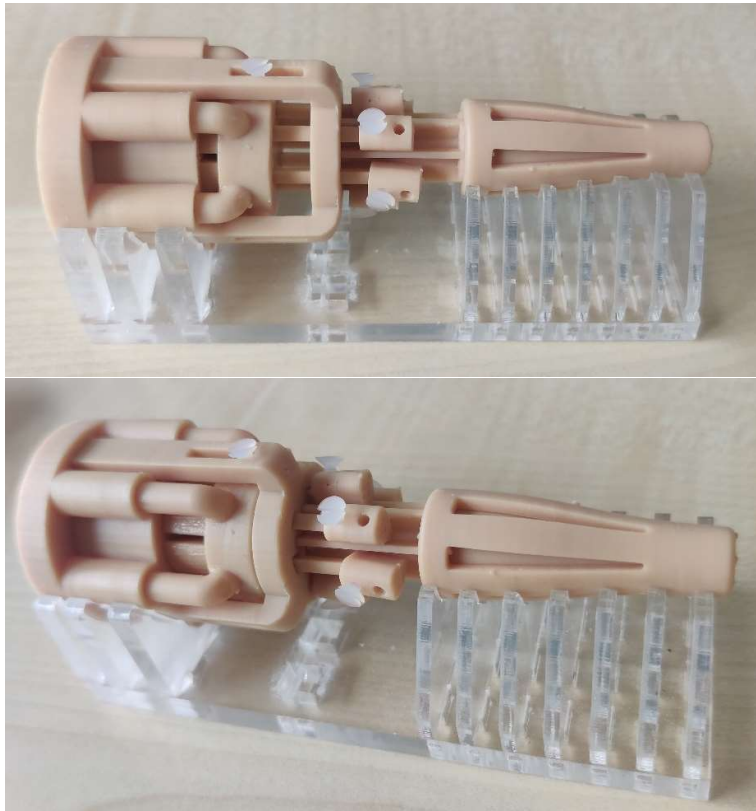
## Prototype 2.1

### Adjusted:

- Bar/guidance part: added tolerance for the screws (0.1) and added tolerance to attach the nose (0.1).
- Reprinted the piston stop because a part of the screw thread broke.
- Sanding the tip of the screws that are used to attach the needle wires to the piston tips. This allows the screws to go deeper.

### Results:

- 3D printed bar/guidance fits better into the nose, still a bit tight but after sanding it works.
- The screw thread for the piston stop still did not work for all three screw threads. However, after manual testing, it was clear that two are sufficient for the stop to hold position.
- After sanding the tip of the screws that are used to attach the needle wires to the piston tips, the needle wires are attached successfully to the design.





#### Prototype 2.2 (Final)

Adjusted:

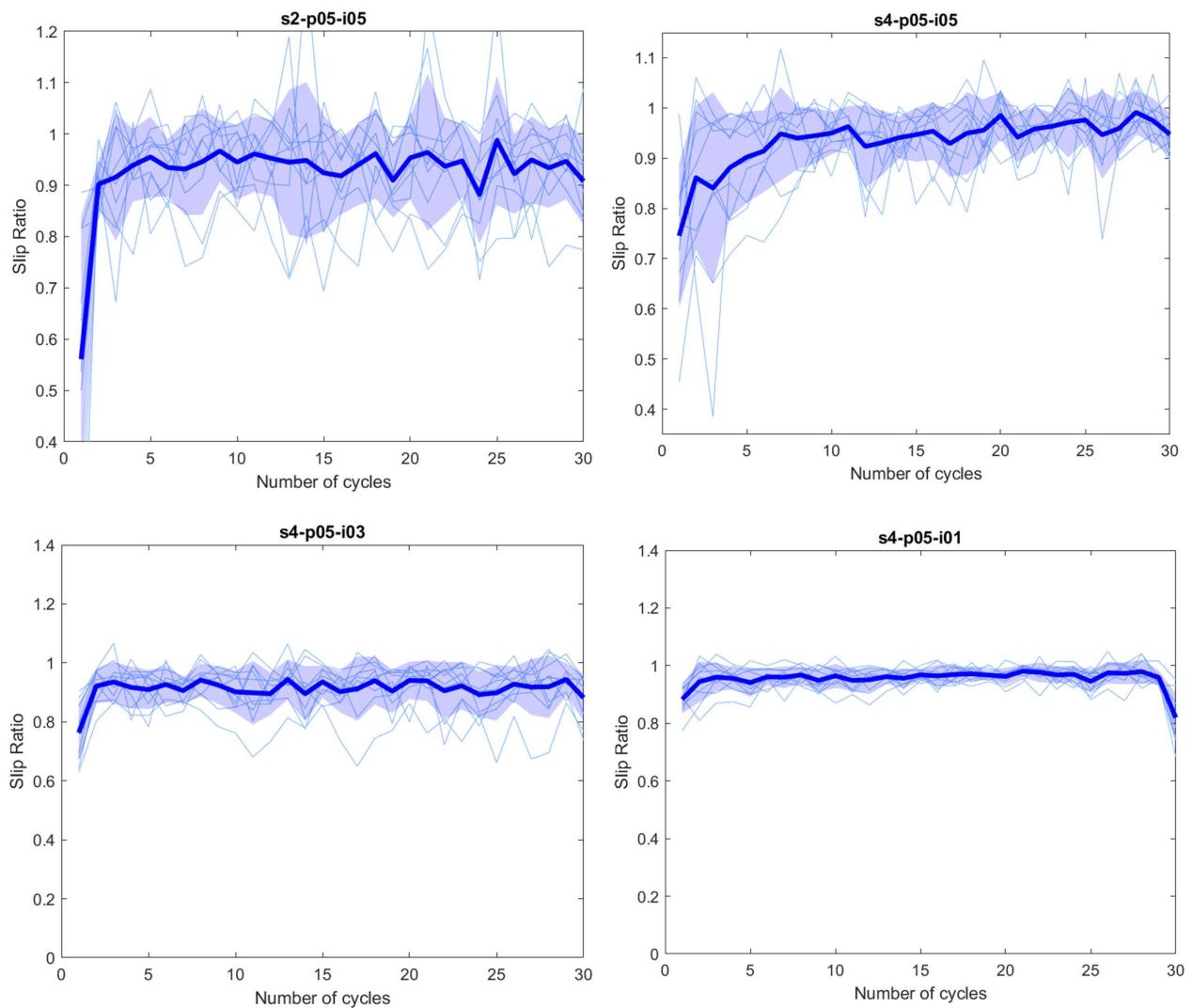
- Screw holes made before curing the print.

Results:

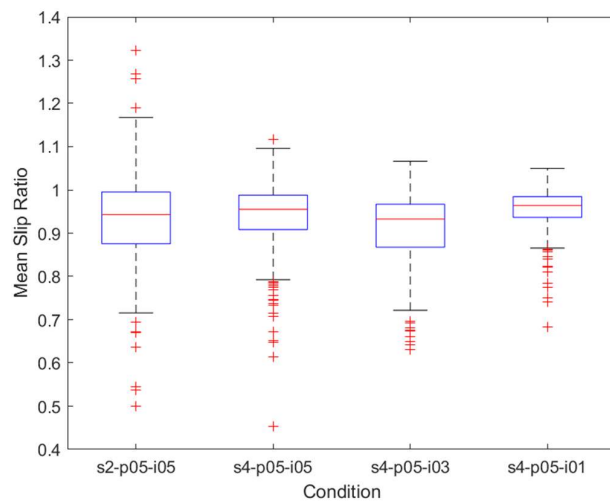
- Screw thread was easier to add and with no failure.

## Appendix H. Figures Data Analysis + Statistical Analysis

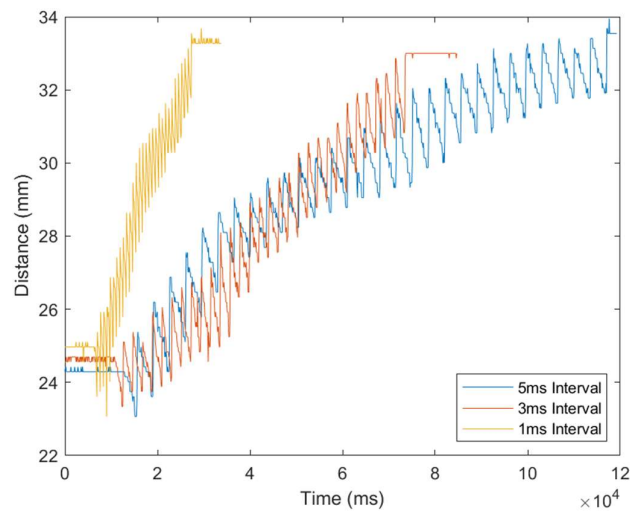
Slip ratio per cycle



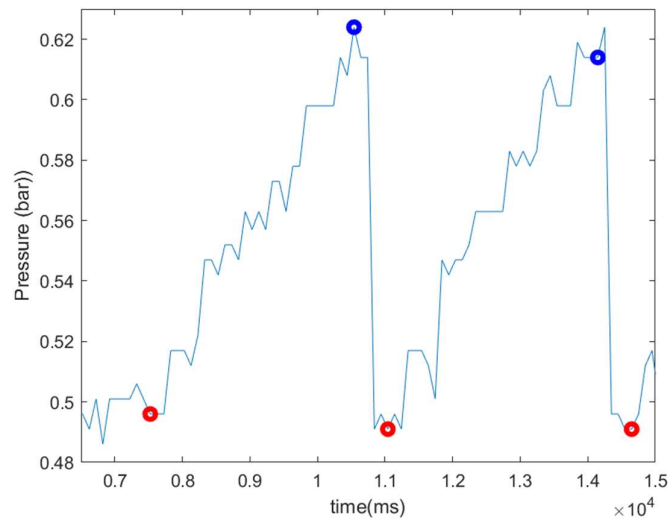
Box plot for the slip ratio per cycle data



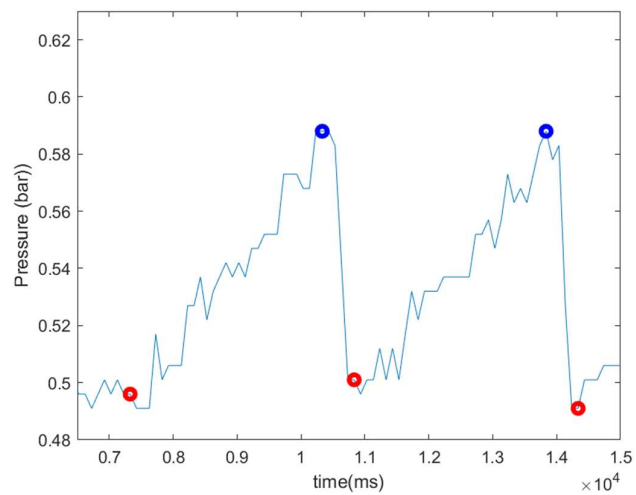
### Unfiltered speed comparison



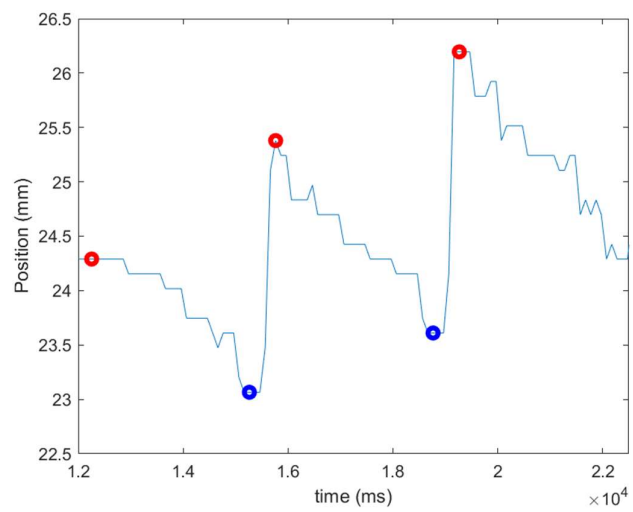
### Unfiltered Pressure data s2-p05-i05



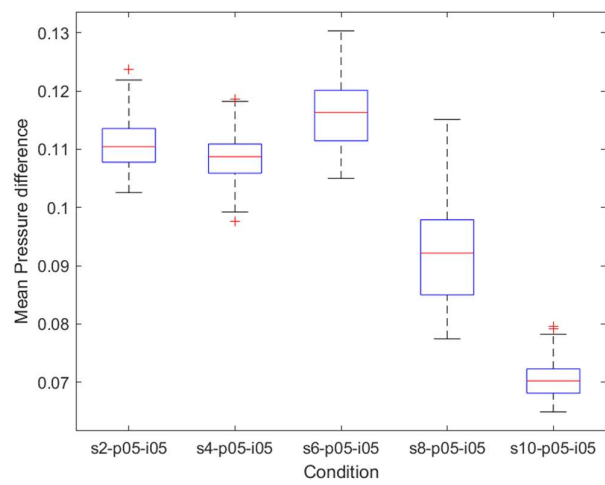
### Unfiltered Pressure data s10-p05-i05



Unfiltered cart distance graph

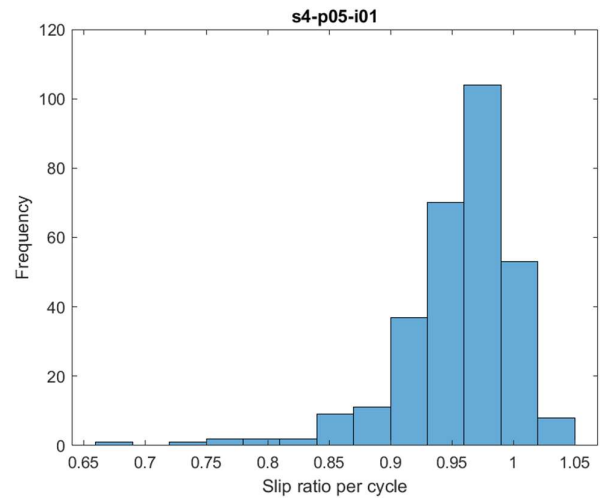
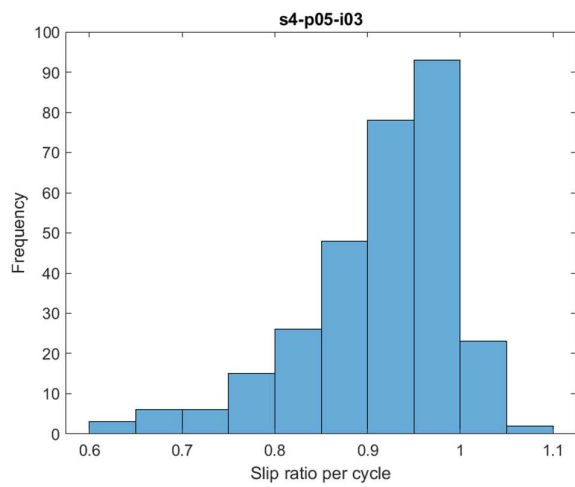
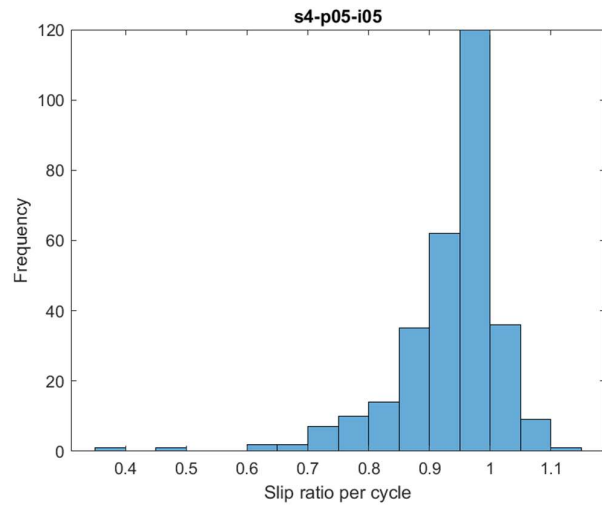
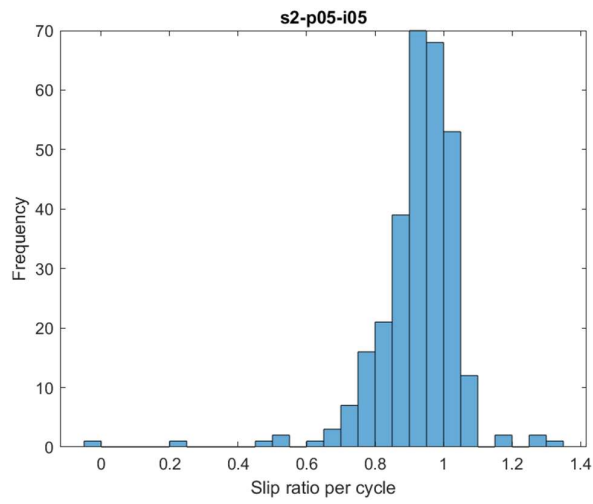


Boxplot mean pressure difference

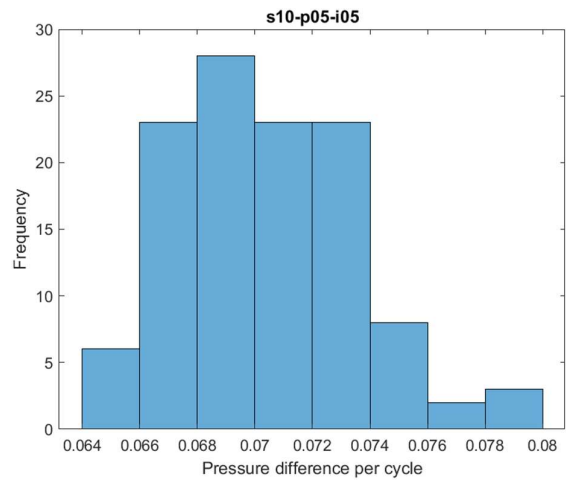
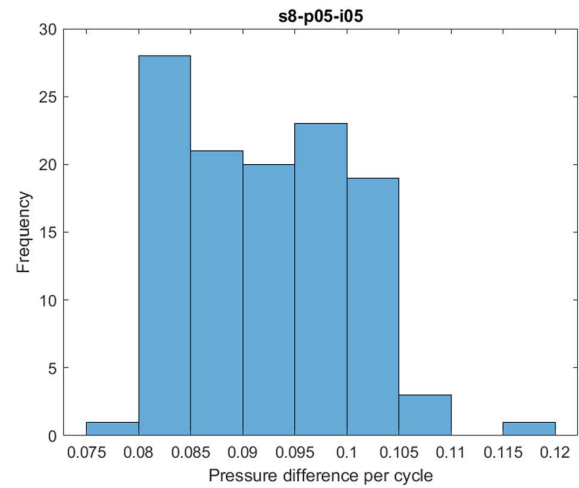
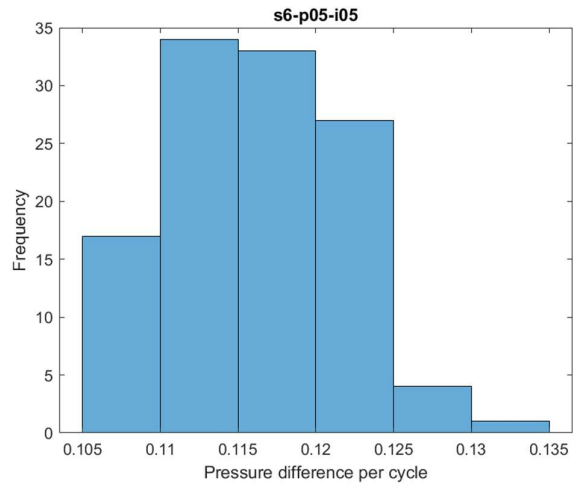
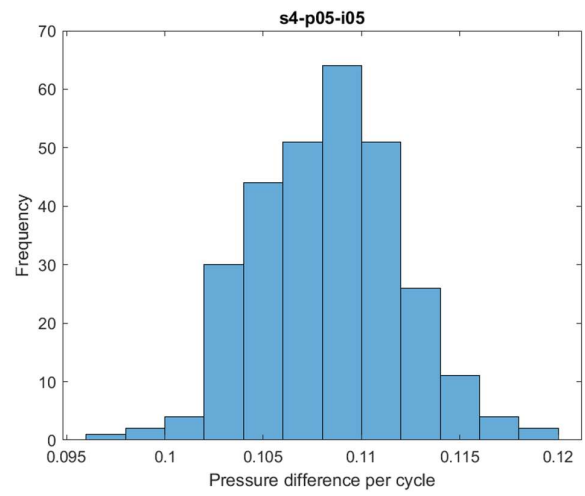
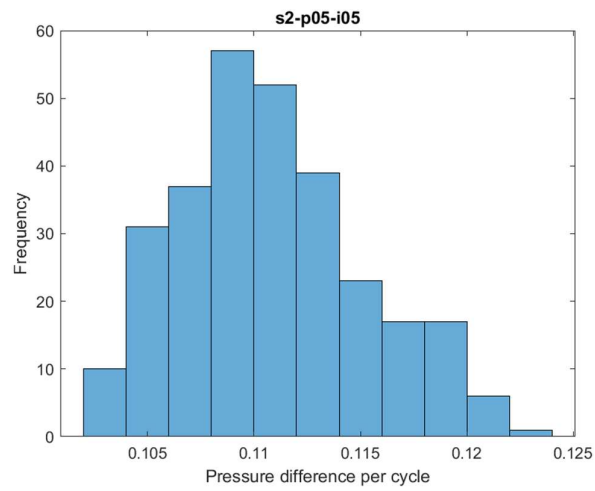




### Histograms for the statistical analysis for the slip ratio per cycle



## Histograms for the statistical analysis for the pressure difference



## Appendix I. Matlab Script Data Analysis

The following code was repeated for each of the conditions:

Only for condition s4-p05-i01, the Savitzky-Golay filter was used with an order of 4 instead of 3. This is because, for these measurements, the interval was small (as small as the measurement interval). This caused the data to look smooth, however, it just had fewer data points for the cycles. This is why smoothening with a larger order was found to work better. Smoothening with a 3<sup>rd</sup> order would smoothen the data too much, causing the peaks to disappear.

```
%% s2-p05-i05

data_dir = ('Data\xlsx\stroke experiments\2mm');
data_files = dir(fullfile(data_dir, '*.xlsx'));

%variables
d_theoretical = 2; %mm
interval = 0.5; %seconds

%Calculate the time of one cycle
cycleTime = (interval*10)*7;

%Open a figure to plot the data in
figure

%Make totalSlip variable
totalSlip = zeros(1,1);

for i = 1:length(data_files)
    data = xlsread(fullfile(data_dir,data_files(i).name));
    time{i} = data(:,1);
    pressure{i} = data(:,3);
    distance{i} = data(:,4);

    %Smooth the data with a Savitzky-Golay filter, order 3, frame length 11.
    distance_smooth{i} = sgolayfilt(distance{i},3,11);

    %Find the peaks and the locations of the peaks
    [pks_d{i},locsp_d{i}] = findpeaks(distance_smooth{i},'MinPeakProminence',0.5);

    %Find the locations of the first and the last peak
    loc_peak1 = locsp_d{i}(1)-cycleTime;
    loc_peak31 = locsp_d{i}(29)+cycleTime;

    %add them to the new locations vector
    locsp{i}(1) = loc_peak1;
    locsp{i}(2:30) = locsp_d{i};
    locsp{i}(31) = loc_peak31;

    pks{i}(1) = distance_smooth{i}(loc_peak1);%Find the first peak
    pks{i}(2:30) = pks_d{i}; %add the found peaks to the new peaks vectors
    pks{i}(31) = distance_smooth{i}(loc_peak31);%Find the last peak

    %Find the valleys and the location of the valleys
    [vall{i},locsv{i}] = findpeaks(-distance_smooth{i},'MinPeakProminence',0.5);
    vall{i} = abs(vall{i}); % As this is negative, use the absolute value

    %Calculate the slip ratio of the peaks and the valleys
    for k = 2:length(pks{i})

        d_measuredp = pks{i}(k) - pks{i}(k-1); %Measured distance (in mm)
        SRp(i,k-1) = 1 - d_measuredp/d_theoretical;;

    end
end
```

```

        %plot the data with the peaks, to check manually
        %plot(locsp{i},pks{i},'**')
        %hold on
        %findpeaks(distance_smooth{i},'MinPeakProminence',0.5);
        %hold on

        %Plot all data points of the Slip Ratio
        plot(1:length(SRp(i,:)),SRp(i,:), 'color', '#80B3FF')
        hold on
    end

    %make a matrix for the mean
    meanSR2 = zeros(1,1);

    for j = 1:30
        %Calculate the mean Slip Ratio of all the data points
        meanSR2(:,j) = mean(SRp(:,j));

        S(:,j) = std(SRp(:,j));
    end

    %Plot the area inbetween the standard deviation
    inBetween = [meanSR2+S, fliplr(meanSR2-S)];
    x2 = [1:length(meanSR2), fliplr(1:length(meanSR2))];
    fill(x2, inBetween, 'b', 'FaceAlpha', .2, 'LineStyle', 'none');
    hold on

    %plot the mean slip ratio
    plot(1:length(meanSR2),meanSR2, 'LineWidth', 3, 'color', 'blue')

    %add labels and a title
    xlabel('Number of cycles')
    ylabel('Slip Ratio')
    title('s2-p05-i05')
    ylim([0.4 1.2]);

    %Add all the slip ratio data to a new vector, for the statistical analysis
    Slips2p05i05 = reshape(SRp.',1,[]);

```

To get the Pressure differences per cycle: (Also repeated for each condition)

```
%% Get the pressure differences for each cycle to compare them (S2)

data_dir = ('Data\xlsx\stroke experiments\2mm');
data_files = dir(fullfile(data_dir, '*.xlsx'));

for i = 1:length(data_files)
    data = xlsread(fullfile(data_dir,data_files(i).name));
    pressure2{i} = data(:,3);

    %Smooth the data with a Savitzky-Golay filter, order 4, frame length 11.
    pressure_smooth10{i} = sgolayfilt(pressure2{i},1,9);

    %Find peaks and valleys
    [pks_press{i},locs_ppress{i}] = findpeaks(pressure_smooth10{i},'MinPeakProminence',0.05); %Find peaks
    [vall_press{i},locs_vpress{i}] = findpeaks(-pressure_smooth10{i},'MinPeakProminence',0.05); %Find valleys

    %calculate the difference in pressure between the valley and the peak

    for j = 1:length(vall_press{i})
        dP2(i,j) = pks_press{i}(j) - abs(vall_press{i}(j));
    end
end
```

For the mean and standard deviation of the slip ratio:

```
%% Calculate the mean and standard deviations for the conditions

mean_s2p05i05 = mean(Slips2p05i05)
std_s2p05i05 = std(Slips2p05i05)

mean_s4p05i05 = mean(Slips4p05i05)
std_s4p05i05 = std(Slips4p05i05)

mean_s4p05i03 = mean(Slips4p05i03)
std_s4p05i03 = std(Slips4p05i03)

mean_s4p05i01 = mean(Slips4p05i01)
std_s4p05i01 = std(Slips4p05i01)
```

For the boxplot to compare the slip ratios:

```
%% Make Boxplot for the slip ratio

figure
boxplot([Slips2p05i05,Slips4p05i05,Slips4p05i03,Slips4p05i01],'Labels',{'s2-p05-i05','s4-p05-i05','s4-p05-i03','s4-p05-i01'})
%title('Slip ratio for each of the conditions')
xlabel('Condition')
ylabel('Mean Slip Ratio')
ylim([0.4 1.4]);
```

Unfiltered speed comparison:

```
%% Unfiltered speed comparison

figure
plot(time4{3},distance4{3})
hold on
plot(time03{3},distance03{3})
hold on
plot(time01{1},distance01{1})

xlabel('Time (ms)')
ylabel('Distance (mm)')
legend('5ms Interval','3ms Interval','1ms Interval','Location','southeast')
```

### Plot the raw pressure data (works the same for the raw position data)

```
%% Plot the raw pressure data of one data set for a 4 mm stroke
figure

plot(time4{2},pressure4{2})
hold on

%Plot the start of the cycles
plot(time4{2}(76),pressure4{2}(76),'o','LineWidth',3,'color','r')
hold on
plot(time4{2}(111),pressure4{2}(111),'o','LineWidth',3,'color','r')
hold on
plot(time4{2}(147),pressure4{2}(147),'o','LineWidth',3,'color','r')
xlim([6500 15000]);

%Plot the moment that all pistons are out
plot(time4{2}(106),pressure4{2}(106),'o','LineWidth',3,'color','b')
hold on
plot(time4{2}(142),pressure4{2}(142),'o','LineWidth',3,'color','b')
hold on

ylim([0.48 0.63]);
xlabel('time(ms)');
ylabel('Pressure (bar)');
```

### Make a boxplot for the mean pressure difference for each of the conditions

```
%% Make Boxplot for the pressure difference per cycle (Experiment 1)

%Make a vector for the data
dP2mm = reshape(dP2.',1,[]);
dP4mm = reshape(dP4.',1,[]);
dP6mm = reshape(dP6.',1,[]);
dP8mm = reshape(dP8.',1,[]);
dP10mm = reshape(dP10.',1,[]);

group = [zeros(length(dP2mm),1); ones(length(dP4mm),1); 2*ones(length(dP6mm),1); 3*ones(length(dP8mm),1); 4*ones(length(dP10mm),1)];

figure
boxplot([dP2mm'; dP4mm'; dP6mm'; dP8mm'; dP10mm'],group,'Labels',{'s2-p05-i05','s4-p05-i05','s6-p05-i05','s8-p05-i05','s10-p05-i05'})
%title('Slip ratio for each of the conditions')
xlabel('Condition')
ylabel('Mean Pressure difference')
```

### Calculate the mean for pressure difference per condition

```
%% Calculate the mean for pressure difference per condition (Experiment 1)

meandP_2mm = mean(reshape(dP2,[],1))
stddP_2mm = std(reshape(dP2,[],1))

meandP_4mm = mean(reshape(dP4,[],1))
stddP_4mm = std(reshape(dP4,[],1))

meandP_6mm = mean(reshape(dP6,[],1))
stddP_6mm = std(reshape(dP6,[],1))

meandP_8mm = mean(reshape(dP8,[],1))
stddP_8mm = std(reshape(dP8,[],1))

meandP_10mm = mean(reshape(dP10,[],1))
stddP_10mm = std(reshape(dP10,[],1))
```

## Appendix J. Matlab Code Statistical Analysis

The outcomes from the statistical analysis of the pressure data might be hard to compare, due to the different sample sizes. The conditions for larger strokes (i.e., 6, 8, and 10 mm) were only measured four times, compared to ten times for the conditions with smaller strokes (i.e., 2 and 4 mm), which makes it hard to conclude something about these outcomes. Another point of discussion regarding the statistical analysis could be the approach that was taken regarding the parametric assumptions. The histograms showed that the data was skewed, but it showed some similarities with a normal distribution. Minor errors in parametric assumptions have no or little effect on the conclusions of a statistical analysis (Garson, 2012). Thus, it could be discussed that the assumption could have been made that the data is normally distributed. To check whether both approaches resulted in the same conclusions, outcomes for both approaches were calculated. The conclusions, about whether there are significant differences, were found to be the same for both approaches.

G. D. Garson. Testing Statistical Assumptions, Statistical Associates Publishing, 2012.

### Histograms + normality tests

```
%% Do a normality check for all experiments
close all

% With histograms
figure
histogram(Slips2p05i05)
xlabel('Frequency')
ylabel('Slip ratio per cycle')
title('s2-p05-i05')
figure
histogram(Slips4p05i05)
xlabel('Frequency')
ylabel('Slip ratio per cycle')
title('s4-p05-i05')
figure
histogram(Slips4p05i03)
xlabel('Frequency')
ylabel('Slip ratio per cycle')
title('s4-p05-i03')
figure
histogram(Slips4p05i01)
xlabel('Frequency')
ylabel('Slip ratio per cycle')
title('s4-p05-i01')

%with the normalitytest script from Öner & Deveci Kocakoc (2017)
normalitytest(Slips2p05i05)
%etc, etc. Manually check for all the data.
```

### Wilcoxon signed rank test for data of experiment 1

```
%% Statistical Analysis Experiment 1

mean_s2 = mean(Slips2p05i05)
std_s2 = std(Slips2p05i05)
mean_s4 = mean(Slips4p05i05)
std_s2 = std(Slips4p05i05)

%Do a Wilcoxon signed rank test, since there are two repeated groups of the
%same size that are not normally distributed

[p,h,stats] = signrank(Slips2p05i05,Slips4p05i05)

if h == 0
    sprintf('The null hypothesis is not rejected, the p-value is %s',num2str(p))
else
    sprintf('The null hypothesis is rejected, the p-value is %s',num2str(p))
end
```



### Friedman + Wilcoxon signed rank test for data of experiment 2

```
%% Statistical Analysis Experiment 2

%Perform a Friedman test for all three conditions
experiments = [Slips4p05i05' Slips4p05i03' Slips4p05i01'];

friedman(experiments)

%The friedman test rejects the null-hypothesis, and thus further examination
%is needed:

%Do a Wilcoxon signed rank test for the three combinations of conditions:
[p1,h1,stats1] = signrank(Slips4p05i05,Slips4p05i03)

[p2,h2,stats2] = signrank(Slips4p05i05,Slips4p05i01)

[p3,h3,stats3] = signrank(Slips4p05i03,Slips4p05i01)
```

### Friedman + Wilcoxon rank-sum test for the pressure data of Experiment 1

```
%% Statistical Analysis for the pressure difference of Experiment 1
dP2mm = reshape(dP2.',1,[]);
dP4mm = reshape(dP4.',1,[]);

%Perform a Friedman test for the three conditions with the same amount of
%measurements
experiments = [dP6mm' dP8mm' dP10mm'];
friedman(experiments)

%Compare the results between the conditions with a wilcoxon signed-rank
%test
%For the measurements with 4 repetitions
[p68,h68,stats68] = signrank(dP6mm',dP8mm')
[p610,h610,stats610] = signrank(dP6mm',dP10mm')
[p810,h810,stats810] = signrank(dP8mm',dP10mm')
%For the measurements with 10 repetitions
[p24,h24,stats24] = signrank(dP2mm',dP4mm')

%conduct a Wilcoxon rank-sum test for the conditions with a different
%amount of repetitions
[p26,h26,stats26] = ranksum(dP2mm',dP6mm')
[p28,h28,stats28] = ranksum(dP2mm',dP8mm')
[p210,h210,stats210] = ranksum(dP2mm',dP10mm')
[p46,h46,stats46] = ranksum(dP4mm',dP6mm')
[p48,h48,stats48] = ranksum(dP4mm',dP8mm')
[p410,h410,stats410] = ranksum(dP4mm',dP10mm')

h = [h24;h26;h28;h210;h46;h48;h410;h68;h610;h810]
p = [p24;p26;p28;p210;p46;p48;p410;p68;p610;p810]
```

### Repeated measures ANOVA + Tukeys HSD test (If the data would have been normally distributed)

```

%% Statistical analysis if the data would have been normally distributed

%the DOF
DOFbetween = 3;
DOFwithin = 1196;

%Calculate the means for the groups
x2mm = mean(Slips2p05i05);
x4mm = mean(Slips4p05i05);
xi03 = mean(Slips4p05i03);
xi01 = mean(Slips4p05i01);

%Put all slip ratios in one vector
allsr = [Slips2p05i05 Slips4p05i05 Slips4p05i03 Slips4p05i01];

%Calculate the grand mean
xg = mean(allsr);

%calculate the sum of squares
SStotal = sum((allsr-xg).^2);
SSwithin = sum((Slips2p05i05-x2mm).^2 + (Slips4p05i05-x4mm).^2 + (Slips4p05i03-xi03).^2 + (Slips4p05i01-xi01).^2);
SSbetween = SStotal - SSwithin;

%Calculate variance (mean square)
MSbetween = SSbetween/DOFbetween;
MSwithin = SSwithin/DOFwithin;

%Calculate the F-value
F = MSbetween/MSwithin

% Tukey's HSD test to find which mean(s) is/are different

q2mm4mm = (x2mm-x4mm)/sqrt(MSwithin/300)
q2mmi03 = (x2mm-xi03)/sqrt(MSwithin/300)
q2mmi01 = (x2mm-xi01)/sqrt(MSwithin/300)

q4mmi03 = (x4mm-xi03)/sqrt(MSwithin/300)
q4mmi01 = (x4mm-xi01)/sqrt(MSwithin/300)

qi03i01 = (xi03-xi01)/sqrt(MSwithin/300)

```

Two sample t-test for the pressure difference data (If the data would have been normally distributed)

```

%% Do a two sample t-test to find if the mean pressures are statistically different

close all
%Check if the data is normally distributed with a histogram
figure
histogram(dP2)
xlabel('Pressure difference per cycle')
ylabel('Frequency')
title('s2-p05-i05')
figure
histogram(dP4)
xlabel('Pressure difference per cycle')
ylabel('Frequency')
title('s4-p05-i05')
figure
histogram(dP6)
xlabel('Pressure difference per cycle')
ylabel('Frequency')
title('s6-p05-i05')
figure
histogram(dP8)
xlabel('Pressure difference per cycle')
ylabel('Frequency')
title('s8-p05-i05')
figure
histogram(dP10)
xlabel('Pressure difference per cycle')
ylabel('Frequency')
title('s10-p05-i05')

%do the t-test. If h=1, the test rejects the null hypothesis at the 5%
%significance level, and 0 otherwise.

[h24,p24] = ttest2(reshape(dP2, 1, []), reshape(dP4, 1, []))
[h26,p26] = ttest2(reshape(dP2, 1, []), reshape(dP6, 1, []))
[h28,p28] = ttest2(reshape(dP2, 1, []), reshape(dP8, 1, []))
[h210,p210] = ttest2(reshape(dP2, 1, []), reshape(dP10, 1, []))
[h46,p46] = ttest2(reshape(dP4, 1, []), reshape(dP6, 1, []))
[h48,p48] = ttest2(reshape(dP4, 1, []), reshape(dP8, 1, []))
[h410,p410] = ttest2(reshape(dP4, 1, []), reshape(dP10, 1, []))
[h68,p68] = ttest2(reshape(dP6, 1, []), reshape(dP8, 1, []))
[h610,p610] = ttest2(reshape(dP6, 1, []), reshape(dP10, 1, []))
[h810,p810] = ttest2(reshape(dP8, 1, []), reshape(dP10, 1, []))

```

## Appendix K. Components for the Control Unit

Part	Amount	Company/Brand	Product Code	Price ea.
Pressure regulator	1	Norgren	B72G-2GK-ST3-RMN	€ 130
Electronic pressure sensor	1	Autosen	/	€ 84.12
Tubes 6 mm OD	/	Festo	PUN-H	/
Tubes 4 mm OD	/	Festo	PUN-H	/
T-connector	1	Festo	T-PK-4	€ 2,42
Tube/screw coupling 1/4"/6 mm	1	Festo	CRCN-1/4-PK-4	€ 17,73
Tube/screw coupling M5/4 mm	12	Festo	CRCN-M5-PK-3	€ 10,08
Mono-stable 5/2-way valve	6	Festo	MHP2-MS1H-5/2-M5	€ 124,78
Electrical connection for valve	6	Festo	NEBV-Z4WA2L-P-E-2.5-N-LE2-S1	€ 21,69
Valve manifold for 2 valves	1	Festo	MHP2-PR2-5	€ 55,32
Valve manifold for 4 valves	1	Festo	MHP2-PR4-5 525123	€ 79.89
Double nipple	1	Festo	NPFC-DS-M5-M5-M	€ 1,81
Reducing nipple	1	Festo	NPFC-R-M7-M5-MF	€ 1,30
Screw plug	1	Festo	NPQH-BK-M5-P10	€ 0,87
24V Power supply	1	Delta Elektronika	SM 66-AR-110	/
Microcontroller	1	Arduino	A000066	€ 25
transistors	6	/	/	/

OD = outer diameter